Isopeptide Bond-Locked Enzymes to Engineer Thermal Resilience



Jisoo Jean

Department of Biochemistry
Wolfson College
University of Oxford

Trinity 2020

This thesis is submitted to the Department of Biochemistry, University of Oxford, in partial fulfilment of the requirements for the degree of Doctor of Philosophy

Abstract

Despite their high utility, enzymes often require thermal stabilisation prior to use in industrial catalysis. Current stabilisation approaches are time-consuming and require the individual engineering of each enzyme requiring stabilisation. Head-to-tail enzyme cyclisation is an alternative strategy that has the potential to serve as a generic yet effective method for the thermal stabilisation of enzymes. Spontaneous isopeptide bond-forming protein partners SpyTag and SpyCatcher have been used to cyclise enzymes to confer thermal resilience.

In this thesis, I established the application of the novel tripartite SnoopLigase conjugation system for enzyme cyclisation. SnoopLigase catalyses the covalent locking of peptide tags SnoopTagJr and DogTag. N-terminal fusion of SnoopTagJr and C-terminal fusion of DogTag enabled the efficient cyclisation of mesophilic enzymes upon addition of SnoopLigase through the formation of an isopeptide bond between the peptide tags. SnoopLigase cyclisation conferred major improvements in thermal resilience to mesophilic enzymes, enabling them to withstand heat-induced aggregation and inactivation even following incubation at 100 °C.

Until now, cyclisation has only been demonstrated for enzymes whose termini are found in relative proximity. To broaden the scope of isopeptide bond-mediated cyclisation, I applied SnoopLigase cyclisation in conjunction with structured linkers to cyclise industrially important enzymes with larger distances between termini. Linker-appended SnoopLigase cyclisation improved the thermal resilience of already thermostable enzymes, demonstrating the potential for one-step enhancement of thermal resilience for a wider range of enzymes.

COVID-19 Statement

In accordance with the guidelines issued by the University of Oxford on the 20th July 2020 regarding thesis submissions during the COVID-19 global pandemic, a statement addressing the impact of the pandemic on this DPhil is provided below:

The COVID-19 global pandemic occurred during the final year of this DPhil. A decision was made to not apply for an extension of the thesis submission deadline and instead, all results were written up into this thesis without additional lab work. Additional experiments could not be performed due to the implementation of national lockdown measures and the closure of the Biochemistry Department.

Authorship Declaration

I declare that all work performed in this thesis is my own, except for cases described below. The thesis has not been submitted for any other degree at the University of Oxford or any other institution.

Experiments performed by others:

Chapter 3
Mass spectrometry was performed by Dr. David Staunton

Publications arising from this thesis are as follows:

Buldun, C.M.*, Jean, J.X.*, Bedford, M.R., and Howarth, M. (2018). SnoopLigase Catalyzes Peptide-Peptide Locking and Enables Solid-Phase Conjugate Isolation. J. Am. Chem. Soc. *140*, 3008–3018.

* joint first author

Acknowledgements

I would like to thank Prof. Mark Howarth for his guidance and assistance during my degree and Prof. Christina Redfield for her support and advice. I would also like to express my gratitude to Dr. Michael Bedford from AB Vista for his time and knowledge. I am grateful to my funding bodies, Wolfson College and the BBSRC, for their financial support that enabled this DPhil.

From the Howarth laboratory, I would like to thank Can, Theo, Irsyad and Eleanor for their support and friendship. I would like to thank all my friends from the Interdisciplinary DTP programme for making my Oxford experiences enjoyable. I am especially grateful to Shahaan and Stuart for helping me find pockets of happiness wherever possible. I am also infinitely grateful for friends who have made the difficult times more manageable - Richard, Michie, Sulo, and Giulia.

I would like to especially thank those without whom this thesis would not have been possible. I thank Emily and Megan from Wolfson for believing in me and Alan for giving me the tools to lift myself up. To Bambi – thank you for being my best friend and for being so very excited every single time I come home. Your fluffy companionship made the writing of this thesis monumentally more enjoyable.

Finally, I would like to express my utmost gratitude to my family for their unconditional love and support. I thank my father for showing me the value of a rigorous work ethic and a dedication to excellence. I thank my mother for showing me the beauty in staying curious and the importance of continuous self-development. I am immensely grateful for every adventure we have shared.

상송상청 - 곧고 귀하게 키워주신 덕분입니다. 사랑합니다. 감사합니다.

Abbreviations

AP	Acceptor peptide
AppA	*Escherichia coli* phytase
ATP	Adenosine triphosphate
BCA	Bicinchoninic acid
Bio	Biotin
BirA	Biotin ligase
BLA	TEM-1 β-lactamase
BSA	Bovine serum albumin
DMSO	Dimethyl sulfoxide
DogT	DogTag
DTT	Dithiothreitol
EDTA	Ethylenediaminetetraacetic acid
epPCR	Error-prone polymerase chain reaction
ESI-MS	Electrospray ionisation mass spectrometry
FACS	Fluorescence-activated cell sorting
GSSM	Gene site saturation mutagenesis
GST	Glutathione S-transferase
HDX-MS	Hydrogen deuterium exchange mass spectrometry
IPTG	Isopropyl β-D-1thiogalactopyranoside
ISM	Iterative saturation mutagenesis
LB	Luria Bertani broth
MS	Mass spectrometry
MWCO	Molecular weight cut-off
Ni-NTA	Nickel nitrilotriacetic acid
OD	Optical density
PAGE	Polyacrylamide gel electrophoresis
PBS	Phosphate-buffered saline
PCR	Polymerase chain reaction

PDB	Protein Data Bank
PhyC	*Bacillus subtilis* phytase
PMSF	Phenylmethylsulfonylfluoride
QB	Quantum Blue
SAXS	Small-angle X-ray scattering
SDS	Sodium dodecyl sulfate
SnL	SnoopLigase
SnTJr	SnoopTagJr
SUMO	Small ubiquitin modifier
T_m	Temperature at which 50% protein is unfolded

Table of Contents

Abstract I
COVID-19 Statement II
Authorship Declaration III
Acknowledgements IV
Abbreviations V
Table of Contents VII
List of Figures and Tables X
Chapter 1: Introduction 1
1.1 Thermal Stabilisation of Enzymes 1
1.1.1 Mutagenesis Using Rational Design 2
1.1.2 Directed Evolution 7
1.1.3 Immobilisation 10
1.1.4 CLEAs and CLECs 14
1.1.5 Protein Supercharging 17
1.1.6 Molecular Chaperones and Thermophilic Protein Fusion 19
1.1.7 Enzyme Caging 22
1.2 Head-to-Tail Cyclisation for Enzyme Stabilisation 23
1.2.1 Intein 24
1.2.2 Sortase 26
1.2.3 Butelase 27
1.3 Cyclisation by Spontaneous Isopeptide Bond-Forming Proteins 28
1.3.1 SpyRing (SpyTag and SpyCatcher) 29
1.3.2 SpyRing-Cyclised Enzymes 31
1.3.3 SnoopRing (SnoopTag and SnoopCatcher) 36
1.4 SnoopLigase 37
1.5 Phytase 39
1.5.1 Phytase Significance 40
1.5.2 Types of Phytase 43
1.5.3 Commercial Stabilised Phytases 46
1.5.4 Quantum Blue 47
1.6 Thesis Objectives 49
Chapter 2: Methods 51

2.1 Cloning 51
2.1.1 Polymerase Chain Reaction 51
2.1.2 Agarose Gel Electrophoresis and PCR Product Purification 52
2.1.3 Gibson Assembly 52
2.1.4 Transformation into *E. coli* 53
2.1.5 Plasmid Preparation 53
2.1.6 DNA Sequence Verification 54
2.1.7 Cloning of SnoopLigase, BLA and PhyC Constructs 54
2.1.8 Cloning of AppA and Quantum Blue Constructs 55
2.2 Protein Expression and Purification 55
2.2.1 Media Composition 55
2.2.2 Protein Expression in *E. coli* 56
2.2.3 Ni-NTA Affinity Chromatography of Soluble His_6-Tagged Proteins 57
2.2.4 Periplasmic Purification of Disulfide Bond-Containing Proteins 58
2.2.5 Quantification of Protein Concentration 58
2.3 Protein Biotinylation 59
2.4 Protein Characterisation 60
2.4.1 SDS-PAGE 60
2.4.2 Electrospray Ionisation Mass Spectrometry 60
2.5 SnoopLigase Cyclisation 61
2.5.1 SnoopLigase Conjugation Reaction 61
2.5.2 SnoopLigase Removal Following Conjugate Formation 61
2.5.2.1 Purification using Glycine Elution 62
2.5.2.2 Purification using Imidazole Elution 63
2.5.2.3 Purification using Competitor Peptide Elution 63
2.6 Characterisation of Enzyme Thermal Resilience 64
2.6.1 Temperature-Dependent Solubility Assay 64
2.6.2 BLA Thermal Resilience Activity Assay 64
2.6.3 PhyC Thermal Resilience Activity Assay 65
2.6.4 AppA/ QB Thermal Resilience Activity Assay 66
2.6.5 Production of Dialysed Cleared Lysate 67
2.6.6 Thermal Resilience Activity Assays in Dialysed Cleared Lysate 67
Chapter 3: Enhancing Thermal Resilience via SnoopLigase Cyclisation 68
3.1 SnoopLigase Cyclisation of TEM-1 β-lactamase 70
3.1.1 Design of Constructs for Cyclisation 73

3.1.2 Verification of BLA Cyclisation 74
3.1.3 Effect on Aggregation of BLA 75
3.1.4 Effect on Thermal Resilience of BLA Activity 77
3.1.5 SnoopLigase Depletion Following BLA Cyclisation 79
3.2 SnoopLigase Cyclisation of *Bacillus subtilis* Phytase (PhyC) 84
3.2.1 Verification of PhyC Cyclisation 86
3.2.2 Effect on Aggregation of PhyC 88
3.2.3 Effect on Thermal Resilience of PhyC Activity 89
3.2.4 SnoopLigase Depletion Following PhyC Cyclisation 91
3.2.5 Comparison to SpyRing-Cyclised PhyC 94
3.2.6 Thermal Resilience in Dialysed Cleared Lysate 95
3.3 Discussion 99
Chapter 4: Cyclisation of Enzymes with Greater Distances Between Termini 105
4.1 Cyclisation of *Escherichia coli* phytase AppA 107
4.1.1 SpyRing Cyclisation of AppA 110
4.1.2 Positioning of Structured Linkers 114
4.1.3 Testing of cTPR, LRR and L9 Linkers 115
4.1.4 SpyRing-Cyclised AppA in Cleared Lysate 118
4.1.5 SnoopLigase Cyclisation of L9-Appended Constructs 119
4.1.6 SnoopLigase-Cyclised AppA in Cleared Lysate 123
4.1.7 SnoopLigase Depletion Following AppA Cyclisation 125
4.2 SnoopLigase Cyclisation of Quantum Blue 126
4.2.1 Quantum Blue 126
4.2.2 SnoopLigase Cyclisation of L9-Appended Quantum Blue 129
4.2.3 SnoopLigase-Cyclised Quantum Blue in Cleared Lysate 131
4.2.4 SnoopLigase Depletion Following QB Cyclisation 134
4.2.5 SnoopLigase Titration Following Depletion 135
4.3 Discussion 143
Chapter 5: Summary and General Discussion 151
Bibliography 158

List of Figures and Tables

Figure 1.1 Schematic of the typical directed evolution cycle 8

Figure 1.2 Multipoint attachment immobilisation and recycling of immobilised enzymes 11

Figure 1.3 Preparation of cross-linked enzyme aggregates and cross-linked enzyme crystals 14

Figure 1.4 Enzyme cyclisation by sortase A and butelase I..... 26

Figure 1.5 Splitting of CnaB2 into SpyTag and SpyCatcher 30

Figure 1.6 SpyRing cyclisation of TEM-1 β-lactamase 32

Table 1 SpyRing-cyclised enzymes……..34

Figure 1.7 Splitting of RrgA C-terminal domain into SnoopTag and SnoopCatcher 36

Figure 1.8 Splitting of RrgA into the SnoopLigase conjugation system 38

Figure 1.9 Phytic acid and its sequential hydrolysis by phytase 41

Figure 1.10 Phytase classification and representative enzymes 45

Table 2 Commercially available thermostable phytases ……..46

Figure 1.11 Structure of Phy9X 48

Figure 3.1 Tripartite and bipartite splitting of RrgA domain 4..... 72

Figure 3.2 Design of BLA constructs for SnoopLigase cyclisation..... 73

Figure 3.3 Timecourse of SnoopLigase cyclisation of BLA..... 75

Figure 3.4 Cyclisation improved BLA resistance to heat-induced aggregation.... 76

Figure 3.5 SnoopLigase cyclisation improved BLA resilience to heat-induced deactivation 78

Figure 3.6 Solid-phase SnoopLigase immobilisation for cyclised enzyme purification 80

Figure 3.7 SnoopLigase could be cleanly removed from cyclised BLA without dramatic compromise in thermal resilience 82

Figure 3.8 Effect of SnoopLigase removal on thermal resilience of cyclised BLA 83

Figure 3.9 Structure and function of PhyC, and its construct design for SnoopLigase cyclisation 84

Figure 3.10 SnoopLigase efficiently cyclised SnoopTagJr-PhyC-DogTag..... 87

Figure 3.11 SnoopLigase cyclization increased the solubility of PhyC ..... **Error! Bookmark not defined.**

Figure 3.12 SnoopLigase cyclisation improved thermal resilience of PhyC..... 90

Figure 3.13 Effect of SnoopLigase depletion on cyclised PhyC. 93

Figure 3.14 SnoopLigase cyclisation was superior to SpyRing in conferring thermal resilience to PhyC..... 94

Figure 3.15 Thermal resilience conferred by SnoopLigase cyclisation is more robust during heating with BSA 97

Figure 3.16 Thermal resilience conferred by SnoopLigase cyclisation is robust during heating in DCL.. 99

Figure 4.1 Distance between termini of AppA..... 106

Figure 4.2 Structured linker candidates for SnoopLigase cyclisation of AppA... 109

Figure 4.3 Design of AppA construct for SpyRing cyclisation 111

Figure 4.4 SpyRing cyclisation is insufficient to confer thermal resilience to AppA 113

Figure 4.5 C-terminal linker placement for SpyRing cyclisation of AppA is superior for thermal resilience. 115

Figure 4.6 SpyRing cyclisation with L9 linker is most effective at improving AppA thermal resilience 117

Figure 4.7 L9-appended SpyRing cyclisation does not improve AppA thermal resilience in dialysed cleared lysate. 118

Figure 4.8 SnoopLigase cyclises SnoopTagJr-AppA-L9-DogTag..... 120

Figure 4.9 SnoopLigase cyclisation with L9 linker improved AppA resilience to heat-induced aggregation..... 122

Figure 4.10 SnoopLigase-cyclised SnoopTagJr-AppA-L9-DogTag is thermally resilient..... 123

Figure 4.11 SnoopLigase-cyclised SnoopTagJr-AppA-L9-DogTag is not thermally resilient in cleared lysate 124

Figure 4.12 SnoopLigase association with cyclised SnoopTagJr-AppA-L9-DogTag is required for thermal resilience..... 125

Figure 4.13 Quantum Blue is more thermally resilient than AppA 128

Figure 4.14 SnoopLigase cyclises SnoopTagJr-QB-L9-DogTag 129

Figure 4.15 SnoopLigase cyclisation with the L9 linker improves the thermal resilience of Quantum Blue 130

Figure 4.16 SnoopLigase-cyclised SnoopTagJr-QB-L9-DogTag is not thermally resilient in cleared lysate 132

Figure 4.17 SnoopLigase cyclisation is ineffective at improving the thermal resilience of QB even at lower concentrations of cleared lysate..... 133

Figure 4.18 SnoopLigase depletion following cyclisation compromises the thermal resilience of Quantum Blue 135

Figure 4.19 Titration of SnoopLigase into SnoopLigase-depleted cyclised SnoopTagJr-QB-L9-DogTag restores improvements in thermal resilience 137

Figure 4.20 SnoopLigase cyclisation of SnoopTagJr-QB-L9-DogTag at varying molar ratios..... 139

Figure 4.21 SnoopLigase cyclisation of SnoopTagJr-QB-L9-DogTag at varying molar ratios with no glycerol 142

Chapter 1: Introduction

1.1 Thermal Stabilisation of Enzymes

Enzymes are critical in maintaining metabolic processes and biological pathways since these processes rely on enzymatic catalysis to progress reactions at rates amenable to the sustenance of cellular function (Copeland, 2013). Due to their high degree of utility, enzymes have been exploited for a diverse range of applications. Today, biotechnology is a prominent field partly due to a greater understanding of enzymes (Li et al., 2012). The industrial enzyme market was valued at $4.2 billion in 2014 and is dominated by hydrolytic enzymes including carbohydrases, proteases and lipases (Li et al., 2012; Singh et al., 2016).

Enzymes are well-suited for industrial use because they often show high selectivity, high efficiency, and low environmental toxicity (Chapman et al., 2018). These qualities translate into economic savings in the form of reduced operating costs and processing time (Chapman et al., 2018; Marrs et al., 1999; Singh et al., 2016). As a result, enzymes have become pervasive in areas including the detergent, food, cosmetics, textiles, pharmaceutical and agricultural industries (Chapman et al., 2018; Silva et al., 2018).

Despite their utility, many enzymes cannot be directly used for industrial applications due to their instability (Choi et al., 2015). To achieve the required level of stability, enzymes may need to be engineered to withstand various industrial conditions including high temperature, varying pH, high salt concentrations, co-solvents, surfactants or shearing forces (Bommarius and Paye, 2013; Silva et al.,

2018). Furthermore, the stabilised catalysts must be amenable to large-scale production at high yields at low cost to be commercially viable (Choi et al., 2015).

Of the challenges posed to industrial enzymes, the most common and problematic is thermal denaturation. Many industrial applications include exposure to high temperatures, such as textile desizing (removal of template size fabric from woven textiles), which is conducted between 80 and 90 °C (Iyer and Ananthanarayan, 2008; Silva et al., 2018). Some industrially important enzymatic processes are also run at higher temperatures for cost effectiveness, due to faster rates of processing and reduced diffusional limitations (Iyer and Ananthanarayan, 2008; Klibanov, 1983). Examples of biocatalysis at higher temperatures include cellulase hydrolysis of cellulose at 65 ~ 70 °C (Bilen and Bakir, 1998), washing with protease detergents at 60 °C (Schmid, 1979) and α-amylase hydrolysis of starch at 85 ~ 110 °C (Iyer and Ananthanarayan, 2008; Klibanov, 1983). Furthermore, high temperature treatment is widely used in the pharmaceutical, food, and animal feed industries to curb bacterial contamination (Iyer and Ananthanarayan, 2008).

Many approaches have been trialled with varying degrees of success to stabilise enzymes against thermal denaturation for industrial application. The following sections will discuss the advantages and shortcomings of the best-studied strategies for enzyme thermal stabilisation.

1.1.1 Mutagenesis Using Rational Design

Rational design involves making modifications to the protein structure using available structural, biochemical and phylogenetic data (Rigoldi et al., 2018). Mutations introduced by rational design are more likely to produce the desired

effects than those introduced in directed evolution, thereby reducing the number of mutants requiring screening (Steiner and Schwab, 2012). However, the efficacy of rational design methods are limited by the availability of structural data, the unreliability of predictive computational tools and the incomplete current understanding of enzyme folding and dynamics (Rigoldi et al., 2018; Rosenfeld et al., 2016). Furthermore, each enzyme for stabilisation requires manual engineering and screening, which makes rational design an ineffective foundation for a generic, modular approach for enzyme stabilisation (Korendovych, 2018; Nixon and Firestine, 2000).

A common method in rational design is engineering novel disulfide bonds into proteins (Dombkowski et al., 2014). Disulfide bonds contribute to thermodynamic stability by placing constraints on the flexibility of the protein to reduce the conformational entropy of the unfolded state (Dombkowski et al., 2014; Pace et al., 1988). Furthermore, disulfide bonds inserted in aggregation-prone regions inhibit the dysfunctional association of proteins to reduce irreversible denaturation of enzymes (Sanchez-Romero et al., 2013).

The introduction of disulfide bonds has been shown to stabilise a range of enzymes, including acetylcholinesterase, α-amylase, phytase and β-lactamase (Liu et al., 2016; Sanchez-Romero et al., 2013; Sauer et al., 1986; Siadat et al., 2006; Siddiqui et al., 2005; Zavodszky et al., 2001). Computational tools to assist in the placement of disulfide bridges have also been developed, including Disulfide by Design 2.0 (DbD2) and the FRESCO algorithm in YASARA (Korendovych, 2018).

Another rational design strategy that works to stabilise proteins similarly by increasing protein rigidity is the introduction of salt bridges. Salt bridges are greatly

enriched in enzymes found in hyperthermophiles when compared to their mesophilic counterparts, and are therefore posited to play an important role in enzyme stability at high temperatures (Kumar, Tsai, Ma, & Nussinov, 2000). However, the contribution of salt bridges to protein thermostability has been contested since salt bridges have been shown to destabilise other proteins (Jelesarov and Karshikoff, 2009; Phelan et al., 2002).

While salt bridges have been reported to destabilise proteins at room temperature due to the desolvation penalty incurred, this energy penalty has been shown to be reduced at high temperatures (Sheinerman et al., 2000). This reduction allows for the stability gain through salt bridge formation to outweigh such penalties, accounting for the efficacy of salt bridge stabilisation at high temperatures (Elcock, 1998; Sadeghi et al., 2006). Salt bridges have been further demonstrated to be stabilising for enzymes, including carboxylesterases, lipases, aqualysin and phytase (Charbonneau and Beauregard, 2013; Jermutus et al., 2001; Sakaguchi et al., 2014).

Other rational design approaches include the improving the packing of hydrophobic cores and the introduction of surface hydrogen bonds (Borgo and Havranek, 2012; Rigoldi et al., 2018; Zhang et al., 2007). Tight packing of hydrophobic cores is a key step in globular protein folding and contributes to overall stability (Farber and Mittermaier, 2008). Like disulfide and salt bridges, surface hydrogen bonds serve to increase the protein rigidity to improve stability (Rigoldi et al., 2018).

In the case of flexible protein loops such as beta turns, proline substitutions have been shown to increase stability by reducing the entropy of the denatured

state (Fu et al., 2009). Since the φ-angle of proline is fixed at around –65°, proline substitutions stabilise protein loops by reducing their conformational entropy (Morris et al., 1992; Trevino et al., 2007). This approach has been used to confer thermal stability to enzymes such as the proteinase K-like serine protease VPR (Óskarsson et al., 2020).

A rational design approach that relies more heavily on sequence data is the sequence consensus method, in which phylogenetic analysis and sequence alignments with homologues are used to guide protein modifications (Rigoldi et al., 2018). The sequence consensus method has been used to construct thermally stabilised enzymes including subtilisin BPN' and phytase by identifying conserved consensus residues that play key roles in stabilisation (Lehmann and Wyss, 2001; Lehmann et al., 2000; Pantoliano et al., 1989).

The sequence consensus approach can further be used to extrapolate ancestral protein sequences using methods such as ancestral sequence reconstruction (ASR) and reconstructing evolutionary adaptive paths (REAP) (Cox and Gaucher, 2014; Okafor et al., 2018). Reconstructed ancestral proteins have been shown to be more thermostable since the environmental temperatures in some regions on Earth were approximately 30 °C hotter around 3.5 billion years ago (Gaucher et al., 2008). Examples include reconstructed Precambrian β-lactamases from 2 ~ 3 billion years ago, which denature ~35 °C above modern mesophilic counterparts (Risso et al., 2013). Such thermostable ancestral proteins can be used to identify mutations that confer thermostability to facilitate rational design. This approach has been used to thermally stabilise β-amylase and 3-isopropylmalate dehydrogenase using ancestral mutations (Watanabe et al., 2006; Yamashiro et al., 2010).

Due to recent technological developments, more computational tools are being developed to better predict the effect of mutations on proteins. These tools include FoldX (Buß et al., 2018), Rosetta (Kellogg et al., 2011), FRESCO (Wijma et al., 2018), ERIS (Yin et al., 2007), HoTMuSiC (Pucci et al., 2016), FireProt (Bednar et al., 2015), PROSS (Goldenzweig et al., 2016) and CUPSAT (Parthiban et al., 2006). As a result, the success rate of computational predictions has greatly increased, only necessitating the experimental characterisation of a few variants (Dou et al., 2018; Marcos et al., 2018).

The latest technological development in protein folding predictions stems from artificial intelligence and deep neural networks, such as those employed in AlphaGo and AlphaGo Zero (Silver et al., 2016). The success of AlphaGo demonstrated the utility of artificial intelligence algorithms in intelligent probing of vast search spaces, which is required for protein structural predictions (Senior et al., 2019). As described by Levinthal's paradox, it would take longer than the age of the universe for a protein to go through all its possible conformations before arriving at its true structure (Levinthal, 1969).

AlphaFold is a protein structure prediction algorithm produced by DeepMind (developers of AlphaGo) that uses deep neural networks to predict pairwise distances and backbone torsion angles between amino acid residues to produce a potential of mean force for each protein (Senior et al., 2020). The generated potential is optimised using a gradient descent algorithm in which small, incremental improvements are made in iterations (Senior et al., 2020). AlphaFold was ranked first place in the 13th Critical Assessment of Techniques for Protein Structure Prediction (CASP13) and produced the most accurate prediction for 24

of 43 proteins, while the second place system was most accurate only for 3 predictions (Senior et al., 2019, 2020).

1.1.2 Directed Evolution

Directed evolution is a three-step process constituting of mutagenesis followed by selection of variants with desired parameters, after which the improved variants are characterised (Figure 1.1) (Nannemann et al., 2011). This approach recreates evolution within a shorter timeframe and is versatile, since it can be used to select for a range of desired traits (organic solvent tolerance, enzyme kinetic parameters, thermostability etc.) through the application of varying selection pressures (Wang et al., 2012). Since thermostability is a desired trait for most industrially relevant enzymes, high temperatures are often used as selection pressure in directed evolution.

The first step of directed evolution is the creation of a mutagenised library that optimally samples the extensive sequence space (Packer and Liu, 2015). A range of genetic diversification techniques have been developed to increase the rate of mutation and better generate libraries of gene variants. Many approaches for gene mutagenesis are available, including site-directed saturation mutagenesis (Miyazaki and Arnold, 1999), DNA shuffling (Stemmer, 1994), OmniChange (Dennig et al., 2011) and transposon-based techniques (Baldwin et al., 2008).

A conventional technique is error-prone PCR (epPCR), which involves the reducing the fidelity of DNA polymerases such as *Taq* polymerase by adding Mn^{2+} or altering dNTP ratios (Arnold and Geurgiou, 2014; Fromant et al., 1995). However, such epPCR methods exhibit mutational biases that prefer mutagenesis at A:T

base pairs and often favour conservative amino acid substitutions (Lin-Goerke et al., 1997; Shivange et al., 2009). The use of mixtures of different polymerases under varied dNTP concentrations has been shown to minimise mutational biases to produce unbiased, balanced libraries (Vanhercke et al., 2005).

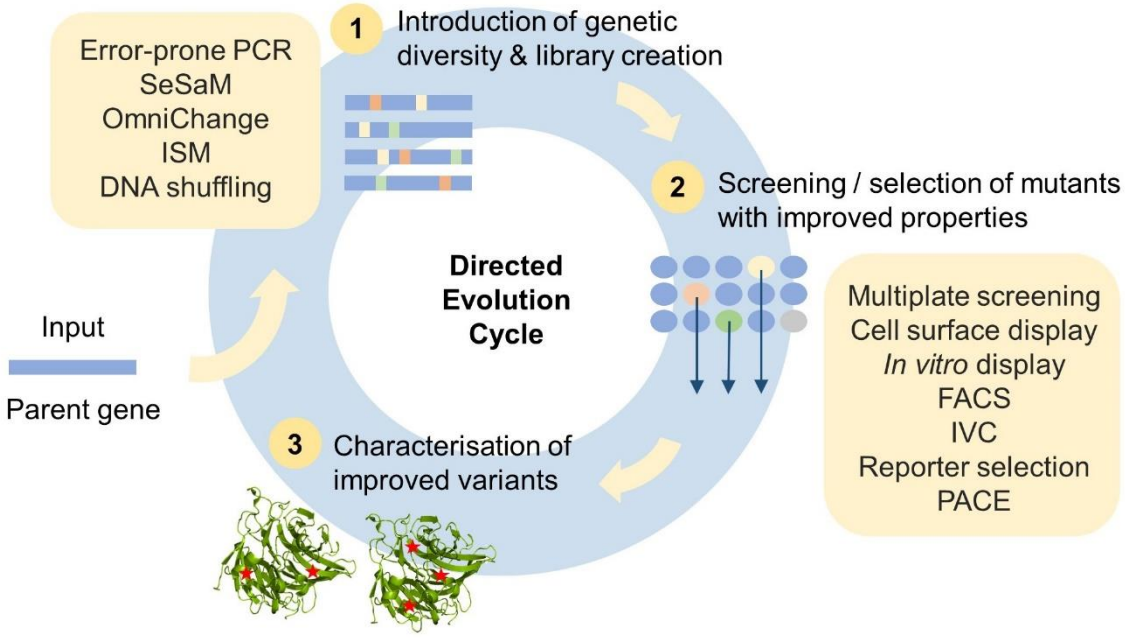

Figure 1.1 Schematic of the typical directed evolution cycle. In directed evolution, a library of variants is created through the introduction of genetic diversity. The genes are expressed into proteins, which are evaluated through screening or selection methods. The resulting variants are subsequently characterised and tested for the desired properties.

A technique that circumvents polymerase-induced mutational bias in library creation is sequence saturation mutagenesis (SeSaM) (Seng Wong et al., 2004).

In SeSAM, single-stranded DNA of random lengths is created, tailed with a nucleotide analogue, and elongated to the full gene length before the incorporated analogues are replaced with standard nucleotides (Seng Wong et al., 2004).

Iterative saturation mutagenesis (ISM) is a technique that allows for more systematic mutagenesis within defined segments of the protein sequence (Acevedo-Rocha et al., 2014). Depending on the protein properties desired, regions of interest are identified and are systematically mutated using methods such as the combinatorial active-site saturation test (CAST) and B-factor iterative test (B-FIT) (Reetz et al., 2005, 2006). ISM of the residues with the highest B-factors was shown to be effective at increasing thermostability, and improved the half-life of the *Bacillus subtilis* lipase at 55 °C from 2 minutes to 980 minutes (Reetz et al., 2006).

Following mutagenesis and the application of selection pressure, the mutants must be screened to select for variants with improvements in desired traits. This step poses the greatest challenge in directed evolution since effective, high-throughput selection and screening methods are scarce, especially in the identification of thermostable enzyme variants. Screening methods evaluate the phenotype of every variant, whereas selection enables the physical sorting of variants with improved properties to circumvent the examination of all mutants (Packer and Liu, 2015).

High-throughput methods for variant screening include the use of colorimetric or fluorometric assays conducted on microtiter plates, fluorescence-activated cell sorting (FACS), cell surface display (bacteria, yeast and mammalian cells), and *in vitro* compartmentalisation (IVC) (Xiao et al., 2015). High-throughput

selection methods include cell-surface display, phage display, SNAP display, mRNA display, reporter-based selection, and phage-assisted continuous evolution (PACE) (Xiao et al., 2015).

Cell-based methods are mostly unavailable for the selection or screening of thermostable variants since they are unequipped to survive incubation at high temperatures during the application of selection pressure. As a result, libraries are commonly screened for thermostability by expressing the enzyme variants, directly heating the expressed library or cell crude extracts and using the heated samples to conduct enzyme activity assays in microtiter plates (Brissos et al., 2014; Madan and Mishra, 2014; Trevizano et al., 2012). Differential scanning fluorimetry has also been used to screen for thermostability (Magnusson et al., 2019; Niesen et al., 2007).

Despite the advances in high-throughput screening and selection methods available, the effective identification of catalytically efficient and thermostable enzyme variants remains challenging. Directed evolution remains a laborious process that needs to be repeated for every enzyme requiring stabilisation. Nevertheless, directed evolution has successfully improved the thermostability of many enzymes (Ruller et al., 2014; Song et al., 2012).

1.1.3 Immobilisation

The immobilisation of soluble enzymes is an effective generic approach for improving enzyme properties prior to industrial application. Immobilisation not only improves enzyme functionality in comparison to soluble enzyme counterparts, but also provides a means to remove and recycle catalysts (Mateo et al., 2007). The

ability to remove catalysts from the reaction media provides control over the enzyme-substrate interactions, and enzyme recycling enables the production of many batches of product using a single set of immobilised catalyst, making it economically efficient (Figure 1.2b) (Basso and Serban, 2019; Mateo et al., 2007).

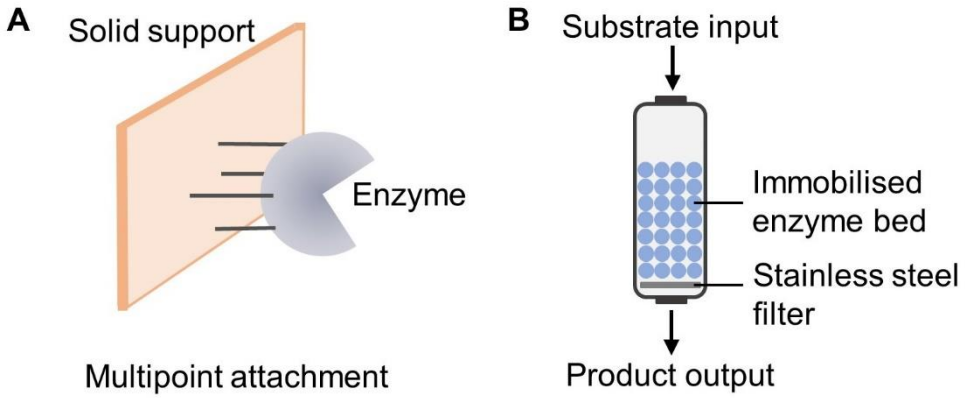

Figure 1.2 Multipoint attachment immobilisation and recycling of immobilised enzymes. a) Enzymes are covalently anchored to solid supports at multiple locations in multipoint attachment. b) Fixed bed reactor for the industrial use of immobilised enzymes. Liquid substrate flows into the packed column bed of immobilised enzyme and product is pumped out. Immobilised enzyme is retained through a stainless-steel mesh filter at the bottom of the reactor and is recycled for many batches.

Immobilisation has become established as an effective method in engineering enzymes for industrial applications, and many examples highlight its utility and efficacy. Immobilised glucose isomerase (IGI) is the most commonly

used form of glucose isomerase in all commercial applications (production of sweeteners for consumption through the conversion of D-glucose to D-fructose), and is the paradigm of success of immobilised catalyst products (DiCosimo et al., 2013). Immobilised penicillin amidase has been used to generate 6-amino penicillanic acid for the production of semisynthetic penicillin antibiotics (Katchalski-Katzir, 1993). A rising application of enzyme immobilisation is hydrolysis of pectin. Pectin produces unwanted thickness and solid suspensions in fruit juice preparations, and immobilised pectin lyase is used to yield a greater degree of liquefaction (DiCosimo et al., 2013).

A critical advantage of immobilisation by covalent multipoint attachment lies in the observed increase in enzyme stability; the multiple attachment points used in immobilisation act as reference points for protein refolding and thereby facilitate the recovery of enzymatic activity (Figure 1.2a) (Miranda et al., 2011). This could be because the distances between each enzyme residue used in immobilisation and the solid support remain unchanged during conformational challenges such as those introduced at high temperatures(López-Gallego et al., 2013). Penicillin G acylase immobilised in glyoxyl-agarose was inactivated and subjected to varying strategies for enzyme reactivation, and the study demonstrated that the attachment points guide the enzyme towards the correct protein conformation to recover its activity (Miranda et al., 2011).

Immobilisation is also permissive of co-immobilisation of multiple enzymes on a single support, allowing for an efficient catalytic cascade (Garcia-Galan et al., 2011). After the first catalytic step, the product of the first reaction will already be available in high local concentrations for the second catalytic step, thereby making the kinetics of the catalytic cascade more favourable (Garcia-Galan et al., 2011).

The co-immobilisation of multiple enzymes into multienzymes complexes has also been demonstrated to improve product yield, such as in the case of the covalently assembled mevalonate biosynthesis pathway (Qu et al., 2019). Co-immobilisation is particularly necessary in cases where the product of the first reaction is unstable or too reactive and requires rapid conversion (Garcia-Galan et al., 2011). The co-immobilisation of D-amino acid oxidase (DAAO) with catalase was successful in preventing the inactivation of DAAO by efficient removal of produced hydrogen peroxide, resulting in >80% yield in the conversion of cephalosporin C to 7-aminocephalosporanic acid (Lopez-Gallego et al., 2005).

However, multipoint attachment is not without disadvantages. The cost of the solid support will contribute to the cost of the immobilised enzyme, which can increase the final cost despite a potential decrease in enzyme activity (Garcia-Galan et al., 2011). The immobilisation process itself incurs additional costs, which when scaled up can render enzyme immobilisation economically unviable (DiCosimo et al., 2013). The costs incurred in biocatalyst production become significant in light of large-scale applications. There is therefore a high incentive to employ methods that enable enzyme recycling, the cost of industrial enzymes is relatively low, with prices averaging between $50~500 per kg enzyme protein (DiCosimo et al., 2013). Therefore, the additional cost of the immobilisation process may not be worth the net gain from enzyme recycling, rendering immobilisation redundant (DiCosimo et al., 2013).

1.1.4 CLEAs and CLECs

Cross-linked enzyme aggregates (CLEAs) and cross-linked enzyme crystals (CLECs) offer methods of immobilisation in the absence of a solid support (Figure 1.3). The absence of a support is beneficial in not only lowering the material cost of biocatalyst production, but also improving the volumetric yield (yield per quantity of input materials) and space-time yield (yield per amount of biocatalyst per unit time) yields (Sheldon et al., 2005). Yield improvement is achieved by eliminating a large proportion of non-catalytic mass (90~99% of total catalyst mass), which is usually introduced by the solid support (Sheldon et al., 2005).

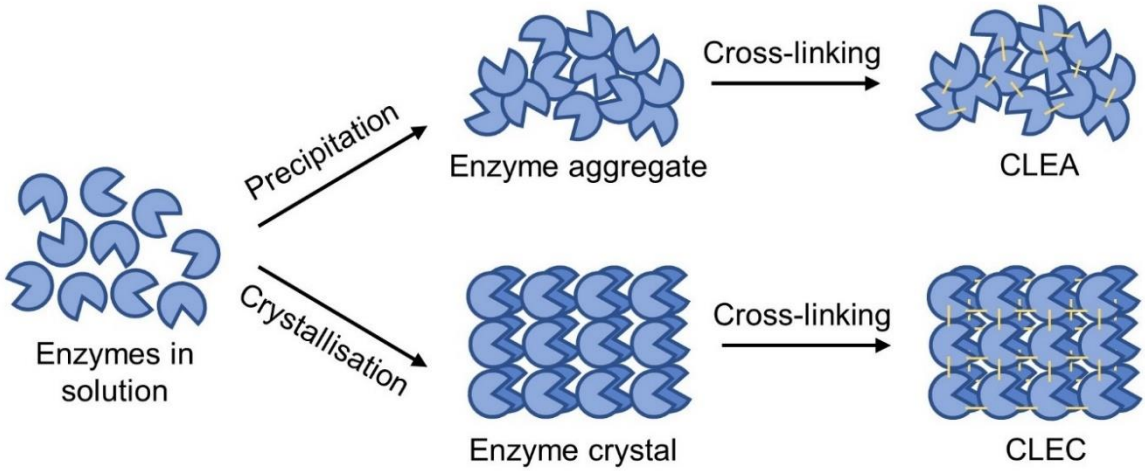

Figure 1.3 Preparation of cross-linked enzyme aggregates and cross-linked enzyme crystals. Enzymes in solution are precipitated to produce aggregates, which are cross-linked to produce CLEAs. Enzymes in solution are crystallised and cross-linked to produce CLECs.

The CLEA method provides an alternative to complex glutaraldehyde cross-linking chemistry and bypasses the need for highly pure enzyme preparations by

combining protein purification and immobilisation into a single process (Sheldon, 2011). CLEA preparation typically results in particles of 5~50 μm diameter with up to 8 million enzyme molecules (Sheldon, 2011; Sheldon et al., 2005). CLEAs also offer additional advantages, including the circumvention of reduced enzymatic activity due to limited diffusion; CLEAs are porous and can therefore overcome reduced activity due to limited diffusion, frequently observed in enzymes immobilised by attachment to solid support (Sheldon, 2011). Furthermore, CLEAs enable effective enzyme recycling, as demonstrated by the R-oxynitrilase CLEA, which was reused 10 times with no significant loss of catalytic activity (van Langen et al., 2005). Nitrile hydratase CLEA was successfully recycled 36 times and exhibited significantly improved operational stability, demonstrating the ease of catalyst removal and recycling offered by the CLEA method (van Pelt et al., 2008).

The CLEA method is also permissive to co-immobilisation of multiple enzymes, enabling the catalysis of multiple reactions with one CLEA aggregate, known as a combi-CLEA. A combi-CLEA of lipase, α-amylase and phospholipase A_2 was prepared from porcine pancreatic acetone powder crude extract and tested for catalytic activity (Dalal et al., 2007). Though the lipase exhibited an increase in thermal stability at 50°C compared to its soluble counterpart, the α-amylase exhibited a significant decrease in the V_{max}/K_m, demonstrating that the combi-CLEA method is not ideal in optimising the catalytic efficiency or stability of all constituent enzymes (Dalal et al., 2007).

CLEA preparation involves many parameters, which may be adjusted to yield optimal enzyme aggregates. The inclusion of bovine serum albumin (BSA) in CLEAs of aminoacylase from *Aspergillus melleus* (10 mg BSA per 100 mg enzyme, denoted CLEA-E-BSA) produced CLEAs that exhibited 82% recovery of catalytic

activity in comparison to 24% recovery in BSA-lacking counterpart CLEAs (denoted CLEA-E) (Dong et al., 2010). Though the improvement in activity recovery was accompanied by an increase in thermostability and the retention of activity after being recycled 10 times, CLEA-E-BSA exhibited a substantial reduction in catalytic activity (k_{cat}/K_m 0.357 to 0.270 mM^{-1} min^{-1}) (Dong et al., 2010). The improvement in CLEAs through BSA addition has been further demonstrated through CLEAs of *Pseudomonas cepacia* lipase; CLEAs prepared with BSA not only exhibited a 12-fold increase in catalytic activity, but also improved operational stability, withstanding over 10 cycles of use with little reduction in residual activity (Shah et al., 2006; Talekar et al., 2013).

Though the CLEA method presents a straightforward method of enzyme immobilisation, the method also presents disadvantages. Firstly, the enzyme aggregates can result in altered selectivity of the enzymes, depending on the conformation of the aggregates (Cao et al., 2000). Secondly, reports on the efficacy of CLEAs in enzyme stabilisation are mixed; though CLEA preparation of certain enzymes improves their catalytic activity, thermostability and activity recovery, some enzymes have not been improved. As a result, it is difficult to predict whether CLEA preparation of an enzyme will yield improvements in all desired areas.

The CLEC method is an alternative to the CLEA method that relies on the initial crystallisation of the enzyme for subsequent crosslinking of the protein microcrystal (Figure 1.3) (Persichetti et al., 1995). When compared to enzymes immobilised through different means, CLECs exhibit greater stability in a wide range of reaction conditions including organic solvents and resilience to proteolytic degradation (Persichetti et al., 1995). Thermolysin CLECs (T-CLECs) demonstrated high operational stability at high temperatures and in organic

solvents, as shown by the retention of T-CLEC catalytic activity through 18 cycles of catalysis at 55 °C in ethyl acetate (Persichetti et al., 1995).

The CLEC method has further been applied to the construction of an amperometric biosensor through the glutaraldehyde and albumin crosslinking of organophosphate hydrolase CLECs (CLEC-OPH) with carbon nanotubes (Laothanachareon et al., 2008). CLEC-OPH demonstrated an increase in catalytic efficiency and a substantial improvement in thermostability compared to the crude enzyme (Laothanachareon et al., 2008). While native organophosphate hydrolase was thermally inactivated from 50 °C, CLEC-OPH retained full activity after incubation ~55 °C and was only gradually inactivated following incubation at 60 °C (Laothanachareon et al., 2008).

Though CLEC has been mostly successful in improving enzyme properties, it is dependent on the initial crystallisation of the enzyme. Since enzyme crystallisation is not always possible, especially with larger enzymes, CLECs are not suitable to function as a generic platform for the thermal stabilisation of enzymes.

1.1.5 Protein Supercharging

Protein supercharging, developed in David Liu's laboratory at Harvard University in 2007, refers to the mutation of neutral surface amino acid residues to charged amino acids, while conserving the folded native protein structure and function, to result in a large net charge (Lawrence et al., 2007). A large net charge is associated with resistance to protein aggregation, as illustrated by intrinsically disordered proteins, which are eukaryotic proteins containing disordered, unfolded

domains that are significantly less prone to aggregation than ordered globular proteins (Fink, 2005).

The first instance of protein resilience conferred by supercharging was demonstrated on green fluorescent protein (GFP), which has a wild-type net charge of -8 and irreversibly aggregates (and therefore loses fluorescence) following heating at 100°C and exposure to 40% trifluoroethanol (TFE) (Lawrence et al., 2007). Exposed surface residues were selected from the crystal structure and mutated to generate supercharged variants with net charges of +36 and -30. The resulting supercharged GFP variants retained solubility and recovered up to 62% fluorescence after incubation at 100 °C or exposure to 40% TFE (Lawrence et al., 2007). The supercharged GFP molecules were also able to associate with and bind macromolecules with the opposite charge, described as “molecular Velcro” – positively (net charge +36) and negatively supercharged (net charge -30) GFP co-precipitated and fluoresced green (Lawrence et al., 2007).

The Liu laboratory has exploited the ability of supercharged GFP to associate with oppositely charged macromolecules to employ positively supercharged GFP in mammalian cell penetration (Mcnaughton et al., 2009). Using Rosetta calculations to select surface mutations, Rosetta-supercharged GFP variants (RscG) ranging from net charges of -11 to -61 and +7 to +58 were created and tested (Der et al., 2013). The study found that RscGs of low and mid-levels of net charge (up to -30 and up to +37) were mostly correctly folded and expressed at high levels, whereas RscGs of high net charges did not express well and exhibited significant levels of unfolding (Der et al., 2013). This showed that protein supercharging is an effective method of increasing refolding yield and protein

solubility, but there is a limit to the mutational load that proteins can withstand (Der et al., 2013).

Supercharging has also been successfully applied to the human recombinant enteropeptidase light chain (hEPL), whose application has been limited by its low solubility (Simeonov et al., 2011). Supercharging of the hEPL surface resulted in an increase in solubility of over 100-fold, an increase in refolding yield of 50%, and an increase in thermal stability (Simeonov et al., 2011). This demonstrates that supercharging can be effective in imparting increased resilience to biotechnologically relevant proteins.

1.1.6 Molecular Chaperones and Thermophilic Protein Fusion

Molecular chaperones increase the stability of the protein of interest to impart resilience, solubility and resistance to aggregation. Chemical chaperones have been used to stabilise various enzymes, such as the *Torpedo californica* acetylcholinesterase (Millard et al., 2003). The addition of a range of osmolytes (low-molecular weight solutes that are used to maintain high osmolality in cells during water stress) was shown to stabilise the enzyme through shifting the equilibrium between native and inactivated enzyme states towards the native form (Millard et al., 2003). Osmolytes were also employed as chemical chaperones for yeast alcohol dehydrogenase (YADH), and the coexistence of YADH with stabilising chaperones was shown to increase the productivity of biocatalysis (Miyawaki et al., 2008).

The study also found that while many osmolytes enhance protein stability, certain solutes serve to destabilise the enzyme; sarcosine and ribose were shown

to decrease the thermodynamic and kinetic stability of YADH (Miyawaki et al., 2008). These results show that while chemical chaperones offer a simple route for achieving moderate increases in thermal stability, it is not always possible to ensure that such solutes are present at their effective concentrations in bioreactors. Industrial bioreactors contain reaction media with numerous ingredients, often with multiple proteins, and the presence of certain solutes may not be optimal for all macromolecules involved.

In addition to chemical chaperones, protein chaperones also offer stabilisation by facilitating the correct folding of proteins. Chaperone proteins are well-documented, with the best studied being the GroEL/GroES and DnaK proteins, which are heat shock proteins often found in prokaryotes (Kohda et al., 1996). Co-expression of proteins with GroEL and GroES increased the recovered activity of the yeast alcohol dehydrogenase from 55% to 90%, and further enabled soluble scFv (single chain antibody protein) recovery from the soluble fraction despite the formation of inclusion bodies (Kohda et al., 1996).

Protein fusions to chaperone proteins have also been tested, such as in the case of the penicillin amidase-rTHS (single-subunit Group II chaperonin from *Methanocaldococcus jannaschii*) enzyme-chaperone chimera (Bergeron et al., 2009). In this chimera, the penicillin amidase and rTHS were connected by an optimised linker, and the chimera demonstrated a rate of turnover 2.8-fold greater than enzymes lacking the chaperone domain (Bergeron et al., 2009). In addition to aiding enzyme turnover, the rTHS-containing penicillin amidase chimeras remained active for 3 times longer than non-chimeric penicillin amidase in 32% methanol (Bergeron et al., 2009). The study showed that fusion to chaperones aids reversibly unfolded species to refold correctly (Bergeron et al., 2009).

In addition to fusion proteins to chaperones, simply fusing proteins to maltose binding protein (MBP) has been shown to enhance solubility and even impart resilience. Fusion of passenger proteins including GFP, dihydrofolate reductase (DHFR) and tobacco etch virus (TEV) protease to *Escherichia coli* MBP yielded the highest percentage of soluble protein compared to His_6-tagged or His_6-glutathione-S-transferase (GST)-tagged counterparts (Raran-Kurussi and Waugh, 2012). The capacity of MBP to enhance solubility has been documented for MBP from a diverse range of bacteria, from *Pyrococcus furiosus* to *Thermotoga maritima* (Fox et al., 2003). The study found that thermophilic PfuMBP (maltodextrin binding protein from *Pyrococcus furiosus*) is an even more potent solubility enhancer than *E. coli* MBP (Fox et al., 2003).

Following the success of thermophilic protein fusion, enzymes have been also inserted into thermophilic proteins such as PfuMBP to successfully enhance kinetic stability (Kim et al., 2009b). Exoinulinase (EI) was inserted into a loop in PfuMBP such that the PfuMBP serves as a stable scaffold for proper EI folding, and the resulting insertional fusion protein demonstrated similar EI activity to wild-type EI (Kim et al., 2009b). At 37 °C, the inserted PfuMBP-EI protein exhibited significantly greater kinetic stability (Kim et al., 2009b).

This effect was also demonstrated using TEM-1 BLA, which was inserted at various positions throughout PfuMBP and *E. coli* MBP (Pierre et al., 2011). The study showed that the success of insertional fusion depends on the insertion site, since insertion of BLA at some MBP positions eliminated expression, whereas insertion at other MBP positions resulted in an increase in kinetic stability (Pierre et al., 2011).

1.1.7 Enzyme Caging

A method of protein stabilisation that builds on the shortcomings of enzyme immobilisation strategies is protein encapsulation. Butyrylcholinesterase encapsulated during the precipitation of biosilica from the diatom *Cylindrotheca fusiformis* was immobilised with 90% efficiency (Luckarift et al., 2004). The biosilica-immobilised butyrylcholinesterase retained 100% catalytic activity at 25 °C after 30 days and after 1 hour at 65 °C, whereas the free enzymes were 85% denatured after 1 hour at 65 °C (Luckarift et al., 2004). The biosilica immobilisation was successfully applied to a “mini-reactor” system in which the immobilised butyrylcholinesterase was continually re-used for 1,000+ column volumes (1 column volume of 500 mL) with no significant reductions in enzyme activity (Luckarift et al., 2004). The biosilica method of enzyme immobilisation confers advantages over the more commonly employed protocols of sol-gel composite and mesoporous silica encapsulation, since the synthesis of such materials requires harsh chemical treatments that may denature the enzymes for encapsulation (Luckarift et al., 2004).

Other improvements have been made to pre-existing methods of silica entrapment of enzymes, such as through the addition of palladium nanoparticles (PdNPs), which serve to impart conductivity and hydrophilicity to carbon-silica foam for enzyme entrapment (Wu et al., 2008b). The resulting PdNP-doped mesocellular carbon-silicate nanocage was used to successfully entrap glucose oxidase and improve its catalytic efficiency to produce a highly sensitive biosensor with a 130-fold improvement in amperometric response compared to free glucose oxidase in solution (Wu et al., 2008b).

In addition to silica-based materials, other materials have been used to create nanocages for enzyme entrapment, including DNA. Glucose oxidase and horseradish peroxidase (HRP) were encapsulated as a pair (GOx ~10 nm and HRP ~5 nm) in DNA nanocages, and the caged enzymes were ~8 times more active than their free counterparts due to the imposed proximity of the enzymes and the high charge density of DNA helices within the nanocage environment (Zhao et al., 2016). Furthermore, the DNA-encapsulated enzymes exhibited resistance to trypsin digestion, whereas free GOx and HRP only retained 50% initial activity (Zhao et al., 2016). Besides DNA, proteins have also been used to build nanocages for enzyme immobilisation, such as the CCMV (cowpea chlorotic mottle virus) capsid caging of *Candida antarctica* lipase B (CalB) (Schoonen et al., 2016).

1.2 Head-to-Tail Cyclisation for Enzyme Stabilisation

Head-to-tail enzyme cyclisation stabilises proteins through joining the N- and C- termini with a peptide bond. In doing so, the peptide bond imbues structure to previously flexible termini to reduce their spatial heterogeneity and thereby reduce the entropy of the unfolded protein to stabilise the native three-dimensional conformation (Borra and Camarero, 2013; Clark and Craik, 2010). Cyclisation-mediated rigidification of the enzyme backbone can not only positively impact catalytic activity and stability, but also protect against exoproteolytic degradation (Borra and Camarero, 2013).

Improving thermal stability through cyclisation circumvents the mutagenesis and evolution steps required to stabilise each enzyme in rational design and

directed evolution approaches. The following subsections will discuss the various strategies for enzyme head-to-tail cyclisation.

1.2.1 Intein

Intein-mediated cyclisation, also known as intein-mediated protein trans-splicing (PTS), was first demonstrated in *E. coli* DHFR (Scott et al., 1999). Inteins (*int*ernal prot*eins*) are proteins that catalyse post-translational modifications such that they are excised from the precursor protein and the flanking regions are ligated (Perler et al., 1997). Using the DnaE split intein from *Synechocystis* sp. PCC6803, cyclised DHFR or cyclic pseudostellarin F (acid tyrosinase inhibitor) were produced (Scott et al., 1999). Like carbodiimide-cyclised bovine pancreatic trypsin inhibitor (BPTI), the cyclised DHFR also demonstrated greater electrophoretic mobility (cyclised DHFR: 21 kDa, linear DHFR: 23 kDa), resilience to proteolytic degradation, and thermal resilience following incubation at 65°C than its linear counterpart (Scott et al., 1999).

Intein-mediated cyclisation has been successfully applied to other enzymes, including *E. coli* DNA helicase (DnaB-N), which was cyclised using the same DnaE split intein from *Synechocystis* (Williams et al.). Cyclisation stabilised the DnaB-N native conformation with a free energy of 2 kcal mol^{-1} through reducing the entropy of the unfolded conformation, manifesting as an increase in T_m of 15°C (Williams et al.). Cyclised *E. coli* glucose transporter, IIA^{Glc} not only retained 100% glucose phosphotransferase activity in comparison to its linear counterpart, but also exhibited increased inherent thermostability (cyclised IIA^{Glc} T_m: 75°C, linear IIA^{Glc} T_m: 70 °C) (Siebold and Erni, 2002). Cyclised IIA^{Glc} also moved faster through the

gel during SDS-PAGE compared to linear IIA^{Glc}, and exhibited a degree of protection against unfolding by guanidinium chloride (Siebold and Erni, 2002).

The intein method of enzyme cyclisation has also been successfully applied to phytase; intein-cyclised phytase was patented in 2010 in China and is available for purchase (平淑珍 et al., 2010). The patented intein-cyclised phytase retained 65% activity following 1 hour at 65 °C, whereas the wild-type phytase retained 39% activity under the same conditions (平淑珍 et al., 2010). Unlike the wild-type phytase, the intein-cyclised phytase resisted degradation by exopeptidases for 12 hours at 25 °C (平淑珍 et al., 2010).

More recently, intein-mediated cyclisation has been applied to the coxsackievirus B3 (CVB3) capsid protein VP1 to produce a more stable, degradation- and aggregation-resistant cyclised VP1 (C-VP1) for more efficient immunisation against CVB3-induced viral myocarditis and pancreatitis (Qi and Xiong, 2017). C-VP1 immunisation of mice induced stronger humoral (quantified anti-CVB3-specific IgG via ELISA) and cellular (quantified CVB3-specific T cell proliferation) immune responses against viral myocarditis, and C-VP1 exhibited complete resistance to carboxypeptidase Y, unlike its linear counterpart (Qi and Xiong, 2017).

Despite the demonstrated high utility of intein-mediated cyclisation, the method requires the genetic fusion of intein domains to the protein of interest, which can negatively affect protein stability and solubility (Borra and Camarero, 2013; Wood and Camarero, 2014). Furthermore, the intein method yields a mixture of linear and cyclised constructs, which can be difficult to separate (Tarasava and Freisinger, 2014).

1.2.2 Sortase

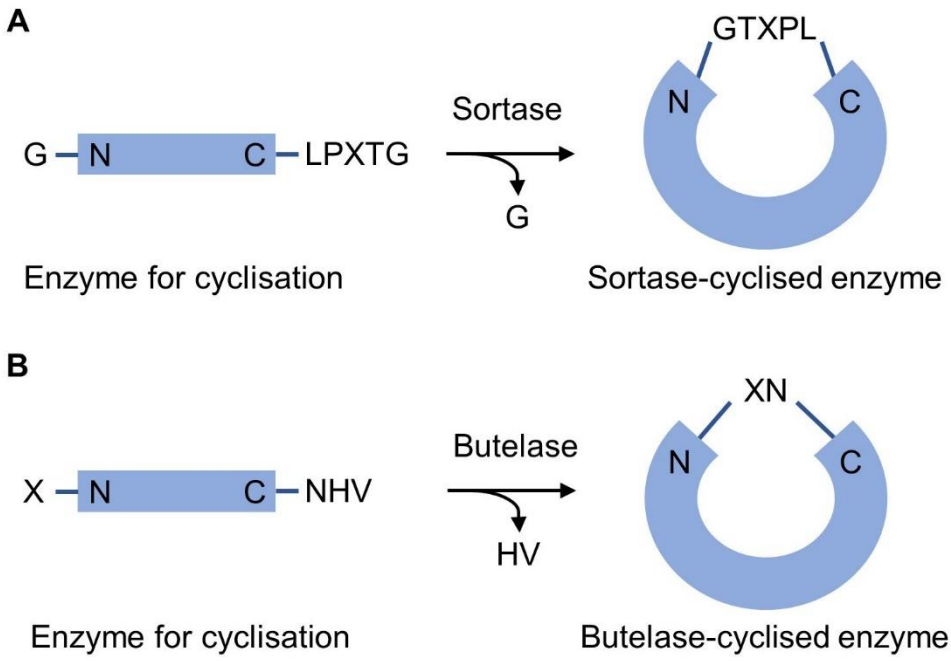

Figure 1.4 Enzyme cyclisation by sortase A or butelase I. a) Sortase A catalyses the transpeptidation between the N-terminal glycine and the C-terminal LPXTG motif. b) Butelase catalyses the transpeptidation between the N-terminus and the C-terminal NHV motif.

Sortase A (SrtA) is a transpeptidase from *Staphylococcus aureus*, which recognises a 5-amino acid C-terminal motif (LPXTGX) to cleave the threonine-glycine peptide bond (Figure 1.4a), and the resulting thioacyl-linked intermediate species is nucleophilically attacked by the N-terminal glycine to form a peptide bond between the C-terminal threonine and the N-terminal glycine (Jia et al., 2014).

Sortase A was successfully used to cyclise disulfide-rich peptide species of special interest due to their therapeutic potential, including kalata B1 and sunflower trypsin inhibitor 1 (SFTI-1) (Jia et al., 2014). Sortase A-mediated cyclisation was

applied to the cytokine human interferon alpha 2 (IFNα2), and the cyclised IFNα2 retained activity even following boiling (in RPMI medium 1640 + 10% heat-inactivated foetal calf serum), demonstrating that sortase cyclisation can dramatically enhance the resilience and half-life of cytokines (Popp et al., 2011). This ability of sortase A to mediate cyclisation of smaller peptides has been exploited recently to produce cyclic oligomers of short (< 15 aa) peptides (Voloshchuk et al., 2017). As the cyclisation reaction progressed (~24 hours), the ratio of cyclised oligomers to linear species increased, showing that sortase A can be used in the production of linear and cyclic oligomers of short peptides (Voloshchuk et al., 2017).

On larger proteins, sortase-mediated cyclisation still occurs at high efficiency, with final yields of over 90% reported for cyclised enhanced GFP (eGFP) and Cre recombinase (Antos et al., 2009a). However, the high yield of sortase cyclisation comes at the cost of time efficiency; sortase A cyclisation reactions typically require incubation periods of over 16 hours (Antos et al., 2009a). Furthermore, sortase A reaction rate is highly variable depending on the substrate (Antos et al., 2009b; Heck et al., 2014).

1.2.3 Butelase

A recent cyclisation strategy that addresses the slow cyclisation rates of intein or sortase-mediated cyclisation involves the use of butelase I (Figure 1.4b). Butelase I is the fastest known ligase with a k_{cat}/K_M of 542,000 M^{-1} s^{-1} and is reported to be capable of cyclising proteins 20,000 times faster than sortase A (Nguyen et al., 2016a, 2016b). Unlike intein and sortase cyclisation reactions,

which commonly take up to 16 hours, butelase-mediated cyclisation takes minutes and has reported yields of ~95 % (Nguyen et al., 2014, 2015).

However, butelase I has only been applied to the cyclisation of peptides and smaller proteins (green fluorescent protein, interleukin-1 receptor antagonist, human growth hormone) and has yet to be tested on larger proteins with greater distances between termini (Nguyen et al., 2015). Similarly to sortase A, butelase I is also limited to intramolecular conjugation between the termini (Nguyen et al., 2016b).

1.3 Cyclisation by Spontaneous Isopeptide Bond-Forming Proteins

Isopeptide bonds are covalent crosslinks that occur between the ε-amino groups of lysine residues and the carboxyl groups of Asn, Asp, Gln or Glu (Asquith et al., 1974). Isopeptide bonds play an important role in protein structure and signal transduction, with many naturally occurring enzymes catalysing isopeptide bond formation. Notable examples include ubiquitin-protein ligases, which catalyse the formation of isopeptide bonds between the C-terminal Gly of ubiquitin and the Lys of the substrate protein (Pickart, 2001). Transglutaminases also catalyse isopeptide bond formation in a calcium-dependent manner to facilitate a wide range of physiological events including wound healing, extracellular matrix stabilisation and cell adhesion (Ahvazi and Steinert, 2003; Odii and Coussons, 2014).

Intramolecular isopeptide bonds contribute to mechanical stability, resistance to proteolytic degradation and stability against thermal and pH stresses

(Alegre-Cebollada et al., 2010; Purkayastha and Kang, 2019). Intramolecular isopeptide bonds were first found in the major pilin protein Spy0128 from *Streptococcus pyogenes* (Kang et al., 2007). Intramolecular isopeptide bonds have since been identified in other Gram-positive surface proteins such as the major pilin GBS52 from *Streptococcus algalactiae* (Cozzi et al., 2015), and RrgB from *Streptococcus pneumoniae* (Paterson and Baker, 2011).

The spontaneous and autocatalytic formation of the intramolecular isopeptide bond is mediated by a reactive triad (Hu et al., 2011). In the *S. pyogenes* pilin subunit Spy0128, the isopeptide bond is formed between the Lys and Asn, catalysed by the autocatalytic Glu residue (Hu et al., 2011). The three residues are all located within the hydrophobic core, which serves to raise the pK_a of the Glu and lower the pK_a of Lys to maintain the residues in their catalytically competent protonation states (Hu et al., 2011). The resulting spontaneous isopeptide bond in Spy0128 confers stability against heat (T_m of 85 °C), pH and mechanical stress (~ 800 pN) (Kang and Baker, 2009, 2011).

1.3.1 SpyRing (SpyTag and SpyCatcher)

Split-protein systems have shown that genetically split proteins can reassemble to reconstitute a functional protein. Examples have included dihydrofolate reductase (Pelletier et al., 1999), β-galactosidase (Rossi et al., 1997), TEM-1 β-lactamase (Galarneau et al., 2002), fluorescent proteins (Zhang et al., 2004) and ubiquitin (Johnsson and Varshavsky, 1994).

Similarly, strategically splitting proteins containing isopeptide bonds such that a reactive residue is located on each protein enabled reconstitution of the

protein and formation of an isopeptide bond upon mixing. The spontaneous intramolecular isopeptide bond-containing Spy0128 domain from *Streptococcus pyogenes* was split into the Isopeptag and Pilin-C system, consisting of a 16 amino acid peptide tag (Isopeptag) and a 32 kDa protein (Pilin-C) (Zakeri and Howarth, 2010). Spy0128 was split such that Isopeptag contained the reactive Asn and Pilin-C contained the reactive Lys and Glu, allowing for isopeptide bond formation upon mixing of the two modules (Zakeri and Howarth, 2010). However, the Isopeptag/Pilin-C system was inefficient, reaching only ~ 60 % yield in 72 hours, and involved the use of a large protein partner (32 kDa).

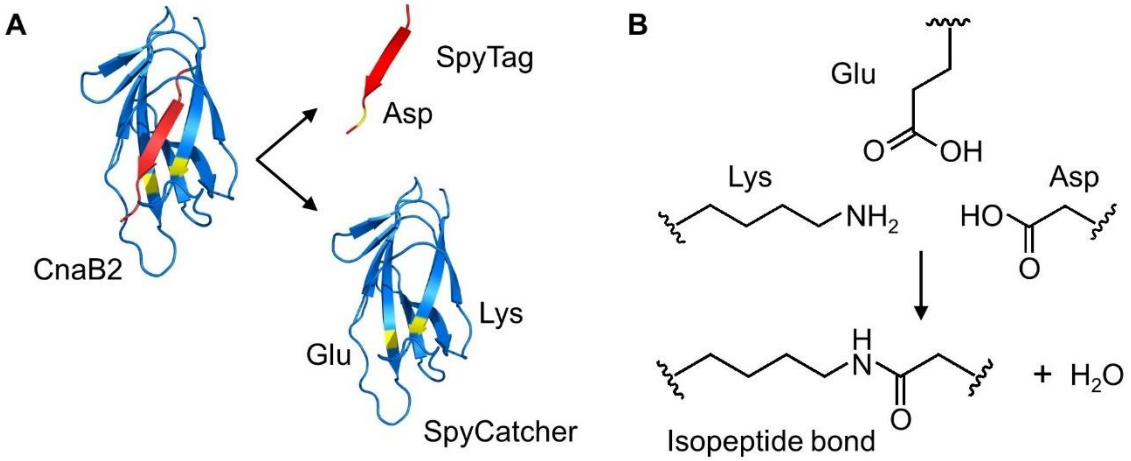

Figure 1.5 Splitting of CnaB2 into SpyTag and SpyCatcher. a) The CnaB2 domain from *Streptococcus pyogenes* (PDB 2X5P) was split to produce spontaneous isopeptide bond-forming protein partners SpyTag and SpyCatcher. The reactive Glu and Lys (shown in yellow) were present on SpyCatcher, with Asp on SpyTag. b) The amidation reaction between the Lys of SpyCatcher and Asp of SpyTag is catalysed by Glu to form an isopeptide bond. A molecule of water is eliminated during the reaction.

To address the shortcomings of the Isopeptag/Pilin-C system, the CnaB2 domain of the fibronectin-binding protein FbaB from *Streptococcus pyogenes* was split to produce SpyTag (13 aa) and SpyCatcher (15 kDa) as shown in Figure 1.5 (Zakeri et al., 2012). SpyTag and SpyCatcher spontaneously associated in a wide range of reaction conditions to form an amide bond between Lys and Asp and was markedly more efficient than the Isopeptag/ Pilin-C system, reaching ~ 80 % yield in 10 min (Zakeri et al., 2012). The peptide bond formed between SpyTag and SpyCatcher exhibited a high degree of mechanical resilience, resisting breakage until >1 nN of applied force (Zakeri et al., 2012).

The SpyTag/ SpyCatcher system has been widely used in a variety of applications including the functionalisation of hydrogels (Sun et al., 2014), decoration of virus-like particles (Brune et al., 2016), whole-cell biocatalysis (Peschke et al., 2017), construction of bispecific antibodies (Yumura et al., 2017), single-molecule DNA sequencing (Stranges et al., 2016) and the construction of multienzyme nanostructures (Liu et al., 2019). Notably, SpyTag and SpyCatcher have also been used in the head-to-tail cyclisation of enzymes to improve thermal resilience in a method denoted SpyRing cyclisation (Schoene, Bennett, & Howarth, 2016; Schoene, Bennett, & Howarth, 2016b; Schoene, Fierer, Bennett, & Howarth, 2014).

1.3.2 SpyRing-Cyclised Enzymes

In SpyRing cyclisation, fusion of SpyTag to the N-terminus and SpyCatcher to the C-terminus results in enzyme cyclisation through peptide bond linkage of the two protein termini (Figure 1.6) (Schoene et al., 2014). SpyRing cyclisation has

been applied to many enzymes and has been shown to be effective at improving thermal resilience of a diverse range of enzymes, ranging in size from 19 ~ 86 kDa and distance between termini of 7 ~ 38 Å (Table 1).

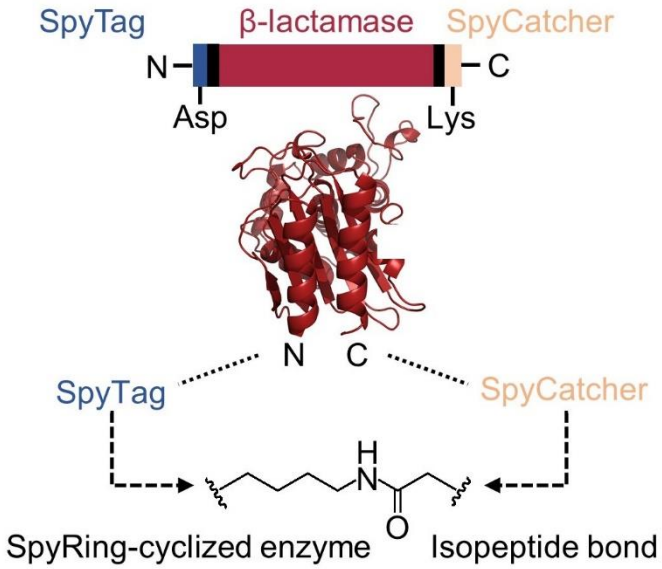

Figure 1.6 SpyRing cyclisation of TEM-1 β-lactamase. The spontaneous isopeptide bond-forming protein partners SpyTag and SpyCatcher were used to cyclise TEM-1 BLA (Schoene et al., 2014). SpyTag was fused to the N-terminus and SpyCatcher to the C-terminus to enable head-to-tail cyclisation.

Such increases in thermal resilience were conferred without compromising the kinetic parameters of the enzyme. In some instances, SpyRing cyclisation even enhanced the substrate affinity and catalytic efficiency of the enzyme, such as in the cases of xylanase and lichenase (Sun et al., 2019; Wang et al., 2016a). SpyRing cyclisation was demonstrated to confer additional benefits including

organic solvent tolerance (Wang et al., 2019a), ion stability (Zhou et al., 2020) and pH stability (Si et al., 2016a).

SpyRing cyclisation was further demonstrated not to interfere with proper folding of the enzyme in structural analyses using circular dichroism (CD). The CD spectra of SpyRing-cyclised and linear enzymes exhibited similar distribution of secondary structures in all cases (Gao et al., 2019; Si et al., 2016a; Sun et al., 2019; Wang et al., 2019b; Zhou et al., 2020). Furthermore, CD analyses showed that SpyRing-cyclised enzymes maintained secondary structures better during heat challenge and subsequent cooling than their linear counterparts, demonstrating the extent of conformational stabilisation imparted by SpyRing cyclisation (Gao et al., 2019; Schoene et al., 2016; Si et al., 2016a; Sun et al., 2019; Wang et al., 2019b; Zhou et al., 2020).

Interestingly, differential scanning calorimetry analyses of SpyRing-cyclised enzymes and their linear counterparts showed relatively small improvements in T_m in comparison to the observed enhancements in thermal resilience. In the case of SpyRing-cyclised BLA, there was little to no increase in T_m compared to the wild-type enzyme, though > 60 °C improvements in thermal resilience to heat-induced aggregation and inactivation could be observed (Schoene et al., 2014). This was also the case for DHFR (Schoene et al., 2014) and phytase (Schoene et al., 2016a).

The relatively small improvements in T_m and the ability of cyclised enzymes to retain secondary structure better during and after heating suggest a mechanism for improving thermal resilience by increasing the reversibility of thermal denaturation (Schoene et al., 2014, 2016a). The SpyTag/ SpyCatcher domain and isopeptide bond function as a reference point and scaffold for refolding of denatured

enzymes, thereby making the denatured state reversible (Schoene et al., 2014, 2016a). This reversibility, in conjunction with rigidification of the protein backbone and reduction in conformational entropy through head-to-tail cyclisation (Borra and Camarero, 2013), account for the major improvements in thermal resilience observed in SpyRing-cyclised enzymes.

Table 1 SpyRing-cyclised enzymes.

Enzyme	Organism of Enzyme origin	PDB ID	Distance between termini*	MW	Improvement in thermal stability/ resilience following SpyRing cyclisation	Reference
Dihydrofolate reductase	*Escherichia coli*	1RX2	15 Å	19 kDa	• Almost all activity and solubility retained after 10 min at 100 °C (negligible activity retained in uncyclised enzyme)	(Schoene *et al.*, 2014)
TEM-1 β-lactamase	*Escherichia coli*	1BTL	7 Å	32 kDa	• Thermal resilience to aggregation/ inactivation improved by >60 °C • Almost all activity and solubility retained after 10 min at 100 °C	(Schoene *et al.*, 2014)
Phytase	*Bacillus subtilis*	3AMR	29 Å	40 kDa	• Retained most solubility after 10 min at 100 °C (uncyclised enzyme mostly aggregated at 75 °C) • Retained most activity after 10 min at 90 °C (uncyclized enzyme mostly inactivated at 75 °C)	(Schoene, Bennett and Howarth, 2016)
Firefly luciferase	*Photinus pyralis*	1BA3	38 Å	61 kDa	• T_m improved from 53 °C to 60.5 °C • Residual activity after 70 min at 45 °C improved from almost 0 % to 17 %	(Si *et al.*, 2016)
Cephalosporin C acylase	*Escherichia coli*	1GM8	10 Å	87 kDa	• Residual activity improved 3.3-fold after 20 min at 50 °C at 0.05 mg/ml protein concentration	(Wang *et al.*, 2020)
Xylanase	*Thermobifida fusca*	3ZSE	22 Å	23 kDa	• Residual activity after 20 min at 90 °C improved from 24 % to 70 %	(Sun *et al.*, 2019)
Xylanase	*Hu sheep fosmid library*	N/A	N/A	54 kDa	• Residual activity after 5 min at 70 °C improved from 29 % to 63 %	(Zhou *et al.*, 2020)
Lichenase	*Bacillus subtilis*	3O5S	12 Å	27 kDa	• 5 °C increase in enzyme optimum temperature • Residual activity after 10 min at 100 °C improved from almost 0 % to >80 %	(Wang *et al.*, 2016)
Trehalose synthase	*Thermomonospora curvata*	N/A	N/A	N/A	• Residual activity after 30 min at 40-50 °C improved from ~60 % to >85 %	(Xu *et al.*, 2018)
L-phenylserine aldolase	*Pseudomonas putida*	1V72	25 Å	39 kDa	• Residual activity after 120 min at 65 °C improved from ~20 % to >70 %	(Wang *et al.*, 2019)
Endo-β-1,4-mannanase	*Bacillus subtilis*	2WHK	6 Å	38 kDa	• Residual activity after 1 h at 60 °C improved from almost 0 % to 67 %	(Gao *et al.*, 2019)

* Distance between termini refer to the last resolved residue. Measured from amine group of N-terminal residue to carboxylate carbon of C-terminal residue

1.3.3 SnoopRing (SnoopTag and SnoopCatcher)

Using the same principle employed in the splitting of the Spy0128 and CnaB2 domains, the C-terminal D4 domain of the pilus-related RrgA adhesin from *Streptococcus pneumoniae* was split and engineered to produce SnoopTag (12 aa) and SnoopCatcher (13 kDa) as illustrated in Figure 1.7 (Veggiani et al., 2016). The C-terminal domain of RrgA was split such that the catalytic Lys was located on SnoopTag (residues 734 – 745) and Glu and Asn on SnoopCatcher (residues 749 – 860) such that an isopeptide bond was formed upon mixing (Veggiani et al., 2016).

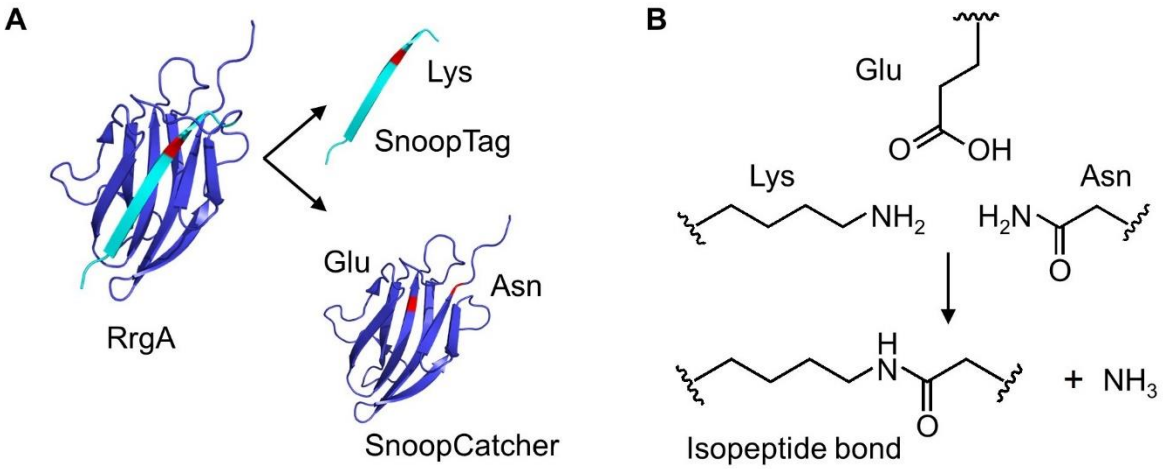

Figure 1.7 Splitting of RrgA C-terminal domain into SnoopTag and SnoopCatcher. a) The C-terminal domain of the RrgA adhesin from *Streptococcus pneumoniae* (PDB 2WW8) was split to produce spontaneous isopeptide bond-forming protein partners SnoopTag and SnoopCatcher. The reactive triad (shown in red) was split, with Lys present on SnoopTag and the reactive Glu and Asn on SnoopCatcher. b) The transamidation reaction between the Lys of SnoopTag and Asn of SnoopCatcher is catalysed by Glu to form an isopeptide bond. A molecule of ammonia is eliminated during the reaction.

SnoopTag and SnoopCatcher were also used to cyclise enzymes through N-terminal fusion of SnoopTag and C-terminal fusion of SnoopCatcher in a method denoted as SnoopRing cyclisation (Schoene et al., 2016a). SnoopRing cyclisation was shown to improve the thermal resilience of BLA to heat-induced aggregation and inactivation despite the slower reaction rate of SnoopTag/SnoopCatcher when compared to SpyTag/ SpyCatcher (Schoene et al., 2016a). Nonetheless, the degree of thermal resilience conferred by SpyRing cyclisation of TEM-1 BLA was demonstrated to be superior than with the SnoopRing (Schoene et al., 2016a).

1.4 SnoopLigase

The C-terminal domain of the RrgA adhesin from *S. pneumoniae* was previously split to yield the bipartite SnoopTag/SnoopCatcher system (Veggiani et al., 2016). However, bipartite tag/ catcher systems require the fusion of the larger catcher protein, which carries the potential to impede protein function. A conjugation system that allows for the ligation of two smaller peptide tags would enable isopeptide bond-locking while circumventing the fusion of larger protein domains.

The RrgA C-terminal domain was split to yield a tripartite system by Can Buldun in the Howarth group, such that the three residues of the reactive triad were placed on different proteins (Buldun et al., 2018). The SnoopLigase tripartite conjugation system was comprised of two peptide tags, SnoopTagJr (12 aa) and DogTag (23 aa), and SnoopLigase (13.3 kDa) as shown in Figure 1.8. The intramolecular isopeptide bond of RrgA is formed between Lys 742 and Asn 854

and is catalysed by the apposed Glu 803. The domain was split such that Lys 742 was placed on SnoopTagJr, Asn 854 on DogTag and Glu 803 on SnoopLigase (Buldun et al., 2018). As a result, SnoopLigase enabled the covalent ligation of SnoopTagJr and DogTag upon mixing.

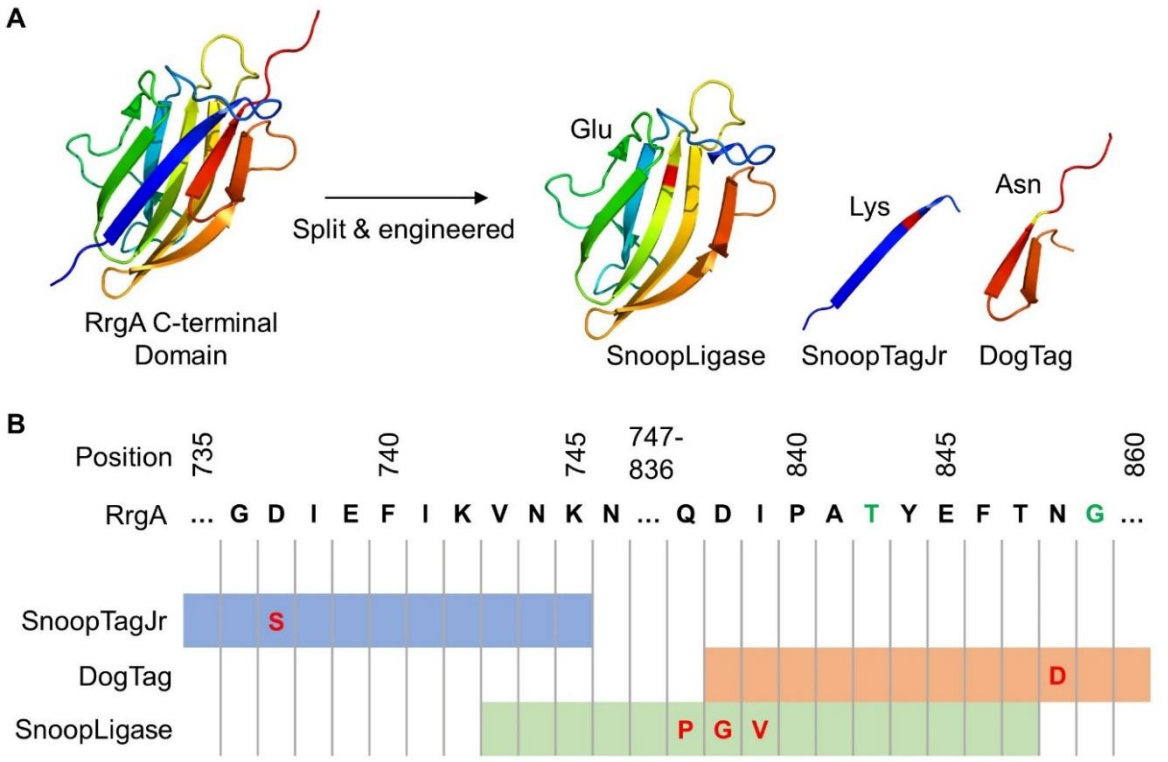

Figure 1.8 Splitting of RrgA into the SnoopLigase conjugation system. a) The C-terminal domain of the RrgA adhesin from *S. pneumoniae* (PDB 2WW8) was split and engineered to produce SnoopLigase, which catalyses the covalent ligation of peptide tags SnoopTagJr and DogTag (Buldun et al., 2018). Each protein component contains a residue from the reactive triad responsible for isopeptide bond formation. b) Sequence alignment of SnoopTagJr, DogTag and SnoopLigase. Green residues indicate point mutations introduced during SnoopCatcher development (Veggiani et al., 2016). Mutations made to each construct are shown in red.

Following splitting, the individual components were further engineered to maximise reactivity and conjugate formation (Buldun et al., 2018). The D737S mutation in SnoopTagJr was introduced since it increased substrate conversion by approximately 60 % compared to wild-type SnoopTag (Buldun et al., 2018). SnoopLigase contains four point mutations (A808P, Q837P, D838G, I839V), which increased the reactivity 66-fold (Buldun et al., 2018). The A808P and Q837P mutations aimed to stabilise the loops using the fixed φ-angle (Buldun et al., 2018; Trevino et al., 2007). The Protein Repair One-Stop Shop (PROSS) algorithm was used to identify stabilising point mutations, of which D838G and I839V were applied to SnoopLigase (Buldun et al., 2018).

Since its development, the SnoopLigase conjugation system has been applied to the modular assembly of vaccines (Andersson et al., 2019). DogTag was fused to the self-assembling nanoparticle IMX313 and could be ligated to SnoopTagJr-fused malarial proteins, demonstrating the utility of SnoopLigase-catalysed peptide-peptide locking in modular vaccine assembly. (Andersson et al., 2019). Furthermore, DogTag can be inserted into protein loops and successfully conjugated by SnoopLigase (Buldun et al., 2018). As a result, the SnoopLigase system shows promise for a range of different applications, including head-to-tail enzyme cyclisation.

1.5 Phytase

Phytase was chosen for cyclisation since it is an industrially and environmentally important enzyme that requires high levels of thermal resilience for

utilisation. Furthermore, phytase was also an enzyme of interest for AB Vista, the industrial partner for this DPhil.

1.5.1 Phytase Significance

Phytic acid (phytate) is the primary form of plant seed phosphate storage and accounts for 60 ~ 70% of total phosphorus in most plant-based matter (Figure 1.9) (Bhavsar and Khire, 2014). However, this phosphorus is indigestible to monogastric animals including poultry, swine and humans (Woyengo and Nyachoti, 2011). As a result, up to 70% of P in animal feed is unutilised and excreted (Jorquera et al., 2008)

In addition to limiting the bioavailability of phosphate, phytic acid also chelates essential cationic dietary minerals including Zn^{2+}, Mg^{2+}, Cu^{2+}, Ca^{2+} and Fe^{2+} through the formation of insoluble complexes (Nunes and Kumar, 2018). Furthermore, phytate has been demonstrated to form complexes with digestive enzymes including trypsin and pepsin to disrupt digestion and limit nutrient uptake (Singh, 2008).

Unlike ruminant animals whose gut rumen flora have endogenous phytases, the endogenous phytases of monogastric organisms (such as broiler chickens) are not sufficiently active (Gessler et al., 2018). Furthermore, broilers are fed a high-calcium diet, which traps phytate in insoluble complexes at non-acidic pH (Sommerfeld et al., 2018). The insoluble calcium-phytate complexes are unavailable for hydrolysis by endogenous chicken phytases, further decreasing P absorption.

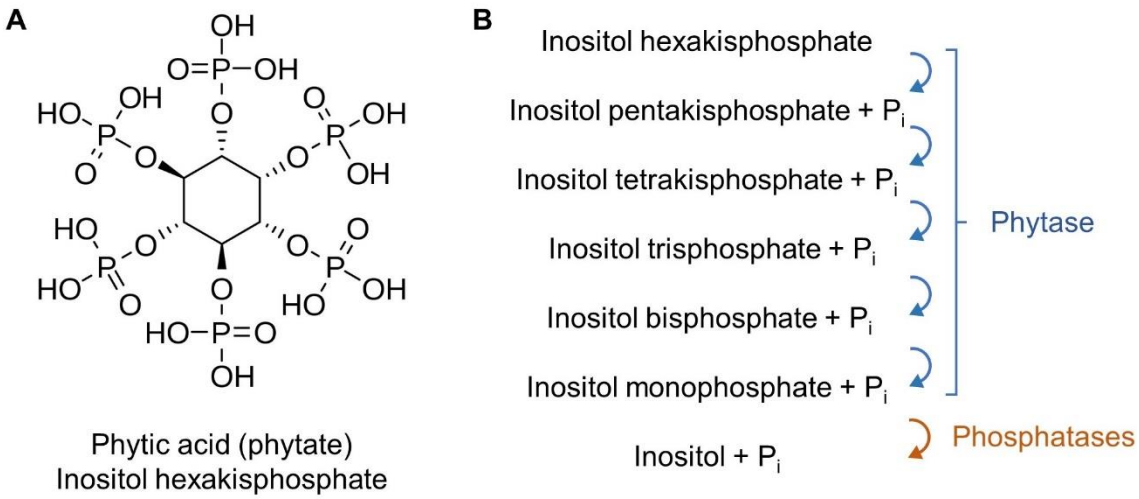

Figure 1.9 Phytic acid and its sequential hydrolysis by phytase. a) Structure of phytic acid. b) Phytic acid is hydrolysed by phytase to release digestible inorganic phosphate in a stepwise manner and each intermediate can exist in many forms. Inositol monophosphate is not a substrate of phytase and requires hydrolysis by other phosphatases.

To facilitate the fulfilment of livestock nutritional requirements, inorganic P is often supplemented into animal feed to combat the indigestibility of phytate. However, P supplementation does not combat the anti-nutrient effects of phytate and is expensive, comprising the third most expensive part of poultry production (Bhavsar and Khire, 2014). Cheaper alternative strategies for P supplementation involve the inclusion of meat and bone meal in animal feed, which incurs the risk of species cross-transfer of diseases including bovine spongiform encephalopathy (Murray, 2011).

Since phytic acid works as an anti-nutrient, it prevents animals from getting the maximal nutritional benefits from animal feed, which is not only economically wasteful and inefficient, but also damaging for the environment. The indigestibility of phytate-bound phosphate leads to a higher concentration of excreted unutilised phosphorus in livestock (Nunes and Kumar, 2018). This results in environmental phosphate pollution and disrupts the phosphorus cycle in nearby ecosystems, causing detrimental phenomena such as eutrophication (Bhavsar and Khire, 2014). In England and Wales, the detrimental effects of eutrophication are estimated to cost up to £114 million each year, including the treatment of drinking water to remove excess nitrogen and the removal of algal toxins (Pretty et al., 2003).

To maximise the nutritional benefits of animal feed and minimise environmental P pollution, animal feed requires supplementation with phytase. Phytases catalyse the sequential hydrolysis of the phosphate groups on phytic acid to release digestible inorganic P and the less phosphorylated inositol intermediates (Figure 1.9b) (Nunes and Kumar, 2018). Phytase supplementation enables the release of phytate-bound P and phytate-complexed minerals to increase the nutritional value of animal feed (Bedford, 2000). Furthermore, phytase renders inorganic P supplementation redundant while maximising the nutritional absorption of animal feed, which translate to significant economic savings (Bedford, 2000; Lee et al., 2017).

A metric that was demonstrated to be improved through phytase superdosing in animal feed was the feed conversion ratio (FCR) (Lee et al., 2017). The FCR measures the efficiency with which animal feed is converted into the mass gained by the animal and is calculated by dividing the mass of the feed input by the mass of the meat output (Lee et al., 2017). Phytase supplementation significantly

improved the FCR and bone content in broiler chickens (Lee et al., 2017). Phytase supplementation also reduced excretion of phosphate by over 50%, thereby preventing environmental phosphate pollution (Konietzny and Greiner, 2004).

Due to the efficacy of phytase supplementation of animal feed, phytase products occupy the largest market share of the animal feed enzymes market, which was valued at $1.3 billion in 2018 (Ahuja and Rawat, 2019). As a result, phytase products have been produced by most major players in the animal feed enzymes market, including BASF, DSM, AB Vista, Adisseo, Novozymes and DuPont Danisco (Ahuja and Rawat, 2019).

1.5.2 Types of Phytase

Though all phytases catalyse the stepwise hydrolysis of phytic acid, they constitute a diverse class of enzymes with varying structures and mechanisms. Phytases have been identified from sources including bacteria, fungi, plants and animals (Nunes and Kumar, 2018). Depending on their catalytic mechanism, phytases can be classified into four classes: histidine acid phytases (HAPhy), β-propeller phytases (BPPhy), purple acid phytases (PAPhy) and protein tyrosine phytases (PTPhy), as shown in Figure 1.10 (Gen Lei et al., 2012).

The best-studied are the histidine acid phytases (HAPhy), which are mostly comprised of microbial phytases (Nunes and Kumar, 2018). HAPhys contain an N-terminal RHGXRXP motif and a C-terminal HD motif that come together to create the phosphate pocket, which serves as the catalytic centre (Gessler et al., 2018; Rigden, 2008). As denoted in the name, the optimal pH for HAPhys is 4.5 ~ 6.0 since the acidic pH allows for the dissociation of divalent metal cations from phytic

acid (Oh et al., 2004). HAPhys are then able to hydrolyse metal-free phytate, which is drawn to the positively-charged HAPhy active site (Gessler et al., 2018; Oh et al., 2004). The HAPhy class of phytases includes phytases with the highest specific activities that have been used as parent enzymes for industrial application, including the phytases from *Aspergillus niger*, *Citrobacter braakii* and *E. coli*.

The β-propeller phytases (BPPhy) resemble six-bladed propellers that contain two high-affinity and three lower-affinity Ca^{2+} binding sites (Ha et al., 2000). Ca^{2+} binding joins loop segments in the enzyme structure to increase thermostability and makes the highly negatively charged phytate-binding cleft electrostatically favourable for substrate binding (Ha et al., 2000). The BPPhy class is the only group that includes alkaline phytases that are capable of hydrolysing phytic acid at > pH 7.0, including the phytase from soil bacterium *Bacillus amyloliquefaciens* (Gessler et al., 2018).

Purple acid phytases (PAPhys) are comprised of mostly plant phytases that contain binuclear metal (Fe-Mn or Fe-Zn) centres (Gessler et al., 2018; Schenk et al., 1999). They contain seven conserved metal-ligating residues that coordinate the metal centres, which varies between enzymes (Schenk et al., 1999). Protein tyrosine phytases (PTPhys), also known as cysteine phytases, are mostly phytases from anaerobic gut rumen bacteria such as *Selenomonas ruminantium* (Gruninger et al., 2014).

A

Classification of Phytases			
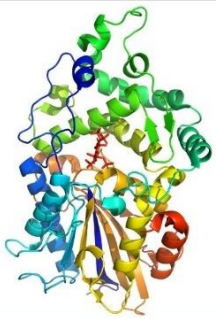	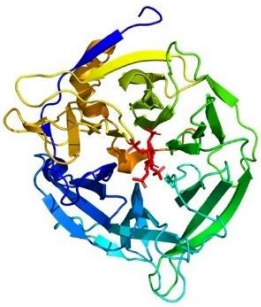		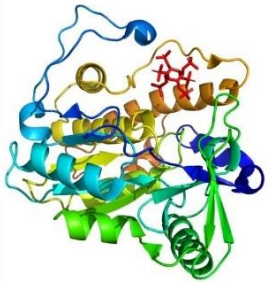
HAPhy	BPPhy	PAPhy	PTPhy
E. coli	*B. subtilis*	Structure Unavailable	*S. ruminantium*

B

Type	Phytase	Specific Activity (U/ mg)	Temperature Optimum
HAPhy	*Escherichia coli* AppA	1700	55 ~ 60 °C
	Citrobacter braakii phytase	3457	50 °C
	Aspergillus niger PhyA	50 ~ 103	55 ~ 58 °C
	Peniophora lycii PhyA	1080	58 °C
BPPhy	*Bacillus subtilis* PhyC	9 ~ 15	55 ~ 60 °C
	Bacillus amyloliquefaciens DS11	20	70 °C
PAPhy	*Triticum aestivum* phytase	137	45 °C
	Glycine max GmPhy	N/A	58 °C
PTPhy	*Selenomonas ruminantium* phytase	N/A	50 ~ 55 °C

Figure 1.10 Phytase classification and representative enzymes. a) Structures of representative enzymes of each type of phytase. The histidine acid phytase (HAPhy) *E. coli* AppA phytase (PDB 1DKQ) is shown in complex with phytate (red). The β-propeller phytase (BPPhy) *B. subtilis* PhyC phytase (PDB 3AMR) is shown in complex with a phytic acid analogue (red). There are no structures available for purple acid phytases (PAPhy). The protein tyrosine phytase (PTPhy) *S. ruminantium* phytase (PDB 1U25) is shown in complex with a phytic acid analogue (red). b) Representative phytases of each class, their specific activities and optimum temperatures (Gen Lei et al., 2012; Greiner and Konietzny, 2006).

1.5.3 Commercial Stabilised Phytases

Phytases must be thermostable for supplementation in animal feed since animal feed requires steam treatment to kill pathogens such as *Enterococcus faecium* and *Salmonella* (Boney et al., 2018; Jones, 2011; Rebello et al., 2017). Steam treatment during pelleting is conducted at 15 ~ 16% moisture and 80 ~ 90 °C, reaching peak temperatures of 92 ~ 104 °C (Rebello et al., 2017). The catalytic activity of most phytases is substantially reduced following exposure to 80 °C (Dersjant-Li et al., 2015). Consequently, phytases require thermal stabilisation to withstand heat-induced inactivation during the pelleting process (Nunes and Kumar, 2018).

As a result of the commercial value of phytase supplementation, substantial work has been undertaken to produce thermostable phytases. The first commercially available thermostable phytase was Natuphos, a stabilised version of the *A. niger* phytase, which was released by BASF in 1991 (Cao et al., 2007). Since then, many others have been released including Ronozyme (from *P. lycii* phytase, Novozymes), Ronozyme HiPhos (from *C. braakii* phytase, Novozymes), Phyzyme (from *E. coli* phytase, Danisco), OptiPhos (from *E. coli* phytase, Huvepharma) and Quantum Blue (from *E. coli* phytase, AB Vista) (Gontia and Tiwari, 2013; Konietzny and Greiner, 2004). Most commercial phytase products were produced through combinations of rational engineering and directed evolution in laborious and costly processes. A comprehensive list of commercially available phytases is shown in Table 2.

Product Name	Company	Source Organism	Production Organism
Allzyme	Alltech	*Aspergillus niger*	*A. niger*
AMAFERM	BioZyme	*Aspergillus oryzae*	*A. oryzae*
Avizyme	Finnfeeds	*Aspergillus awamori*	*Trichoderma reesei*
Finase	Roal	*A. awamori*	*T. reesei*
Natuphos	BASF	*A. niger*	*A. niger*
OptiPhos	Huvepharma	*Escherichia coli*	*Pichia pastoris*
Phyzyme XP	Danisco	*E. coli*	*Schizosaccharomyces pombe*
Quantum	AB Enzymes	*E. coli*	*P. pastoris*
Quantum Blue	AB Vista	*E. coli*	*T. reesei*
Ronozyme	DSM	*Peniophora lycii*	*A. oryzae*
Ronozyme HiPhos	DSM	*Citrobacter braakii*	*A. oryzae*
Rovabio PHY	Adisseo	*Penicillium funiculosum*	*P. funiculosum*

Table 2. Commercially available thermostable phytases (Cao et al., 2007; Gen Lei et al., 2012; Haefner et al., 2005; European Food Safety Authority 2011, European Food Safety Authority 2013)

1.5.4 Quantum Blue

Quantum Blue™ (QB) is the latest commercially available thermostable phytase product by AB Vista. QB is a genetically engineered and intrinsically thermostable *E. coli* AppA phytase that is reported by AB Vista to improve FCR by ~4 points (reduction in FCR of ~0.04) in broiler chickens and reduce feed cost by ~$20 per tonne (Quantum Blue Poultry Brochure, AB Vista). QB is an improved version of its predecessor, Quantum™ (reported in literature as Phy9X), which is a thermostable variant of AppA containing 8 total mutations generated through gene site saturation mutagenesis (Figure 1.11) (Garrett et al., 2004).

Superdosing (administration of phytase at high doses, typically >2500 FTU/kg) of phytases promotes broiler growth by i) reducing levels of residual anti-

nutrient phytic acid, ii) increasing the release of phosphorus and iii) generating inositol (Cowieson et al., 2011; Fernandes et al., 2019). Inositol is an important nutrient with demonstrated beneficial effects on alopecia in mice, fatty liver syndrome in rats and tocopherol deficiency in chicks (Cowieson et al., 2011). Furthermore, inositol is used in cell membrane and lipoprotein synthesis and signalling pathways, is required for prenatal and postnatal development, and is a key regulator of fat transport and deposition (Lee and Bedford, 2016). As a result, myo-inositol confers 30 – 35% of the total benefits seen from phytase superdosing (Lee et al., 2017).

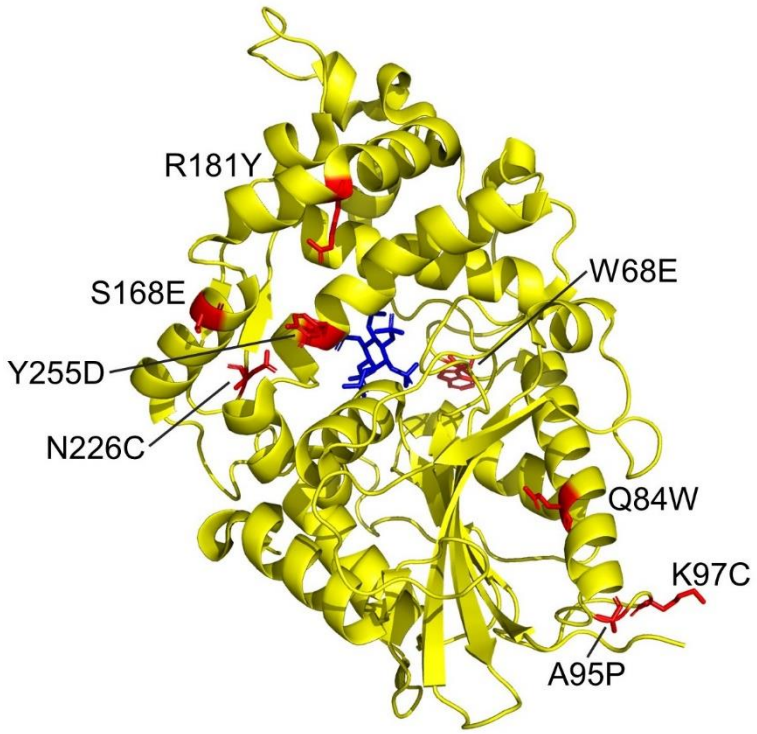

Figure 1.11 Structure of Phy9X. The eight mutations made to produce the thermostable variant Phy9X are shown in red on a structure of the *E. coli* AppA phytase (PDB 1DKQ). Phytate is shown in blue.

Superdosing QB in animal feed improved gizzard inositol levels and body weight gain in broilers and even enabled the breakdown of lower phosphorylated inositol intermediates (IP4 and IP3) to maximise inositol release (Walk et al., 2014; Williams, 2014). Furthermore, QB supplementation improved the digestible nutrient intake and yielded ~ 96 % phytate and phytate ester hydrolysis in the gizzard (at 4,000 FTU/kg) (Walk and Olukosi, 2019). Administration of QB was also shown to be superior to Ronozyme® HiPhos (stabilised *C. braakii* phytase, Novozymes) in increasing the bioavailability of P, with 2,000 FTU/kg of Ronozyme equating to the addition of 2.0 g of P_i and 1,000 FTU/kg of QB equating to 2.4 g of P_i (Ribeiro et al., 2016). These results demonstrate that supplementation of QB in animal feed maximises nutritional benefits from feed to greatly improve the FCR, which may directly translate to economic and environmental benefits.

1.6 Thesis Objectives

The main objective of this thesis was to produce a novel method of enzyme cyclisation that would i) enable the efficient cyclisation of enzymes, ii) confer substantial improvements in thermal resilience, iii) be generically applicable to a wide range of enzymes and iv) expand the range of enzymes suitable for cyclisation. A cyclisation method that satisfies these criteria would allow for the thermal stabilisation of industrially important enzymes without the need to individually engineer each catalyst. Furthermore, a cyclisation approach that is effective on enzymes with greater distances between termini would vastly expand the range of candidates suitable for cyclisation.

The first goal was to apply the SnoopLigase bioconjugation system to the head-to-tail cyclisation of enzymes while i) circumventing the fusion of a larger Catcher domain and ii) allowing for the purification of cyclised enzyme. To better determine the efficacy of SnoopLigase cyclisation in comparison to the efficacy of Tag/Catcher-mediated cyclisation strategies, SnoopLigase cyclisation was applied to mesophilic enzymes.

The subsequent goal was to expand the range of enzymes suitable for cyclisation to include those with greater distances between termini, notably the industrially important *E. coli* AppA phytase. The aim was to optimise the use of structured linkers to facilitate bridging of the gap between termini and extend the scope of the cyclisation platform.

Chapter 2: Methods

2.1 Cloning

2.1.1 Polymerase Chain Reaction

Constructs and primers were designed using SnapGene version 4.3.8 (GSL Biotech), and corresponding lyophilised DNA oligonucleotides were ordered from Integrated DNA Technologies (IDT). The oligonucleotides were reconstituted in 10 mM Tris-HCl pH 8.5 to 100 µM and stored at -20 °C for storage. All polymerase chain reactions (PCRs) were conducted using a C1000 Thermal Cycler (Bio-Rad).

For amplicons smaller than 4 kb, PCRs were prepared to a final volume of 25 µl, containing 0.5 µM each forward and reverse primers, 0.2 ng of template DNA and 12.5 µl of 2× Q5 High-Fidelity DNA Polymerase Master Mix (New England Biolabs). Cycling conditions for Q5 reactions were: initial denaturation at 95 °C for 30 s, followed by 25 cycles of denaturation at 95 °C for 30 s, annealing of primers at 60 °C for 20 s, elongation at 70 °C for 40 s per kb, finished with a final elongation step at 70 °C for 2 min before being cooled to 10 °C. Amplicons smaller than 500 bp were amplified using Q5 for 35 cycles.

For amplicons greater than 4 kb, PCRs were prepared to a final volume of 25 µl, containing 1× KOD Hot Start Buffer, 0.2 µM each forward and reverse primer, 30 ng template DNA, 2.5 mM $MgSO_4$, 0.2 mM mixed dNTPs, 3% (v/v) DMSO and 0.02 U/µl KOD Hot Start DNA Polymerase. Cycling conditions for KOD reactions were: initial denaturation at 95 °C for 3 min, followed by 25 cycles of denaturation at 95 °C for 30 s, annealing of primers at 60 °C for 30 s, and elongation at 68 °C

for 40 s per kb, finished with a final elongation step at 68 °C for 10 min before being cooled to 10 °C.

2.1.2 Agarose Gel Electrophoresis and PCR Product Purification

PCR products at 25 µl were mixed with 5 µl of 6× Purple Gel Loading Dye (New England Biolabs) and loaded on to 0.5 – 2% (w/v) agarose gels containing 0.01% (v/v) SybrSafe (Thermo Fisher Scientific), depending on the size of the DNA product. Agarose gels were run in 1× TAE buffer (40 mM Tris Base, 20 mM acetic acid, 1 mM EDTA, pH 8.0) at 130 V for 40 min. Gels were imaged on the XcitaBlue Conversion Screen and Filter (Bio-Rad) in the ChemiDoc XRS+ (Bio-Rad) and analysed using ImageLab software version 6.0 (Bio-Rad). PCR products were excised from agarose gels and purified using the Wizard SV Gel and PCR Clean-Up Kit (Promega). The concentration of purified DNA was quantified from the OD_{260} measurement using the ND-1000 NanoDrop (NanoDrop).

2.1.3 Gibson Assembly

Gibson isothermal assembly was performed as described (Gibson et al., 2009). A 2× master mix, produced using Taq Ligase (NEB), T5 Exonuclease (NEB) and a Phusion-like DNA polymerase expressed and purified in the Howarth lab, was stored in aliquots of 10 µl at -20 °C until use.

Purified DNA fragments were mixed on ice to a final volume of 10 µl such that DNA fragments of similar size were equimolar, and smaller inserts were present in 3× molar excess. The DNA mixture was combined with the 2×Gibson

master mix and immediately incubated at 50 °C for 1.5 – 3 hours in a preheated C1000 Thermal Cycler (Bio-Rad).

2.1.4 Transformation into *E. coli*

Following Gibson assembly, 8 µl of assembled plasmid was transformed into 50 µl aliquots of chemically competent *E. coli* NEB Turbo cells, stored at -80 °C. Competent cells were thawed on ice for 20 min, incubated with DNA for 20 min, transformed by heat shock for 45 s at 42 °C in a water bath, and incubated on ice for 5 min. For plasmid propagation, 0.5 – 1 µl of plasmid were transformed in the same manner. For Gibson assembly reactions involving more than 3 DNA fragments, 1 – 2 µl of Gibson assembly mix was electroporated into 50 µl aliquots of electrocompetent *E. coli* NEB Turbo using the Ec2 setting (2.5 kV) on the MicroPulser (Bio-Rad).

Following transformation, cells were recovered in 200 µl of SOC media at 37 °C, 200 rpm for 1 hour before plating on LB agar plates containing the corresponding antibiotic (kanamycin 50 µg/mL or ampicillin 100 µg/mL).

2.1.5 Plasmid Preparation

Bacterial colonies were used to inoculate overnight cultures of 10 mL in LB and the appropriate antibiotic for plasmid preparation. The GeneJET Plasmid Miniprep Kit (Thermo Fisher Scientific) was used to purify plasmids. The resulting plasmid DNA concentration was quantified using the OD_{260} measurement using the ND-1000 NanoDrop (NanoDrop).

2.1.6 DNA Sequence Verification

The DNA sequences of all produced constructs were verified by Sanger sequencing, conducted by Eurofins Genomics (Germany) or Source Bioscience (UK).

2.1.7 Cloning of SnoopLigase, BLA and PhyC Constructs

pET28a SnoopLigase (GenBank accession no. MG867372) and pET28a AviTag-SnoopLigase (Addgene plasmid ID 105626) were cloned by Dr. Can Buldun in the Howarth laboratory (Buldun et al., 2018).

The constructs pET28a BLA, pET28a SnoopTag-BLA-SnoopCatcher (GenBank accession no. KU608331) and pET28a SpyTag-BLA-SpyCatcher (Addgene plasmid ID 70943, GenBank accession no. KJ645919) were cloned by Dr. Christopher Schoene in the Howarth laboratory as previously described (Schoene, Bennett, & Howarth, 2016; Schoene, Fierer, Paul Bennett, & Howarth, 2014). pET28a SnoopTagJr-BLA-DogTag (GenBank accession no. MG867373) was derived from pET28a BLA and two constructs cloned by Dr. Can Buldun as: pET28a SnoopTagJr-Her2Affi and pET28a SUMO-DogTag (Addgene plasmid ID 105629, GenBank accession no. MG867376) (Buldun et al., 2018).

The constructs pET28a SpyTag-PhyC-SpyCatcher (GenBank accession no. KU608330) and pET28a PhyC were cloned by Dr. Christopher Schoene as previously described (Schoene et al., 2016). pET28a SnoopTagJr-PhyC-DogTag was derived from pET28a PhyC (Buldun et al., 2018).

2.1.8 Cloning of AppA and Quantum Blue Constructs

The *Escherichia coli* AppA phytase insert (GenBank NC000913.3) was cloned into the SpyTag/SpyCatcher and SnoopTagJr/DogTag cassettes as previously described to produce pET28a SpyTag-AppA-SpyCatcher and pET28a SnoopTagJr-AppA-DogTag. The sequence of Quantum Blue was obtained from AB Vista and was synthesised as two gBlock gene fragments (Integrated DNA Technologies). The gBlock fragments were assembled using Gibson assembly to produce pET28a Quantum Blue.

pET28a SnoopTagJr-cTPR-AppA-DogTag and pET28a SnoopTagJr-AppA-cTPR-DogTag constructs were derived from pET28a Spycatcher002ΔN1-cTPR-SnoopCatcher (cloned by Dr. Irsyad Kharil, Howarth laboratory). pET28a SnoopTagJr-AppA-LRR-DogTag was derived from pET28a SpyCatcher002ΔN1-LRR-SnoopCatcher (cloned by Dr. Irsyad Khairil). pET28a SnoopTagJr-AppA-L9-DogTag and pET28a SnoopTagJr-QB-L9-DogTag were derived from pET28a SpyCatcher002-L9-SnoopCatcher (cloned by Dr. Irsyad Khairil).

2.2 Protein Expression and Purification

2.2.1 Media Composition

All media was produced by the Media Glassware Sterilisation Laboratory at the Department of Biochemistry, University of Oxford. Lysogeny Broth (LB) high salt contained 10 g tryptone, 5 g yeast extract, 10 g NaCl in Milli Q water to a final volume of 1 L. Media was sterilised by autoclaving at 121 °C for 20 min and stored

at 25 °C until use. Terrific Broth (TB) contained 12 g tryptone, 24 g yeast extract, 4 mL of 87% glycerol (v/v) in Milli Q water to a final volume of 900 mL and autoclaved. Following sterilisation, 100 mL of sterilised 10× salt solution (23.13 g KH_2PO_4, 123.41 g K_2HPO_4 in Milli Q H_2O to final volume of 1 L) was added. Autoinduction media (AIM, Formedium) contained 10 g tryptone, 5 g yeast extract, 3.3 g ammonium sulfate, 6.8 g KH_2PO_4 , 7.1 g Na_2HPO_4, 0.5 g glucose, 2.0 g lactose, 0.15 g $MgSO_4$ and 0.03 g trace elements in MilliQ water to a final volume of 1 L.

2.2.2 Protein Expression in *E. coli*

Constructs in pET28a were expressed in *E. coli* BL21 DE3 RIPL (Agilent). Single colonies were picked from LB agar plates and used to inoculate starter cultures in LB containing 50 µg/mL kanamycin, which were grown overnight at 37 °C, 200 rpm. 10 mL of starter culture was used to inoculate 1 L of media (1:100 dilution).

Soluble constructs expressed in the cytoplasm were grown in LB media with kanamycin supplemented with 0.8% glucose (w/v), apart from SnoopTagJr-BLA-DogTag, which was expressed without glucose to minimise post-translational gluconoylation (Aon et al., 2008; Schweida et al., 2019). Cultures were grown at 37 °C, 200 rpm until cells reached OD_{600} of approximately 0.5 and induced with 0.42 mM IPTG for 5 hours at 30 °C, 200 rpm. The cells were harvested by centrifugation at 4,000 g for 20 min at 4 °C, and the resulting pellets were stored at -80 °C.

AppA and Quantum Blue constructs were expressed with a periplasmic signal sequence to enable correct folding in the periplasm, a reducing environment

favourable for the formation of the disulfide bonds. Periplasmic constructs were grown in autoinduction media (AIM) with kanamycin, directly inoculated using a single colony from an LB agar plate. Cultures were grown at 30 °C, 200 rpm for 24 hours. Cells were harvested by centrifugation at 4,000 g for 20 min at 4 °C, and the pellets were processed immediately.

2.2.3 Ni-NTA Affinity Chromatography of Soluble His_6-Tagged Proteins

Proteins containing the polyhistidine tag were purified using Ni-NTA affinity chromatography at 4 °C. Cell pellets obtained from 1 L of culture were resuspended in 10 mL ice-cold Ni-NTA binding buffer (50 mM Tris base, 300 mM NaCl, pH 7.8) supplemented with 10 mM phenylmethylsulfonylfluoride (PMSF) and 1× EDTA-free mixed protease inhibitors (Roche, 1 tablet was dissolved in 1.5 mL Milli Q water to constitute 100× stock solution). Samples were sonicated 4 times on ice using a Sonics Vibra-Cell Sonicator (Ultrasonic Processor) for 60 s, with 60 s break on ice in between each sonication (50% duty cycle, micro tip limit 4). Cell lysate samples were centrifuged at 17,000 g at 4 °C for 20 min, and the supernatant was incubated with washed and equilibrated Ni-NTA resin (Qiagen, 0.5 mL packed resin per L of culture) at 4 °C for 30 min on a roller incubator to keep the resin in suspension. Samples were loaded on to poly-prep columns (Bio-Rad), washed 5 times with 10 resin volumes of 10 mM imidazole in Ni-NTA binding buffer, then washed once with 2 resin volumes of 30 mM imidazole in Ni-NTA binding buffer. Samples were eluted 6 times with 1 resin volume of 200 mM imidazole in Ni-NTA binding buffer. For each elution, elution buffer was applied to the resin in capped columns and incubated for 3 min before elution to maximise elution yield. Elution fractions with high protein concentrations (ascertained by OD_{280}) were pooled for dialysis. Samples were

dialysed in a Spectra/Por 3,500 Da MWCO membrane (Spectrum Labs) 3 times at 1:1000 dilution at 4 °C against the corresponding buffer, each for a minimum of 3 hours. Typically, constructs were dialysed into PBS (137 mM NaCl, 2.7 mM KCl, 10 mM Na_2HPO_4, 2 mM KH_2PO_4, pH 7.4), including BLA and DHFR constructs. PhyC constructs were dialysed into 50 mM Tris-HCl, 2 mM $CaCl_2$, pH 7.0. Samples for mass spectrometry were dialysed into 10 mM ammonium acetate.

2.2.4 Periplasmic Purification of Disulfide Bond-Containing Proteins

Cell pellets were resuspended in 250 mL of ice-cold TES buffer (50 mM Tris, 1 mM EDTA, 20% sucrose (w/v), pH 8.0) per L of culture and incubated with stirring at 4 °C for 15 min, then centrifuged at 34,000 g at 4 °C for 20 min. The supernatant was discarded and pellet resuspended in 100 mL of ice-cold 5 mM $MgCl_2$ and incubated with stirring at 4 °C for 15 min. Samples were centrifuged again at 34,000 g at 4 °C for 20 min. The supernatant osmotic shock fluid was then incubated with washed and equilibrated Ni-NTA resin (Qiagen, 0.5 mL packed resin per L of culture) and purified by Ni-NTA affinity chromatography as described in 2.2.3.

2.2.5 Quantification of Protein Concentration

Protein concentration was primarily ascertained by OD_{280} measurements taken using the ND-1000 NanoDrop (Nanodrop) and molar extinction coefficients calculated using the ExPASY ProtParam web tool (Gasteiger et al., 2005). For dialysed cleared lysate samples, protein concentration was determined using the bicinchoninic acid (BCA) assay, as per the manufacturer's instructions (Thermo Fisher Scientific).

2.3 Protein Biotinylation

Protein biotinylation was conducted as previously described (Fairhead and Howarth, 2015). AP-SnoopLigase was biotinylated in PBS with 5 mM $MgCl_2$ and 1 mM ATP. GST-BirA (expressed and purified by Dr. Can Buldun, Howarth laboratory) was added such that the molar ratio of AP-SnoopLigase: GST-BirA was 15:1. D-Biotin was added such that the molar ratio of AP-SnoopLigase: D-Biotin was 1:15. The biotinylation reaction was incubated at 25 °C for 1 h. Following 1 h incubation, the same amount of GST-BirA was added to the reaction, mixed well, and incubated for another 1 h at 25 °C.

Following biotinylation, GST-BirA was removed by incubation with Hi-Cap Glutathione matrix (Qiagen) for 1 h at 4 °C on a rotor. Samples were then centrifuged at 17,000 g for 30 s. The supernatant was collected and dialysed three times in a Spectra/Por 3,500 Da MWCO membrane (Spectrum Labs) at 1:1000 dilution at 4 °C against 50 mM TB pH 10, each for a minimum of 3 hours.

A gel shift assay was used to ascertain whether the biotinylation process was effective. Biotinylated AP-SnoopLigase was incubated with Streptavidin at molar ratios of 2:1, 1:1 and 1:2 for 1 h at 25 °C. 6× SDS loading buffer (0.23 M Tris-HCl, pH 6.8, 24% (v/v) glycerol, 120 µM bromophenol blue, 0.23 M SDS) was added to samples and loaded on to a 12% SDS-PAGE gel. Gels were run at 200 V for 1 h on ice and stained using InstantBlue (Expedeon).

2.4 Protein Characterisation

2.4.1 SDS-PAGE

Sodium dodecyl sulfate polyacrylamide gel electrophoresis (SDS-PAGE) was conducted using Tris-glycine gels. Gels were run using XCell SureLock Mini-cell gel chambers (Thermo Fisher Scientific) in Tris-glycine running buffer [25 mM Tris-HCl, 192 mM glycine, 0.1% (w/v) SDS] at 200 V for 1 h at 25 °C. Samples were prepared for SDS-PAGE through the addition of 6× SDS loading buffer (0.23 M Tris-HCl, pH 6.8, 24% (v/v) glycerol, 120 µM bromophenol blue, 0.23 M SDS) to 1× concentration. Following the addition of loading dye, samples were heated to 99 °C for 3 min in a C1000 thermal cycler (Bio-Rad) and cooled to 25 °C prior to loading. Samples containing disulfide bonds were reduced through the addition of DTT to a final concentration of 2 mM. Pre-stained PageRuler (Thermo Fisher Scientific) was used as the molecular weight marker.

Gels were stained with InstantBlue (Expedeon) Coomassie stain and destained in MilliQ water. Destained gels were imaged using a ChemiDoc XRS+ Imager (Bio-Rad).

2.4.2 Electrospray Ionisation Mass Spectrometry

Samples were prepared for mass spectrometry by dialysis using Spectra/Por 3,500 Da MWCO membrane (Spectrum Labs) into 10 mM ammonium acetate pH 7.0 at 1:1000 dilution three times, each for a minimum of 3 hours. Electrospray ionisation mass spectrometry (ESI-MS) was performed by Dr. David Staunton at the Molecular Biophysics Suite at the Department of Biochemistry. An m/z (mass/ charge) spectrum was obtained for each sample using a Micromass LCT time-of-

flight (TOF) ESI-MS (Micromass UK). The obtained m/z spectra were converted to molecular mass spectra using the Maximum Entropy algorithm on MassLynx V 4.00.00 (Water Corporation). Mass spectra were evaluated in relation to predicted masses calculated using ProtParam (Gasteiger et al., 2005).

2.5 SnoopLigase Cyclisation

2.5.1 SnoopLigase Conjugation Reaction

To cyclize enzymes flanked by SnoopTagJr and DogTag, 10 μM enzyme construct and 10 μM SnoopLigase was incubated in TB pH 7.25 + 15% (v/v) glycerol at 4 °C for 16 hours. Cyclization reactions of SnoopTagJr-PhyC-DogTag for thermal resilience activity assays were supplemented to a final concentration of 2 mM $CaCl_2$. The cyclized enzymes were then subject to temperature-dependent solubility and thermal resilience activity assays. For the cyclization timecourse, cyclization was terminated through the addition of 6× SDS loading buffer (0.23 M Tris-HCl, pH 6.8, 24% (v/v) glycerol, 120 μM bromophenol blue, 0.23 M SDS) to a final concentration of 1×.

2.5.2 SnoopLigase Removal Following Conjugate Formation

Cyclisation reactions were set up with equimolar quantities of biotinylated SnoopLigase and SnoopTag/DogTag-flanked enzyme at 10 μM in 50 mM Tris-borate pH 7.25 + 15% (v/v) glycerol and allowed to proceed overnight at 4 °C. Following cyclisation, reactions were coupled to washed and equilibrated HiCap Streptavidin Agarose (Thermo Fisher Scientific) for 30 min on a rotating platform at

25 °C. 10 µl packed washed and equilibrated resin was used for every 100 µl of cyclisation reaction at 10 µM. Samples were then transferred to 1 mL polyprep columns (Bio-Rad) and centrifuged for 1 min at 300 g at 25 °C. Polyprep columns (Bio-Rad) for use in imidazole purification were prepared by washing once with 1 M imidazole + 0.01% (v/v) Tween-20 in Tris phosphate pH 7.0 (25 mM phosphoric acid adjusted to pH 7.0 with Tris base)

Following SnoopLigase removal, enzymes were dialysed into their optimal buffers and concentrated using 5 kDa molecular weight cutoff filters (Vivaspin 500, GE Healthcare).

2.5.2.1 Purification using Glycine Elution

Purification using glycine elution was conducted at 4 °C with ice-cold buffers. The Streptavidin agarose with immobilised SnoopLigase-cyclised enzyme was washed twice with five resin volumes of 50 mM glycine pH 3.0 + 300 mM NaCl, then washed three times with five resin volumes of 50 mM glycine pH 3.0. After each addition of wash buffer, samples were centrifuged for 1 min at 300 g. Following all five washes, samples were centrifuged a final time at 500 g for 1 min to remove all remaining buffer. To elute cyclised enzyme free from SnoopLigase, the resin was incubated with one resin volume of 50 mM glycine pH 2.0 for 1 min at 4 °C, then centrifuged for 1 min at 500 g into an Eppendorf tube containing 0.3 resin volumes of 1 M Tris-HCl pH 9.5. The elution step was repeated twice into the same tube without addition of more Tris-HCl buffer.

2.5.2.2 Purification using Imidazole Elution

Purification using imidazole elution was performed at 25 °C. The Streptavidin agarose with immobilised SnoopLigase-cyclised enzyme was washed five times with five resin volumes of 0.5 M imidazole in Tris phosphate pH 7.0 (25 mM phosphoric acid adjusted to pH 7.0 with Tris base) + 0.01% (v/v) Tween-20. After each addition of wash buffer, samples were centrifuged for 1 min at 300 g. Following all five washes, samples were centrifuged a final time at 500 g for 1 min to remove all remaining buffer. To elute cyclised enzyme free from SnoopLigase, 1 column volume of elution buffer [2.5 M imidazole in Tris phosphate pH 7.0 + 0.01% (v/v) Tween-20] was added. Samples were incubated at 25 °C for 5 min at 500 rpm on a ThermoMixer comfort (Eppendorf) before centrifugation at 300 g for 1 min. The elution step was repeated twice.

2.5.2.3 Purification using Competitor Peptide Elution

Conjugate purification using SnoopTagJr:DogTag competitor peptide elution was conducted at 25 °C. The SnoopTagJr:DogTag competitor peptide (obtained from Dr. Can Buldun, Howarth laboratory) was designed to outcompete the cyclised enzyme from SnoopLigase and circumvent enzyme exposure to low pH or high imidazole concentrations during SnoopLigase depletion (Buldun et al., 2018; Pollard, 2010) The Streptavidin agarose with immobilised SnoopLigase-cyclised enzyme was washed five times with five resin volumes of Tris-borate pH 7.0 + 0.01% (v/v) Tween-20. Following all five washes, samples were centrifuged a final time at 500 g for 1 min to remove all remaining buffer. To elute, 2 µl of elution buffer [100 µM SnoopTagJr:DogTag peptide in Tris-phosphate pH 7.0 + 0.01% (v/v) Tween-20] was added per µl of resin. Samples were then incubated at 25 °C for 4 h at 300

rpm on a ThermoMixer comfort (Thermo Fisher Scientific). After 4 h, samples were spun for 1 min at 16,000 g to elute cyclised enzyme.

2.6 Characterisation of Enzyme Thermal Resilience

Enzyme thermal resilience assays were conducted in triplicate using the same protein preparation.

2.6.1 Temperature-Dependent Solubility Assay

For BLA constructs, 20 µl of 10 µM construct in PBS with 100 mM DTT was incubated at 10, 25, 37, 55, 75, 90 and 100 °C for 10 minutes, then cooled to 10 °C (ramp rate 3 °C/second) on a C1000 thermal cycler (Bio-Rad). For PhyC constructs, 20 µl of 10 µM construct in 50 mM Tris-HCl pH 7.0, 2 mM $CaCl_2$ was incubated at 10, 25, 37, 55, 75, 90 and 100 °C for 10 minutes, then cooled to 10 °C in the same manner. Following heating, irreversibly aggregated proteins were pelleted by centrifugation at 4 °C, 17,000 g for 30 minutes. The supernatant was harvested for analysis by SDS-PAGE, as described in the previous section. The samples held at 10 °C were defined as 100% soluble, and gel band densitometry was conducted via ImageLab 3.0 (Bio-Rad).

2.6.2 BLA Thermal Resilience Activity Assay

96-well clear flat-bottom polystyrene plates (Greiner) were blocked with 200 µl PBS, 3% BSA (bovine serum albumin, ≥ 98%, Sigma-Aldrich) in each well at 37 °C for a minimum of 2 hours. Blocked plates were washed twice with 0.1 M

$NaHPO_4$ pH 7.0, 1 mM EDTA. 20 µl of 25 µM BLA construct was incubated at 10, 25, 37, 55, 75, 90 and 100 °C for 10 minutes, then cooled to 10 °C (ramp rate 3 °C/second) on a C1000 thermal cycler (Bio-Rad). The samples were diluted to a final concentration of 62.5 nM using 0.1 M $NaHPO_4$ pH 7.0, 1 mM EDTA, 1% BSA. Nitrocefin (Merck) substrate solution was prepared to a concentration of 105 µM through the addition of 0.1 M $NaHPO_4$ pH 7.0, 1 mM EDTA. The diluted BLA constructs were reacted with at a final concentration of 3 nM construct to 100 µM nitrocefin.

The SpectraMax M3 microplate reader (Molecular Devices) was used to measure the OD_{486} every 15 seconds for 10 minutes (41 measurements total) at 20 °C, with the automix setting on for 3 seconds between measurements. Blanks consisted of all components bar the enzyme.

2.6.3 PhyC Thermal Resilience Activity Assay

96-well clear flat-bottom polystyrene plates (Greiner) were blocked with 200 µl 50 mM Tris-HCl pH 7.0 with 2 mM $CaCl_2$ and 3% (w/v) BSA at 37 °C for 2 hours. Blocked plates were washed twice with 50 mM Tris-HCl pH 7.0 with 2 mM $CaCl_2$ and 10% glycerol. 10 µM enzyme was incubated at 25, 37, 55, 75, 90 or 100°C for 10 minutes, then cooled to 10 °C (ramp rate 3°C/second) on a C1000 thermal cycler (Bio-Rad). The samples were diluted to 380 nM using 50 mM Tris-HCl pH 7.0 with 2 mM $CaCl_2$. 20 µM phytic acid sodium salt (Sigma-Aldrich) substrate solution was prepared using 50 mM Tris-HCl pH 7.0 with 2 mM $CaCl_2$. In the final reaction, 76 nM phytase construct reacted with 16 µM phytic acid at 50 °C, 350 rpm on a Thermomixer comfort (Eppendorf). All reactions were set up such that all timepoints

finished at the same time. 100 µl Biomol Green (Enzo Life Sciences) was added immediately to each well, and the plate was incubated at 25 °C for 25 minutes for colour development. The SpectraMax M3 microplate reader (Molecular Devices) was used to measure the OD_{620} at 20 °C. Blanks consisted of all components bar the enzyme.

2.6.4 AppA/ QB Thermal Resilience Activity Assay

96-well clear flat-bottom polystyrene plates (Greiner) were blocked with 200 µl 0.1 M sodium acetate pH 4.5 and 3% (w/v) BSA at 37 °C for 2 hours. Blocked plates were washed twice with 0.1 M sodium acetate pH 4.5. 10 µM enzyme was incubated at 25, 37, 55, 75, 90 or 100°C for 10 minutes, then cooled to 10 °C (ramp rate 3°C/second) on a C1000 thermal cycler (Bio-Rad). The samples were diluted to 16.67 nM using 0.1 M sodium acetate pH 4.5. 6.25 µM phytic acid sodium salt (Sigma-Aldrich) substrate solution was prepared using 0.1 M sodium acetate pH 4.5. In the final reaction, 3.33 nM phytase construct was reacted with 5 µM phytic acid at 37 °C, 450 rpm on a Thermomixer comfort (Eppendorf). All reactions were set up such that all timepoints finished at the same time. 100 µl Biomol Green (Enzo Life Sciences) was added immediately to each well, and the plate was incubated at 25 °C for 25 minutes for colour development. The SpectraMax M3 microplate reader (Molecular Devices) was used to measure the OD_{620} at 20 °C. Blanks consisted of all components bar the enzyme.

2.6.5 Production of Dialysed Cleared Lysate

SpyCatcher ΔN1 (inactive SpyCatcher mutant, obtained from Dr. Irsyad Khairil, Howarth laboratory) was expressed in *E. coli* BL21 DE3 RIPL (Agilent) and cultured in LB as described in section 2.2. Cells were harvested and frozen as previously described. The pellet was thawed in 15 mL buffer (0.1 M sodium acetate pH 4.5 for AppA and QB constructs, 50 mM Tris-HCl pH 7.0 with 2 mM $CaCl_2$ for PhyC constructs) per L of culture, 1× EDTA-free mixed protease inhibitors (Roche), and PMSF.

Samples were sonicated 4 times on ice using a Sonics Vibra-Cell Sonicator (Ultrasonic Processor) for 60 s, with 60 s break on ice in between each sonication (50% duty cycle, micro tip limit 4). Cell lysate samples were centrifuged at 17,000 g at 4 °C for 30 min. The supernatant was dialysed into the optimum activity buffer for the enzyme construct of interest in Spectra/Por 3,500 Da MWCO membrane (Spectrum Labs) 3 times at 1:1000 dilution at 4 °C against the corresponding buffer, each for a minimum of 3 hours. Aliquots were frozen and stored at -20 °C.

2.6.6 Thermal Resilience Activity Assays in Dialysed Cleared Lysate

96-well plates and substrate solution were prepared as previously described in section 2.6.3 and 2.6.4. Cyclisation reactions were set up at 20 μM, and samples were prepared at 20 μM. Samples were then mixed with dialysed cleared lysate (DCL) at a ratio of 1:1 such that the final enzyme concentration was 10 μM. The samples were incubated at 25, 37, 55, 75, 90 or 100°C for 10 minutes, then cooled to 10 °C (ramp rate 3°C/second) on a C1000 thermal cycler (Bio-Rad). Assays were conducted with the prepared samples as previously described.

Chapter 3: Enhancing Thermal Resilience via SnoopLigase Cyclisation

Enzymes as biocatalysts are particularly desirable for industrial applications due to their high selectivity, ability to efficiently orchestrate such specific chemistries under mild conditions, biodegradability and natural richness in enzyme diversity (Marrs et al., 1999). Enzymes are used extensively in a wide range of industries, from the production of household staples such as fruit juice, detergent and painkillers, to the enhancement of nutritional value of animal feed in agriculture (Singh et al.).

Despite their abundant potential, many enzymes remain unfit for application due to instability, low catalytic efficiency or lack of specificity (Choi et al., 2015). For industrial use, enzymes must be able to withstand processing, which can involve steps such as extrusion, vigorous mixing and heat treatment, and therefore require stabilisation prior to implementation. In addition, the cost of enzyme engineering and production in industrial quantities must be considered. To qualify for commercialisation, catalysts must be able to be produced at high yields at low cost using minimally sophisticated technology (Choi et al., 2015).

Currently, the gold standard for engineering thermal stability into industrial enzymes is directed evolution, where large libraries are generated via mutagenesis and screened for enhanced thermal stability (Johannes et al., 2005; McLachlan et al., 2008). However, this method is labour-intensive, takes a long time and often results in meagre improvements in thermal stability. For example, the melting temperature (T_m) of glucose 6-phosphate dehydrogenase was only increased by

3.4 °C following four rounds of random mutagenesis and screening, and the T_m of T4 lysozyme was only increased by 8.3 °C in one multiple mutant in a pool of over 700 mutants (Baase et al., 2010; Huang et al., 2018).

A similar strategy to improve thermostability that requires specific engineering for each enzyme is the introduction of additional disulfide bonds, given the stabilising effect of native disulfide bonds against heat inactivation (Voutilainen et al., 2010). However, there is conflicting data on whether disulfide bond engineering positively impacts thermal stability, since in some destabilised mutants, the stability gained by the additional covalent linkage is offset by the disruption of the native state (Pecher and Arnold, 2009).

Head-to-tail cyclisation, or the covalent ligation of the N- and C-termini, of enzymes is a more modular approach that stabilises enzymes by imbuing structure to previously flexible termini. This reduces their spatial heterogeneity, and therefore the entropy of the unfolded protein, thereby stabilising the native three-dimensional conformation (Borra and Camarero, 2013; Clark and Craik, 2010; Iwai and Plückthun, 1999). Methods include carbodiimide cross-linking (Goldenberg and Creighton, 1983), split inteins (Scott et al., 1999), sortases (Jia et al., 2014), butelases (Nguyen et al., 2015) and the SpyRing (Schoene et al., 2016a).

The Howarth laboratory has previously produced the SpyRing method of cyclisation using spontaneous isopeptide bond-forming partners, SpyTag (13 aa) and SpyCatcher (12 kDa) (Schoene et al., 2016a). SpyRing cyclisation conferred significant improvements in thermal resilience to TEM-1 β-lactamase (BLA), phytase (PhyC) and dihydrofolate reductase (DHFR), including increasing the resistance of BLA to heat-induced aggregation by > 60 °C (Schoene et al., 2016a).

Other SpyRing-cyclised enzymes include firefly luciferase (Si et al., 2016b), xylanase (Gilbert et al., 2017), lichenase (Wang et al., 2016b), L-phenylalanine aldolase (Wang et al., 2019a), mannanase (Gao et al., 2019) and trehalose synthase (Xu et al., 2018). Despite its efficacy, the SpyRing involves the C-terminal conjugation of the larger SpyCatcher domain, which carries the potential to compromise enzymatic activity, such as through steric hindrance. In addition, SpyTag and SpyCatcher spontaneously form an isopeptide bond, leaving no room for the temporal control of cyclisation.

In this chapter, I describe the application of the novel SnoopLigase system for peptide-peptide ligation to the head-to-tail cyclisation of BLA, a well-characterised model enzyme whose termini are in proximity (7 Å), and to phytase, an environmentally and agriculturally important enzyme. I demonstrate that SnoopLigase cyclisation of BLA and PhyC confers significant improvements in thermal resilience, enabling both enzymes to retain high solubility and activity following boiling.

3.1 SnoopLigase Cyclisation of TEM-1 β-lactamase

Unlike the SpyRing platform, the SnoopLigase system is tripartite, resulting from the three-part splitting of the RrgA adhesin from *Streptococcus pneumoniae* by Can Buldun (Figure 3.1). RrgA was split such that the three residues responsible for the formation of its intramolecular isopeptide bond of RrgA (found in the D4 Ig-like domain, between Lys 742 and Asn 854, catalysed by apposed Glu 803) were placed on separate proteins (Buldun et al., 2018). Following splitting, SnoopLigase was further engineered, including loops stabilisation through proline substitutions,

which stabilise the folded protein by limiting the conformational flexibility due to its fixed φ-angle (Buldun et al., 2018; Fu et al., 2009). The resulting SnoopLigase system is comprised of two peptide tags, SnoopTagJr (12 aa, incl. reactive lysine) and DogTag (23 aa, incl. reactive asparagine), which are covalently locked upon SnoopLigase addition (13.3 kDa, incl. reactive glutamate). Peptide-peptide locking occurs via transamidation, during which ammonia is released (Buldun et al., 2018).

The RrgA protein has also previously been split into a conventional Tag-Catcher system in the Howarth lab to produce SnoopTag (including reactive Lys) and SnoopCatcher (including reactive Asn and Glu), protein partners that form a spontaneous isopeptide bond (Figure 3.1E) (Veggiani et al., 2016).SnoopTag and SnoopCatcher (denoted “SnoopRing”) have been used to cyclise BLA to enable the retention of solubility and activity even after incubation at 100 °C, but the SnoopRing was outperformed by the SpyRing (Schoene et al., 2016a).

The SnoopLigase technology developed by Can Buldun and the application of Tag and Catcher protein partner systems to enzyme cyclisation by Chris Schoene laid the foundation for the use of the SnoopLigase system in head-to-tail cyclisation of enzymes to confer thermal resilience.

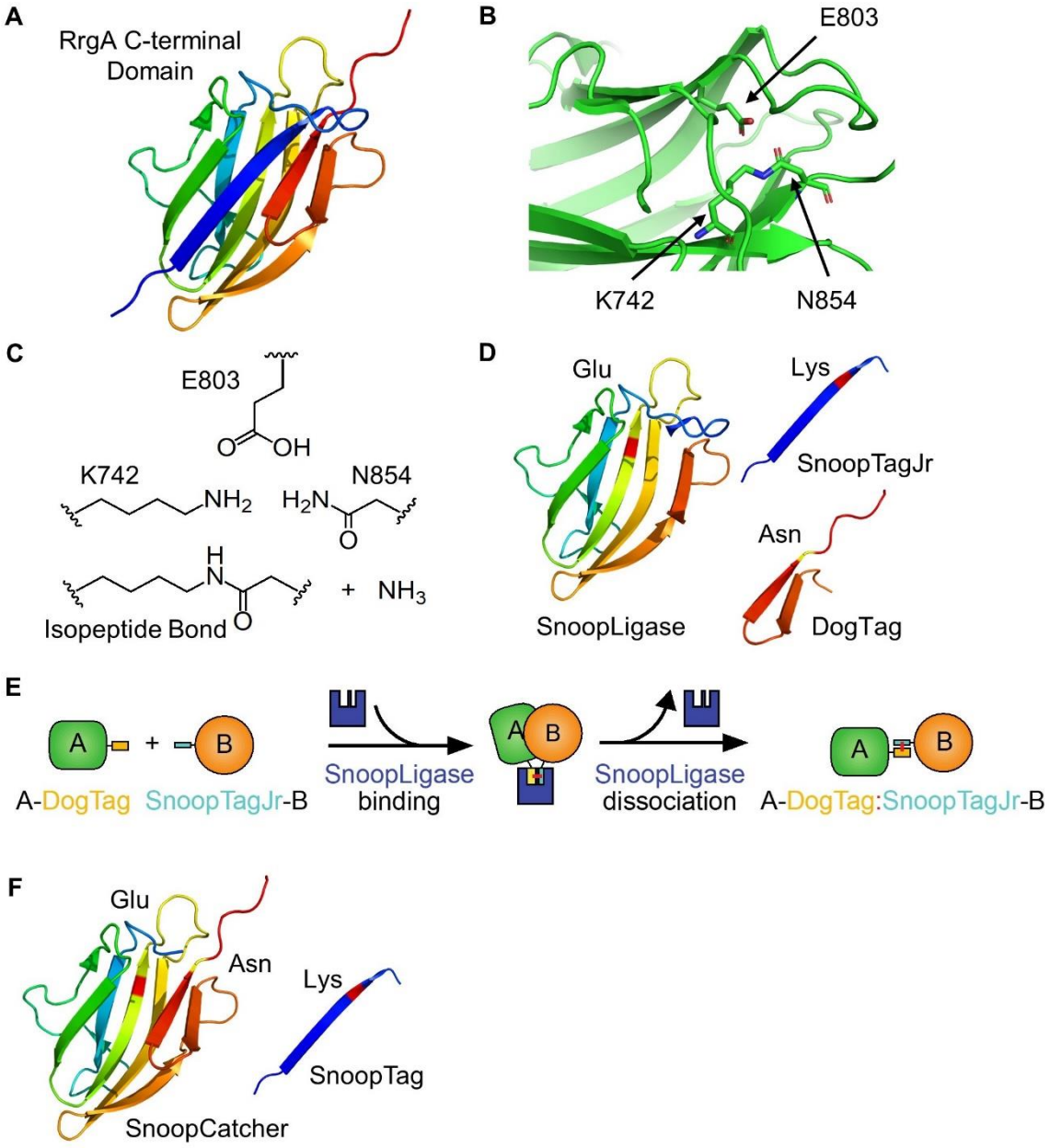

Figure 3.1 Tripartite and bipartite splitting of RrgA domain 4. a) The C-terminal domain of the *Streptococcus pneumoniae* adhesin (Protein Data Bank 2WW8) contains a spontaneous isopeptide bond. b) The reactive triad is comprised of Lys 742, Asn 854 and Glu 803. c) The isopeptide bond is formed via transamidation between Lys 742 and Asn 854, catalysed by the apposed Glu 803, eliminating ammonia. d) The RrgA domain was split and engineered by Can Buldun such that a catalytic residue was placed on each constituent to result in the SnoopLigase

system. SnoopTagJr and DogTag are ligated upon addition of SnoopLigase. e) The SnoopLigase system enables peptide-peptide ligation by effectively reconstituting the parent domain. The isopeptide bond is shown in red. f) RrgA domain 4 was also split into two components, SnoopTag and SnoopCatcher, which spontaneously form an isopeptide bond.

3.1.1 Design of Constructs for Cyclisation

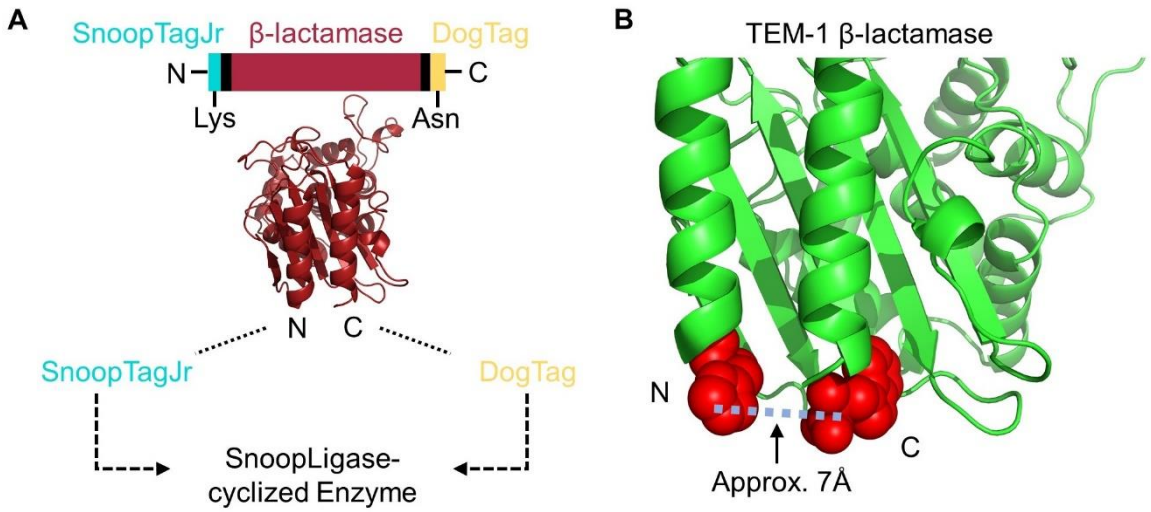

Figure 3.2 Design of BLA constructs for SnoopLigase cyclisation. a) To enable head-to-tail cyclisation upon SnoopLigase addition, SnoopTagJr was genetically encoded at the N-terminus and DogTag at the C-terminus of BLA (Protein Data Bank 1BTL). b) The termini of BLA are in relative proximity, located 7 Å apart (measured from the Nitrogen atoms of the amine groups of the N-terminal histidine and C-terminal tryptophan).

Figure 3.2 shows the BLA construct designed for SnoopLigase-mediated cyclisation. The enzyme is flanked by N-terminal SnoopTagJr and C-terminal DogTag, separated from the enzyme by a flexible $(GSG)_2$ linker to enable the permissive orientation of both peptide tags for ligation by SnoopLigase. The termini of BLA are in relative proximity (approximately 7 Å apart) and are located far from the active site, which make it favourable for SnoopLigase cyclisation. The ligation mechanism of SnoopLigase is derived from the reconstitution of the parent domain through covalent bonding of the two peptide tags, catalysed by the apposed glutamate on SnoopLigase. As a result, SnoopLigase remains associated to its ligated product following reaction. It is important that the termini for conjugation are located away from the active site due to the possibility of steric obstruction of the active site by SnoopLigase.

3.1.2 Verification of BLA Cyclisation

Since SnoopTagJr and DogTag alone cannot form a peptide bond without the catalytic glutamate residue located on SnoopLigase, the expression of SnoopTagJr-BLA-DogTag resulted in monomeric enzyme species. To test whether the produced SnoopTagJr-BLA-DogTag construct was able to be successfully cyclised by SnoopLigase, equimolar quantities of enzyme and SnoopLigase were mixed in the optimal buffer for SnoopLigase activity and incubated at 4 °C (Figure 3.3).

Following incubation with SnoopLigase, SnoopTagJr-BLA-DogTag was cyclised over time, as indicated by the increase in electrophoretic mobility (Figure 3.3). Most of the linear enzyme had been cyclised following incubation with SnoopLigase for 4 hours, though the reaction continued to proceed even after 24

hours, at which point only a slight trace band of linear substrate remained visible on the SDS-PAGE gel. The reaction generated a minimal quantity of dimeric and multimeric species, and primarily resulted in the formation of monomeric cyclic species (Figure 3.3).

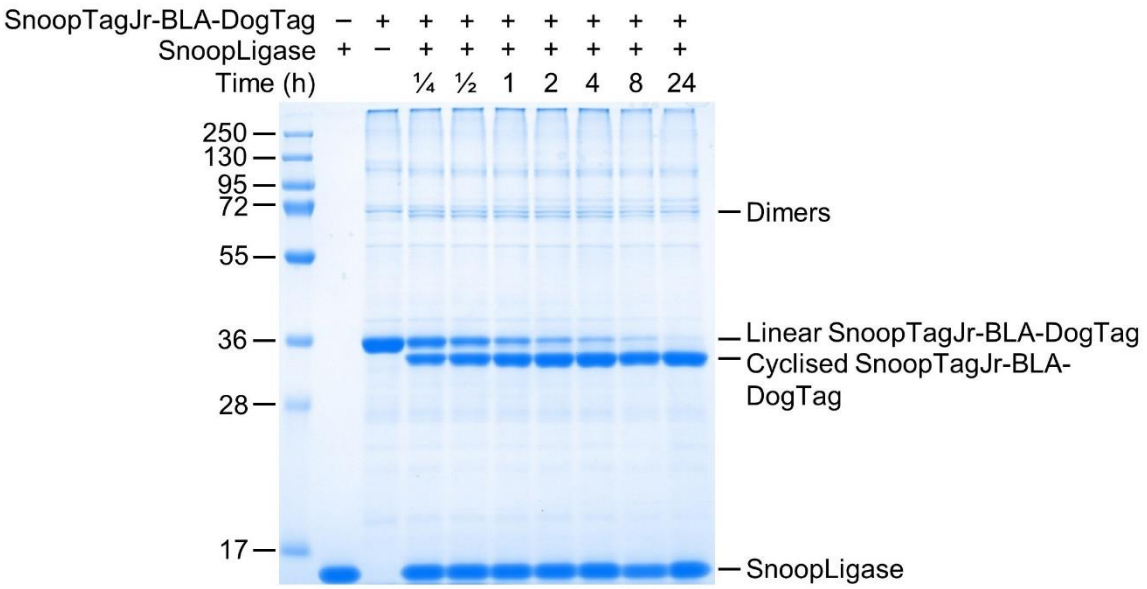

Figure 3.3 Timecourse of SnoopLigase cyclisation of BLA. SnoopLigase efficiently cyclises SnoopTagJr-BLA-DogTag. Both constructs were expressed in *E. coli* and purified by Ni-NTA chromatography. Equimolar quantities (10 µM) of SnoopLigase and SnoopTagJr-BLA-DogTag were incubated at 4 °C for 0.25 – 24 h, prior to SDS-PAGE with Coomassie staining.

3.1.3 Effect on Aggregation of BLA

To determine whether SnoopLigase cyclisation increased the resilience of BLA to heat-induced aggregation, constructs were heated to various temperatures and assessed for the proportion of protein remaining in the soluble fraction (Figure 3.4). Wild-type BLA irreversibly aggregated following 10 min at 37 °C, with only 1.6 %

of protein remaining in the soluble fraction (Figure 3.4). The conjugation of peptide tags, SnoopTagJr and DogTag, had a solubilising effect on BLA, and the uncyclized SnoopTagJr-BLA-DogTag construct exhibited improved resilience to heat-induced aggregation (Figure 3.4).

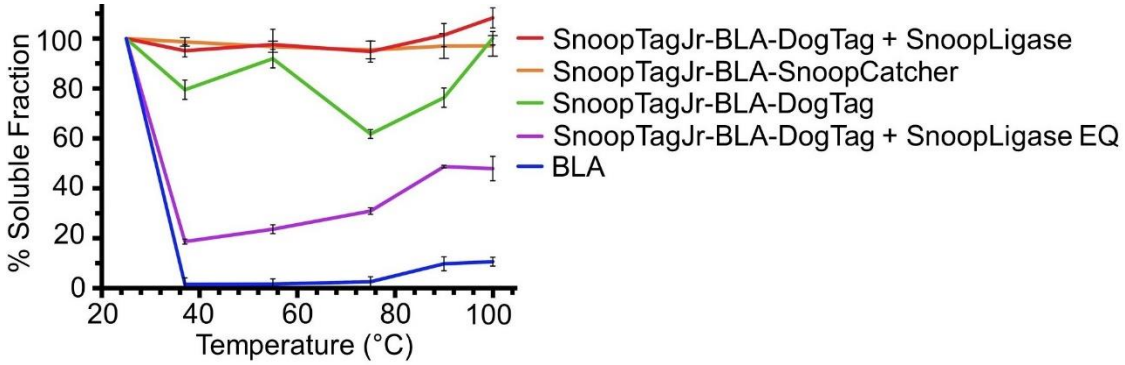

Figure 3.4 Cyclisation improved BLA resistance to heat-induced aggregation. Constructs were held at the temperatures indicated above for 10 min, cooled to 10 °C, then centrifuged to remove insoluble aggregates. The soluble enzyme remaining in the supernatant was assessed by SDS-PAGE with Coomassie staining. Quantification was conducted by gel densitometry and the band intensity of the 25 °C-incubated sample defined as 100% soluble. All are mean of triplicate ± 1 SD. An inactive SnoopLigase mutant, SnoopLigaseEQ was used as a control.

However, the most improvement to aggregation could be seen in the cyclised BLA constructs, SnoopLigase-cyclised SnoopTagJr-BLA-DogTag and SnoopTagJr-BLA-SnoopCatcher. This improvement could not be seen in the SnoopTagJr-BLA-DogTag construct incubated with an inactive SnoopLigase mutant, SnoopLigaseEQ, highlighting the importance of the covalent bond in

conferring thermal resilience. Both forms of cyclisation enabled BLA to retain almost full solubility throughout heating at all temperatures. Even following 10 min at 100 °C, SnoopLigase-cyclised BLA remained fully soluble and SnoopRing-cyclised BLA remained 97 % soluble, presenting an approximate 10-fold improvement over the wild-type enzyme (Figure 3.4).

In the case of BLA constructs that display a low degree of thermal resilience to heat-induced aggregation, such as wild-type BLA and SnoopTagJr-BLA-DogTag incubated with SnoopLigaseEQ, the lowest soluble fraction can be observed following incubation at 37 °C, after which increases in solubility can be observed with increasing temperature.

3.1.4 Effect on Thermal Resilience of BLA Activity

The activity of BLA was measured through the hydrolysis of nitrocefin, whose β-lactam ring is readily cleaved by BLA. Following hydrolysis, nitrocefin changes colour from yellow (380 nm) to red (486 nm), enabling the colourimetric monitoring of BLA activity.

Temperature-dependent solubility assays (Chapter 2.6.1) showed that over 98 % of wild-type BLA aggregated out of solution following incubation at 37 °C (Figure 3.4). Similarly, thermal resilience activity assays (Chapter 2.6.2) demonstrated that BLA is most active when unheated (following 10 min incubation at 25 °C). Following incubation at 37 °C, its activity is significantly compromised, and BLA is effectively inactive following incubation at all temperatures higher than 37 °C (Figure 3.5a).

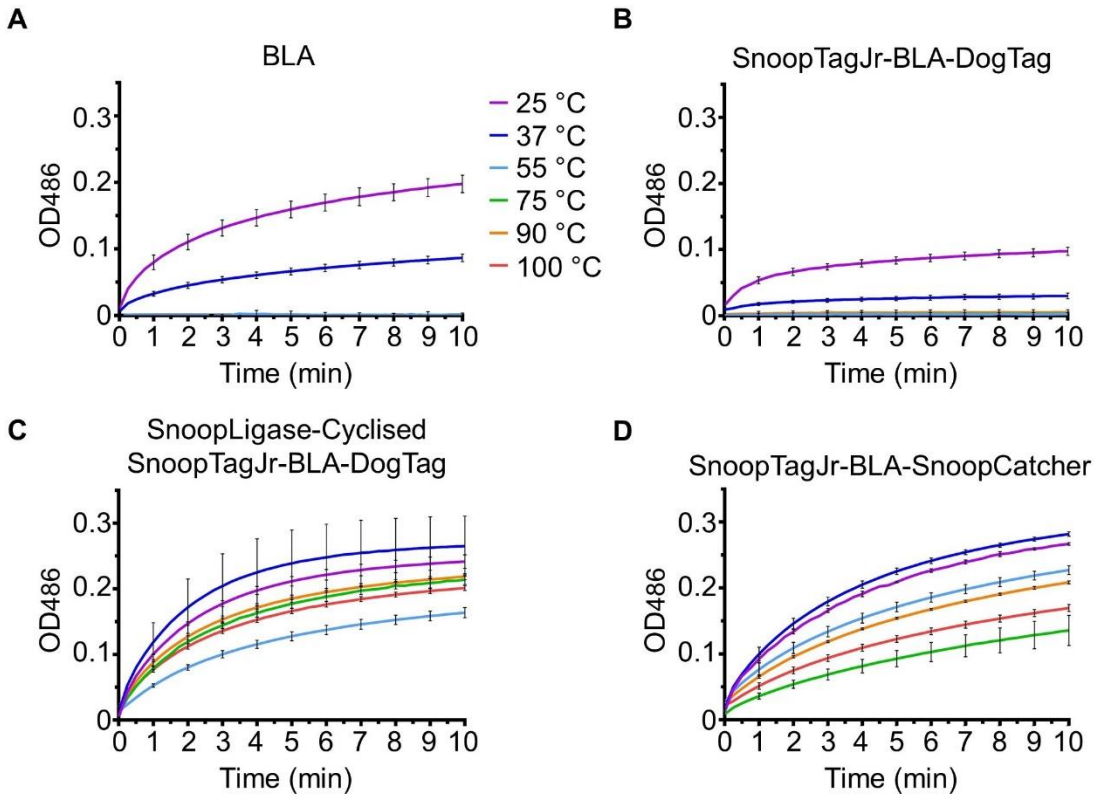

Figure 3.5 SnoopLigase cyclisation improved BLA resilience to heat-induced deactivation. BLA constructs were held at the temperatures indicated above for 10 min, cooled to 10 °C, then assayed for residual activity through colorimetric monitoring of nitrocefin hydrolysis at 20 °C. All are mean of triplicate ± 1 standard deviation. a) WT BLA activity was abolished following incubation at temperatures above 55 °C. b) Uncyclised SnoopTagJr-BLA-DogTag exhibited no improvements in thermal resilience but lower activity overall. c) SnoopLigase cyclisation conferred dramatic improvements in thermal resilience to BLA, enabling retention of activity following incubation at all temperatures. d) SnoopRing cyclisation improved BLA thermal resilience.

The conjugation of SnoopTagJr and DogTag appeared to have a solubilising effect on BLA, increasing the retained soluble fraction from 1.57 % to 79.5 %

following incubation at 37 °C (Figure 3.4b). However, this did not translate to corresponding improvements in thermal resilience to heat-induced deactivation. SnoopTagJr-BLA-DogTag was less active overall than its untagged counterpart and presented no improvement in thermal resilience, becoming effectively inactive following incubation at temperatures over 37 °C.

SnoopLigase-cyclised SnoopTagJr-BLA-DogTag demonstrated dramatic improvements in thermal resilience compared to its uncyclized counterpart and wild-type BLA and retained almost full activity throughout incubation at all temperatures, even following boiling for 10 min (Figure 3.5). SnoopLigase cyclisation was more effective than SnoopRing cyclisation at conferring thermal resilience to BLA. SnoopTagJr-BLA-SnoopCatcher retained full enzymatic activity following incubation at 25 and 37 °C, but following incubation at temperatures above 37 °C, BLA activity was compromised to varying degrees (Figure 3.5).

3.1.5 SnoopLigase Depletion Following BLA Cyclisation

During SnoopLigase cyclisation, SnoopTagJr and DogTag are ligated by SnoopLigase, which each contain a residue of the reactive triad, to reconstitute the parent RrgA domain. As a result, SnoopLigase remains stably associated to its ligation product. To investigate the effects of SnoopLigase presence following cyclisation on thermal resilience of cyclised enzymes, SnoopLigase was removed from its cyclisation product through solid-phase immobilisation.

The SnoopLigase removal method was developed by Can Buldun to enable conjugate product purification from solid-phase catalyst and unreacted substrates. SnoopLigase removal employs the biotin and streptavidin interaction, which is

widely used due to its robustness to a wide range of temperatures or pH levels and femtomolar affinity (Duan et al., 2012; Stayton et al., 1999). The SnoopLigase removal process is shown in Figure 3.6. Within this method, elution can be achieved using i) low pH (glycine), ii) 2 M imidazole or iii) SnoopTagJr:DogTag competitor peptide (Buldun et al., 2018). Solid-phase SnoopLigase could also be reused for up to eight reaction cycles without loss in reactivity, demonstrating the efficiency of SnoopLigase resin regeneration (Buldun et al., 2018).

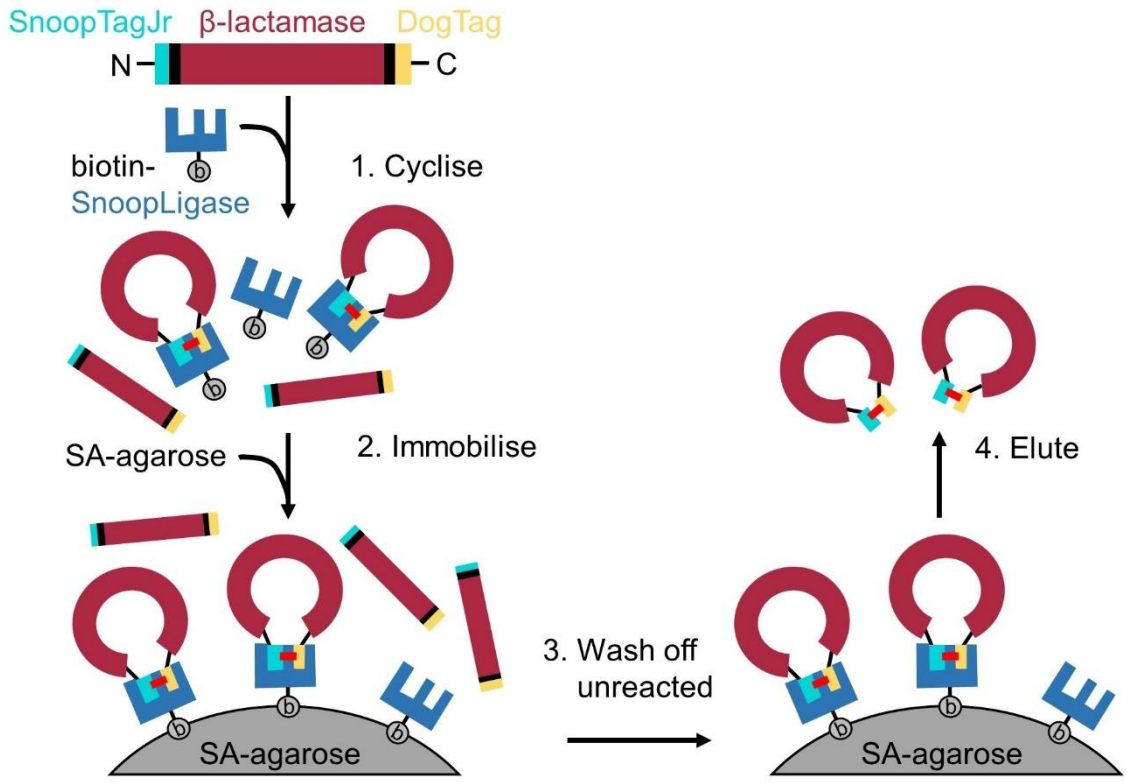

Figure 3.6 Solid-phase SnoopLigase immobilisation for cyclised enzyme purification. Enzymes with N-terminal SnoopTagJr and C-terminal DogTag are cyclised upon incubation with biotinylated SnoopLigase, which covalently links the enzyme termini. Following cyclisation, SnoopLigase is immobilised on streptavidin agarose resin, enabling washing steps to remove unreacted substrates. Subsequently, elution yields cyclised enzyme product free from linear enzyme and SnoopLigase.

SnoopLigase-cyclised SnoopTagJr-BLA-DogTag was depleted of SnoopLigase using the method outlined in Figure 3.6. Using the peptide competition method (Chapter 2.5.2.3), unreacted, uncyclized enzyme substrate was effectively washed away to allow for the elution of only cyclised BLA (Figure 3.7). The competitor peptide in the eluted product could be removed through dialysis. SnoopLigase-depleted cyclised BLA retained much thermal resilience to heat-induced deactivation and remained active following incubation at all temperatures (Figure 3.7b). Compared to its SnoopLigase-associated counterpart, the degree of resilience had been compromised. However, even following SnoopLigase removal, cyclised BLA remained more resilient than the wild-type enzyme, which was inactivated following incubation at temperatures over 37 °C.

Cyclised BLA before and after SnoopLigase removal was further assayed for solubility and activity (Figure 3.8). The removal of the associated SnoopLigase following cyclisation did not affect solubility, and both cyclised BLA constructs retained full solubility throughout heating at all temperatures (Figure 3.8a). Conversely, SnoopLigase removal negatively impacted the thermal resilience of activity of cyclised BLA (Figure 3.8b). Compared to the activity of cyclised BLA that remained associated with SnoopLigase, the activity of SnoopLigase-depleted cyclised BLA was affected to a greater degree by heat treatment. Interestingly, different methods of SnoopLigase depletion (imidazole or peptide competition) seemed to yield slightly different results (Figure 3.8b). This could be the consequence of exposure to high concentrations of imidazole, which could cause irreversible changes in enzyme conformation.

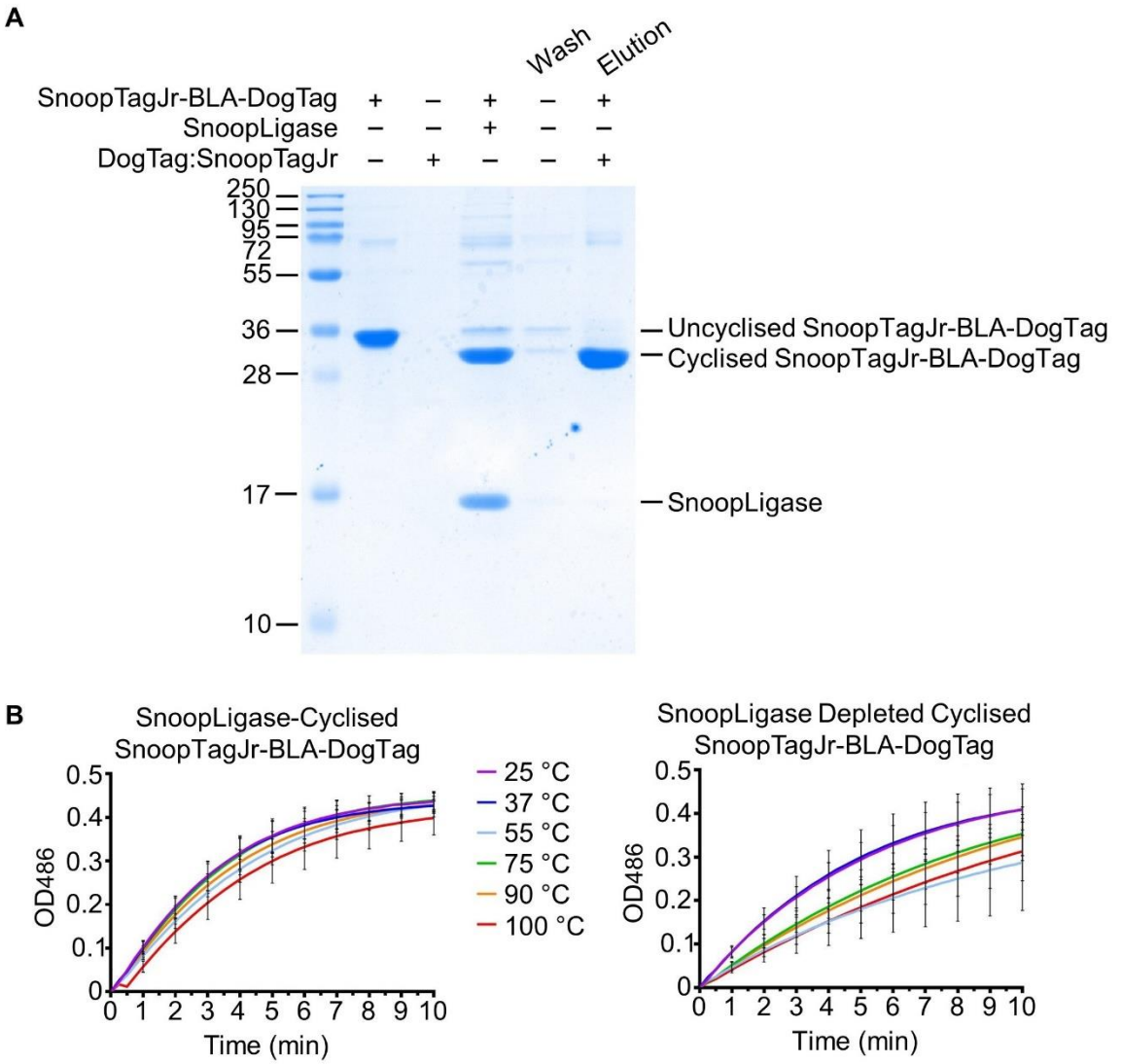

Figure 3.7 SnoopLigase could be cleanly removed from cyclised BLA without dramatic compromise in thermal resilience. a) Following cyclisation, SnoopLigase was removed from cyclised BLA using the SnoopTagJr:DogTag competitor peptide and fractions analysed by SDS-PAGE with Coomassie staining. Solid-phase immobilisation allowed efficient removal of unreacted enzyme substrate. b) Cyclised SnoopTagJr-BLA-DogTag before and after SnoopLigase removal by peptide competition were incubated at the above indicated temperatures for 10 min, cooled and used in a colorimetric assay monitoring the hydrolysis of nitrocefin. Though SnoopLigase removal negatively impacted the

degree of thermal resilience to heat-induced inactivation, SnoopLigase-removed cyclised BLA still remained more resilient than wild-type BLA.

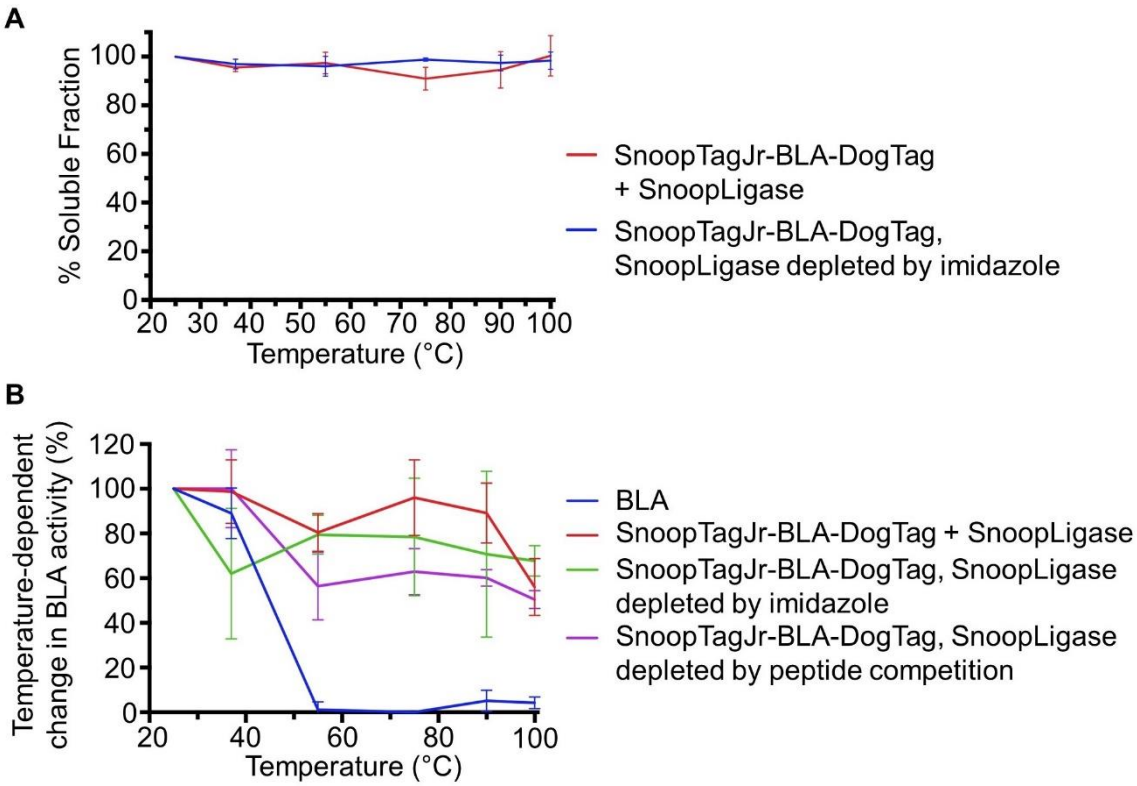

Figure 3.8 Effect of SnoopLigase removal on thermal resilience of cyclised BLA. a) SnoopLigase removal has little effect on temperature-dependent solubility of cyclised BLA, which remains soluble even after boiling for 10 min. SnoopLigase-cyclised SnoopTagJr-BLA-DogTag before and after SnoopLigase removal by imidazole depletion was incubated at the temperatures indicated above for 10 min and centrifuged to remove insoluble aggregates. The soluble protein remaining in the supernatant was quantified by SDS-PAGE. All are mean of triplicate ± 1 SD. b) BLA constructs were incubated at the temperatures shown above for 10 min, cooled to 10 °C, then assayed for residual activity through colorimetric monitoring of nitrocefin hydrolysis at 20 °C. All are mean of triplicate ± 1 SD.

3.2 SnoopLigase Cyclisation of *Bacillus subtilis* Phytase (PhyC)

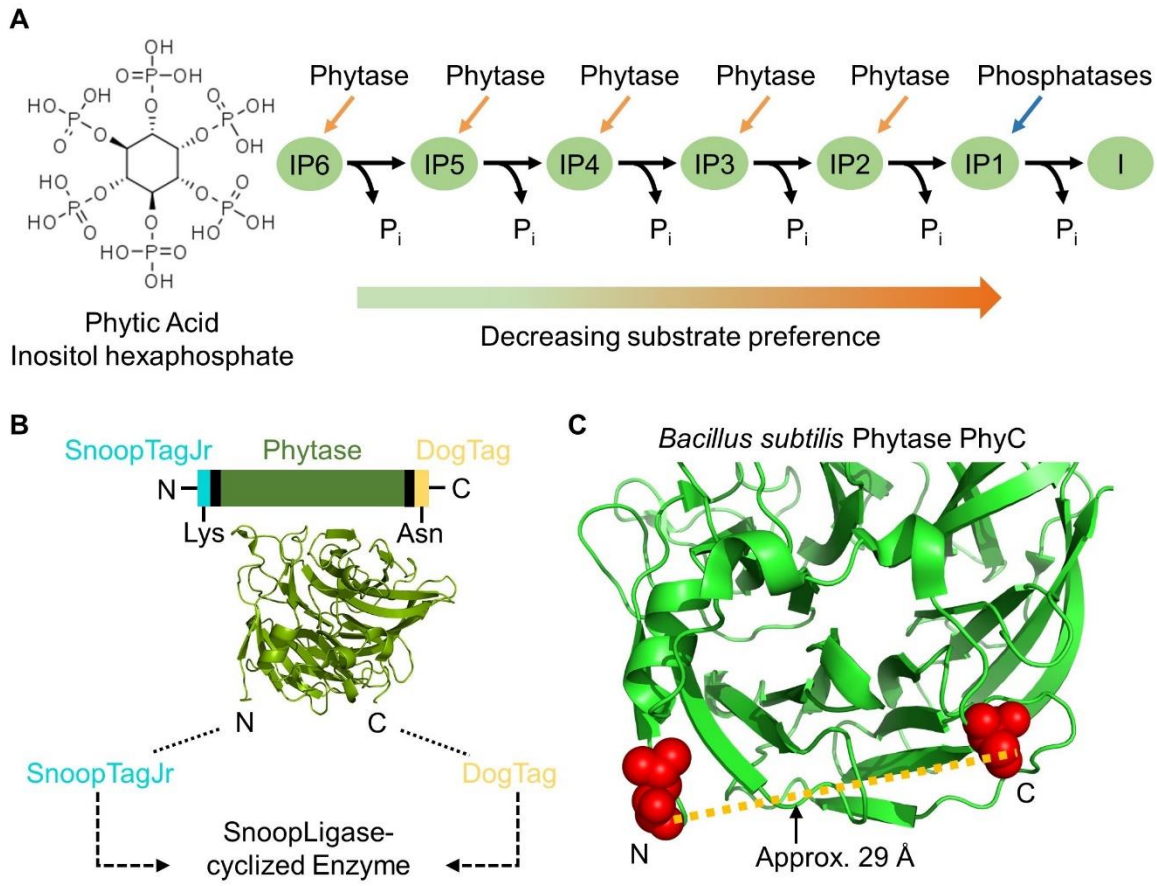

Figure 3.9 Structure and function of PhyC, and its construct design for SnoopLigase cyclisation. a) PhyC breaks down phytic acid through stepwise hydrolysis to release inorganic phosphate. PhyC has highest affinity for high-phosphate substrates and is unable to hydrolyse inositol monophosphate, whose last remaining phosphate is removed by phosphatases. b) To enable head-to-tail cyclisation upon SnoopLigase addition, SnoopTagJr was genetically encoded at the N-terminus and DogTag at the C-terminus of PhyC (Protein Data Bank 3AMR). c) The distance between the termini of PhyC is approximately 29 Å apart (measured from the Nitrogen atoms of the amine groups of the N-terminal lysine and C-terminal lysine).

Bacillus subtilis PhyC is a β-propeller phytase that attacks phytic acid and its less-phosphorylated downstream molecules to sequentially remove phosphates, thereby releasing digestible inorganic phosphate and cations that were previously bound by phytate (Shin et al., 2001). Phytic acid is the predominant form of phosphate storage in plants, accounting for up to 85% of total phosphorus in plants (Reddy et al., 1982). However, it is not only mostly indigestible by monogastric animals, but is also a potent anti-nutrient that chelates micronutrients such as iron, zinc, magnesium and manganese (Gupta et al., 2015). Consequently, up to 70% of total phosphorus in animal feed is not absorbed and excreted (Jorquera et al., 2008).

To combat this, phytase is superdosed into animal feed, which has been demonstrated to maximise the nutritional efficiency and improve feed conversion ratios (FCR) (Lee et al., 2017). Furthermore, phytase application is projected to significantly reduce the environmental footprint of the agricultural industry by displacing the need for inorganic phosphate supplementation to minimise environmental phosphorus pollution (Nielsen and Wenzel, 2007). However, despite extensive research, phytases are seldom effectively used since animal feed processing involves heating at high temperatures (often including steam treatment at over 95 °C) to eliminate pathogens (Rebello et al., 2017). Thermostable phytases are therefore highly coveted for agricultural, industrial and environmental purposes.

The *Bacillus* phytase PhyC has been shown to be thermally stabilised through intein-mediated cyclisation (Ping et al., 2010) and by SpyRing cyclisation (Schoene et al., 2016a). As a result, it was selected as a candidate for SnoopLigase cyclisation.

The catalytic action of PhyC is dependent on the presence of Ca^{2+}, and a total of six Ca^{2+} ions are present in the enzyme (Ha et al., 2000; Kerovuo et al., 2000). Of the six, three calcium ions are bound with high affinity and stabilise the enzyme structure by strengthening the inner tunnel of PhyC, which also translates to a significant increase in melting temperature by approximately 29 °C (Ha et al., 2000; Kerovuo et al., 2000). The remaining three Ca^{2+} ions bind with low affinity to the negatively charged substrate-binding cleft, which is dominated by aspartate and glutamate residues (Ha et al., 2000). Calcium binding shifts the active site to be more electrostatically favourable for phytate binding (Ha et al., 2000). Consequently, all experiments involving PhyC were conducted in buffers supplemented with $CaCl_2$.

Though the termini of PhyC are located away from the active site, they are approximately 29 Å apart, which is over 4 times greater than the distance between the termini of BLA (7 Å). This presents a greater challenge for head-to-tail cyclisation since the aim of cyclisation is to imbue backbone rigidity and constrain the enzyme to minimise conformational entropy. Forcibly joining termini that are too far apart could overly constrain the enzyme structure to hinder enzyme function. Like the BLA construct for SnoopLigase cyclisation outlined in chapter 3.1.1, PhyC was genetically fused to N-terminal SnoopTag and C-terminal DogTag with flexible $(GSG)_2$ linkers for ligation upon addition of SnoopLigase (Figure 3.10b).

3.2.1 Verification of PhyC Cyclisation

In the absence of SnoopLigase, SnoopTagJr-PhyC-DogTag remained uncyclised since SnoopTagJr and DogTag alone are unable to form an isopeptide bond. Upon incubation with SnoopLigase, SnoopTagJr-PhyC-DogTag was

successfully cyclised, as indicated by an increase in electrophoretic mobility on SDS-PAGE (Figure 3.10a). This gel shift was also observed with SnoopTagJr-BLA-DogTag upon cyclisation and is indicative of successful cyclisation (Figure 3.3).

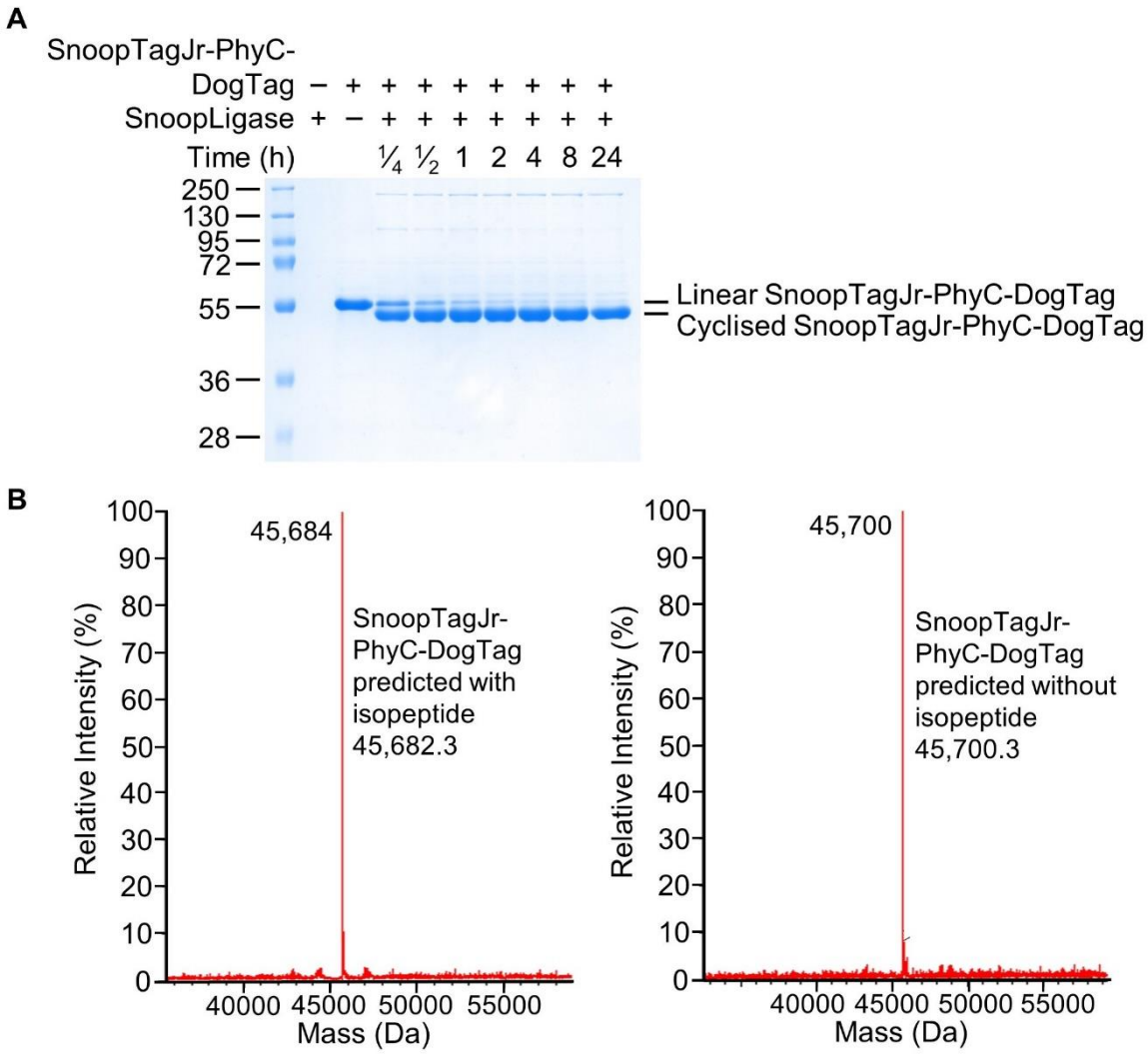

Figure 3.10 SnoopLigase efficiently cyclised SnoopTagJr-PhyC-DogTag. a) SnoopLigase efficiently cyclised PhyC, nearing completion following 4 hours. Equimolar quantities of SnoopLigase and SnoopTagJr-PhyC-DogTag were incubated at 4 °C for 0.25 – 24 h, prior to SDS-PAGE with Coomassie staining. b) Electrospray ionisation mass spectrometry was conducted on SnoopTagJr-PhyC-DogTag and SnoopLigase-removed cyclised SnoopTagJr-PhyC-DogTag. Predicted mass calculations were conducted using the ProtParam online tool.

To further verify the identity of the cyclised product, electrospray ionisation mass spectrometry (Chapter 2.4.2) was conducted on SnoopTagJr-PhyC-DogTag before and after SnoopLigase cyclisation (Figure 3.10b). Following incubation with SnoopLigase, SnoopTagJr-PhyC-DogTag lost 18 Da, corresponding to the single ammonia molecule released during the SnoopLigase transamidation reaction between SnoopTagJr and DogTag.

3.2.2 Effect on Aggregation of PhyC

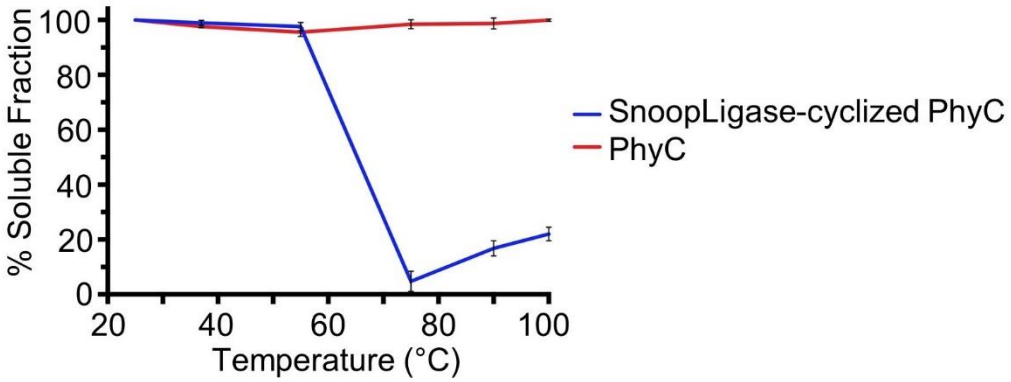

Figure 3.11 SnoopLigase cyclization increased the solubility of PhyC. PhyC constructs were incubated for 10 min at the indicated temperature and centrifuged to remove aggregates, and enzyme remaining in the supernatant was quantified by SDS-PAGE with Coomassie staining. All are mean of triplicate ± SD.

Following SnoopLigase cyclisation, SnoopTagJr-PhyC-DogTag and wild-type PhyC were incubated at 25, 37, 55, 75, 90 and 100 °C before being assayed for remaining soluble enzyme. Wild-type PhyC retained full solubility after incubation at 55 °C, but following incubation at temperatures above 55 °C, PhyC

aggregated (Figure 3.11). This suggests that the energetic trap for PhyC exists around 55 °C, such as it did for BLA at around 37 °C (Figure 3.11).

Conversely, SnoopLigase-cyclised PhyC maintained full solubility throughout all temperatures. There was little to no loss of soluble protein throughout, demonstrating the efficacy of SnoopLigase cyclisation in conferring resilience to heat-induced aggregation (Figure 3.11).

3.2.3 Effect on Thermal Resilience of PhyC Activity

Phytase activity, and therefore the hydrolysis of phytic acid, was measured by quantifying the phosphate release over time. Phytase hydrolysis of phytic acid releases orthophosphate, which complexes with ammonium molybdate to subsequently form the malachite green phosphomolybdate complex, producing a colorimetric reaction. This was achieved using Biomol Green (Enzo Life Sciences), a reagent based on the malachite green assay for phosphate detection (Feng et al., 2011).

Wild-type PhyC remained fully active following incubation at temperatures up to 55 °C but became inactivated at all higher temperatures (Figure 3.12). This was consistent with the solubility data in figure 3.11, in which PhyC aggregated at temperatures above 55 °C. Uncyclised SnoopTagJr-PhyC-DogTag demonstrated no improvement in thermal resilience to heat-induced inactivation, demonstrating that the conjugation of peptide tags does not improve thermal resilience of enzymatic activity. However, SnoopLigase-cyclised PhyC showed a dramatic improvement in thermal resilience and remained fully active throughout incubation at all temperatures, even following boiling for 10 min.

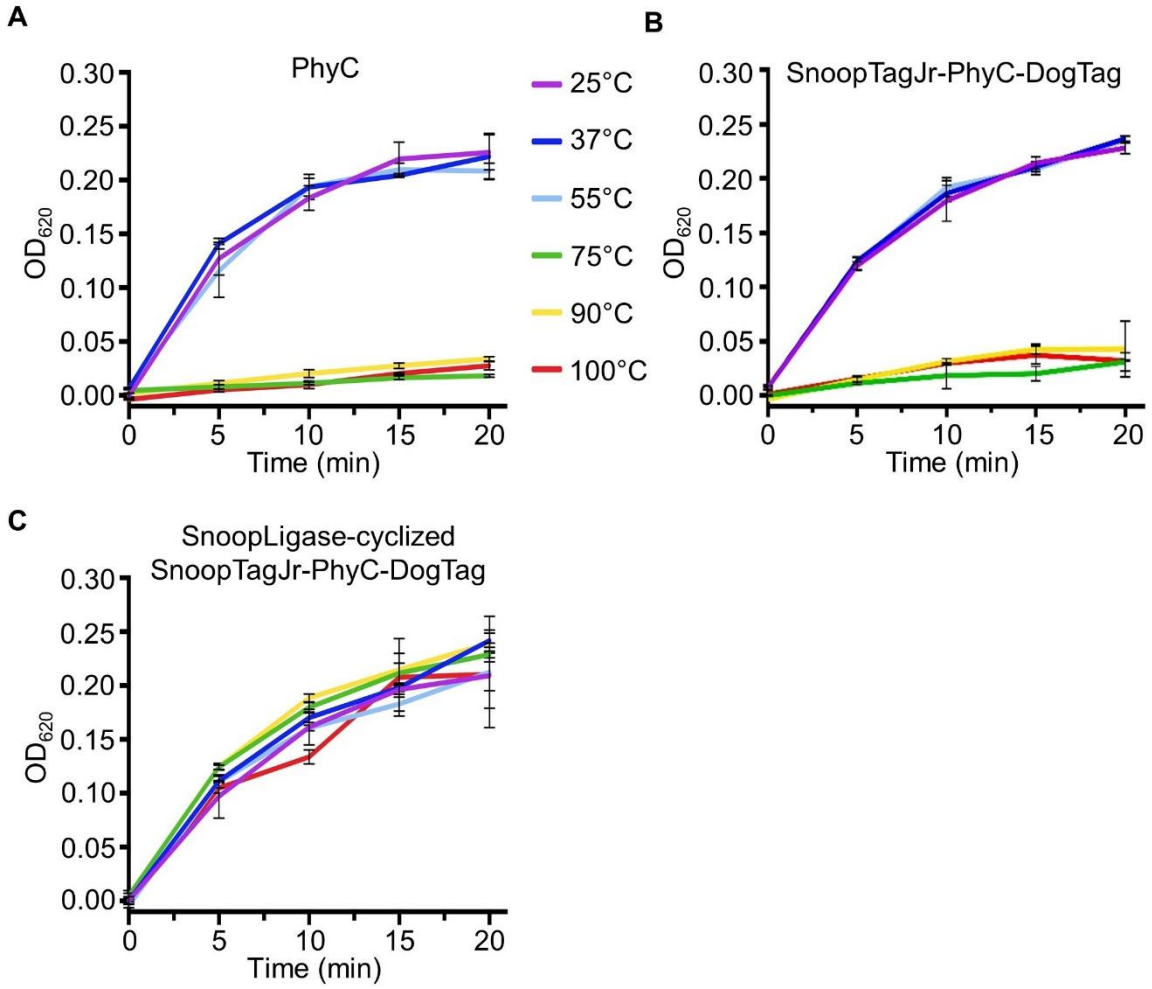

Figure 3.12 SnoopLigase cyclisation improved thermal resilience of PhyC. PhyC constructs were incubated at the above indicated temperatures for 10 min, cooled to 10 °C and used in a colorimetric assay to quantify phosphate release from phytic acid hydrolysis (Chapter 2.6.3). All are mean of triplicate ± 1 SD. a) PhyC activity was abolished following incubation at temperatures over 75 °C. b) Uncyclised SnoopTagJr-PhyC-DogTag exhibited no improvements in thermal resilience. c) SnoopLigase-cyclised PhyC exhibited improvements in thermal resilience, enabling retention of full activity throughout incubation at all temperatures.

3.2.4 SnoopLigase Depletion Following PhyC Cyclisation

The dramatic improvement in thermal resilience from uncyclised SnoopTagJr-BLA-DogTag and SnoopTagJr-PhyC-DogTag and their SnoopLigase-cyclised counterparts in figure 3.5 and figure 3.12 highlights the importance of cyclisation in conferring such improvements. Since SnoopLigase remains stably associated to its conjugate product, assayed SnoopLigase-cyclised enzymes are likely to be in their SnoopLigase-bound form following cyclisation.

Being bound to a larger, stable protein domain has been shown to impart thermal stability to enzymes. Notably, chaperone proteins have been applied to confer resilience, such as the well-studied GroEL/GroES and DnaK proteins, which are heat shock proteins from *E. coli* (Kohda et al., 1996). This was demonstrated on the penicillin amidase-rTHS (single-subunit Group II chaperonin from *Methanocaldococcus jannaschii*) enzyme-chaperone chimera (Bergeron et al., 2009). The chimera not only demonstrated a rate of turnover 2.8-fold greater than enzymes lacking the chaperone domain, but also remained active for 3 times longer than non-chimeric penicillin amidase in 32% methanol (Bergeron et al., 2009). The study further showed that fusion to chaperones aids all reversibly unfolded species to refold correctly (Bergeron et al., 2009).

In addition to fusion proteins to chaperones, simply fusing proteins to maltose binding protein (MBP) has been shown to enhance solubility and even impart resilience. Fusion of passenger proteins including GFP, DHFR and TEV protease to *E. coli* MBP yielded the highest percentage of soluble protein compared to His_6-tagged or His_6-GST-tagged counterparts (Raran-Kurussi and Waugh, 2012). The capacity of MBP to enhance solubility has been documented for MBP from a diverse range of bacteria, from *Pyrococcus furiosus* to *Thermotoga maritima* (Fox

et al., 2003). The study found that thermophilic PfuMBP (maltodextrin binding protein from *Pyrococcus furiosus*) is an even more potent solubility enhancer than *E. coli* MBP (Fox et al., 2003).

Given SnoopLigase (13.3 kDa) is a stable protein domain that is substantially larger than peptide tags, the improvement in thermal resilience observed in SnoopLigase-cyclised BLA and PhyC could be attributed to not only the cyclisation itself, but also the stabilising effect of the bound SnoopLigase. To better understand the individual contributions of the cyclisation and the SnoopLigase binding to the total observed improvement in thermal resilience, SnoopLigase was removed following cyclisation of SnoopTagJr-PhyC-DogTag and the resulting construct was assayed for solubility and activity (Figure 3.13).

SnoopLigase removal following cyclisation has a minimal impact on solubility, and SnoopLigase-removed cyclised PhyC retains solubility throughout heating at all temperatures (Figure 3.13). This suggests that SnoopLigase binding is not critical in conferring resilience to heat-induced aggregation, potentially due to the solubilising effect of the peptide tags as seen in figure 3.4. However, SnoopLigase depletion has a greater effect on the thermal resilience to heat-induced inactivation of PhyC. Following SnoopLigase removal, cyclised PhyC exhibited reduced activity following incubation at 75 and 90 °C, with the greatest reduction in activity following boiling for 10 min (Figure 3.13).

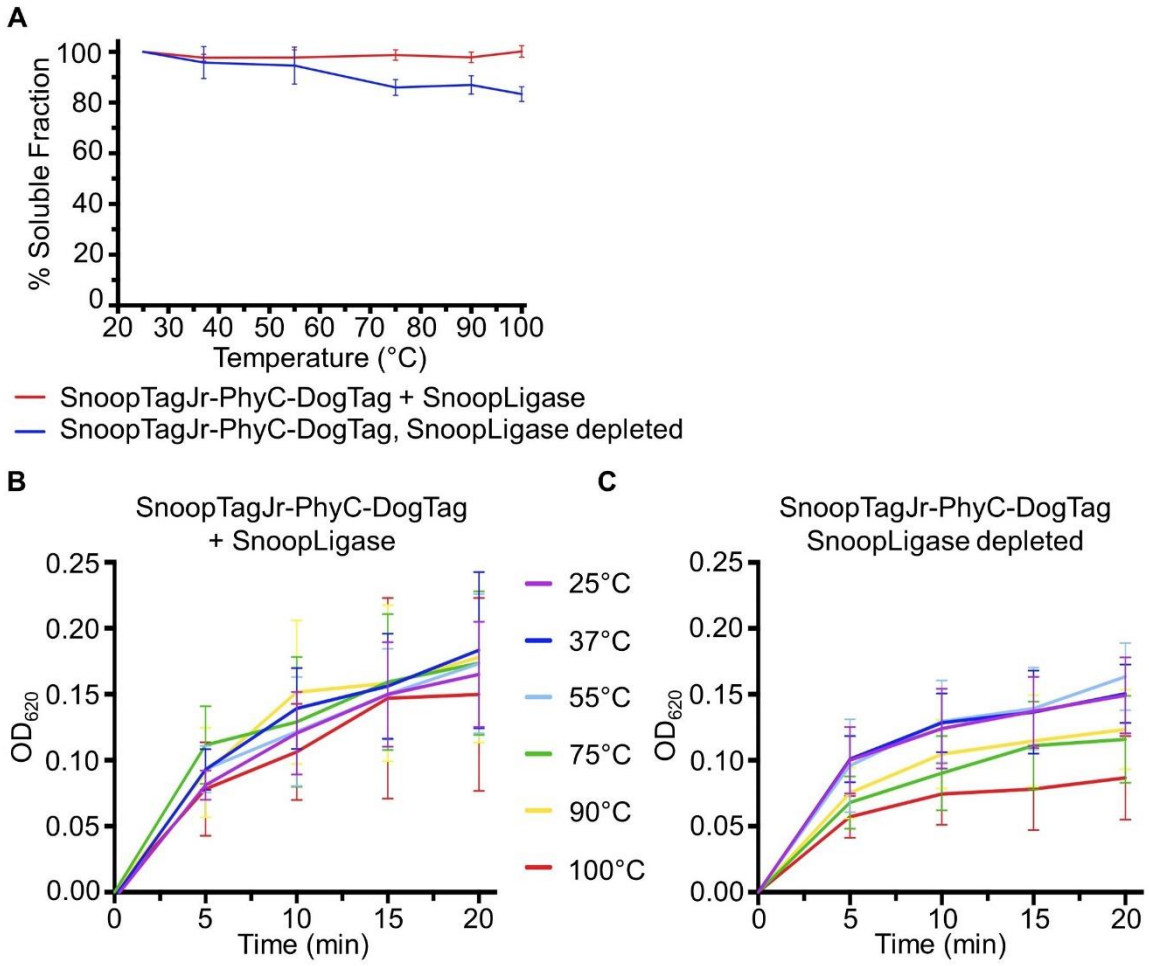

Figure 3.13 Effect of SnoopLigase depletion on cyclised PhyC. (a) Cyclized PhyC before and after SnoopLigase removal by imidazole elution was incubated for 10 min at indicated temperatures. Samples were centrifuged to remove aggregates and then soluble protein in the supernatant was quantified. Results are mean of n=6 ± 1 SD. (b) Cyclized PhyC before SnoopLigase removal was incubated at the indicated temperatures for 10 min, cooled to 10 °C and used in colorimetric assays to quantify phosphate release from the hydrolysis of phytic acid. Results are mean of n=9 ± 1 SD. (d) SnoopLigase removal compromised the thermal resilience of enzymatic activity of cyclized PhyC. Cyclized PhyC following SnoopLigase removal by imidazole was incubated at the indicated temperatures for 10 min at the indicated temperatures, cooled to 10 °C and used in colorimetric

assays to quantify phosphate release from the hydrolysis of phytic acid. Results are mean of n=9 ± 1 SD.

3.2.5 Comparison to SpyRing-Cyclised PhyC

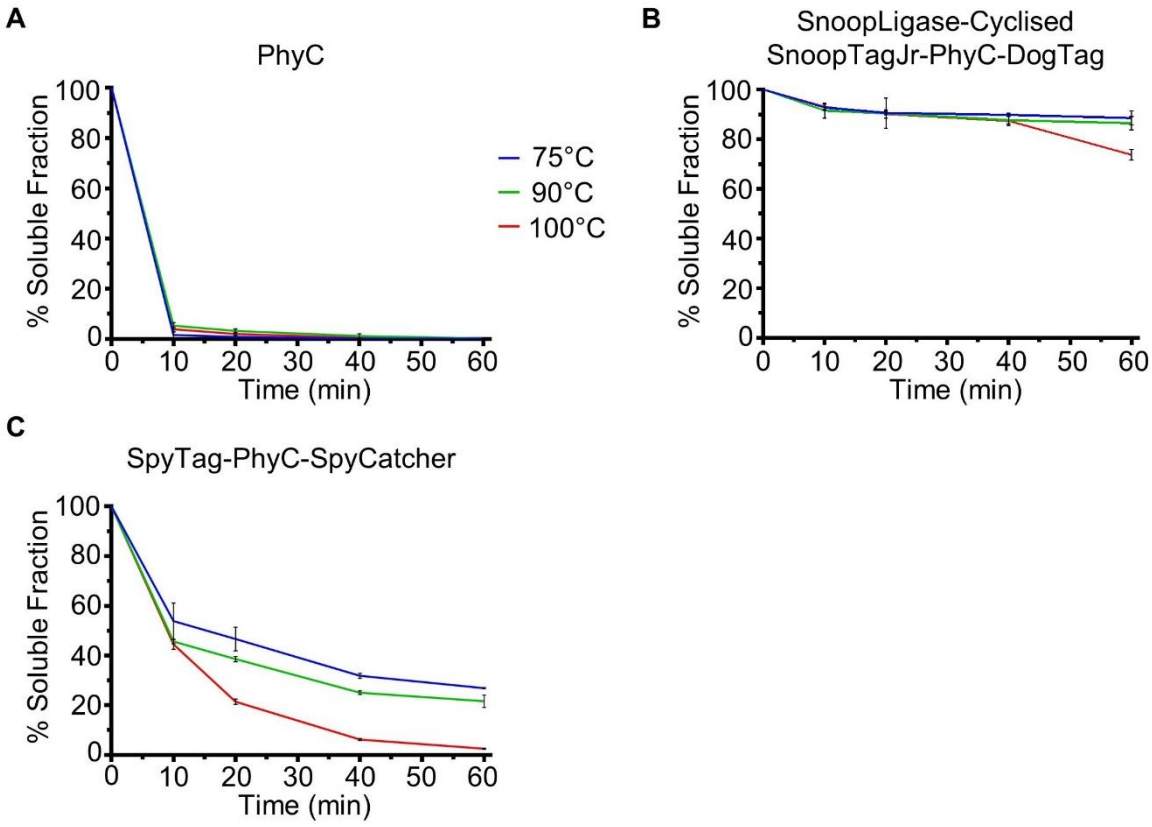

Figure 3.14 SnoopLigase cyclisation was superior to SpyRing in conferring thermal resilience to PhyC. PhyC constructs were heated to 75, 90 and 100 °C for 10, 20, 40 and 60 min, cooled to RT and centrifuged to remove insoluble aggregates. The supernatant was assessed for remaining soluble enzyme using SDS-PAGE with Coomassie staining. All are mean of triplicate ± 1 SD. (a) Wild-type PhyC aggregated following 10 min at all temperatures. (b) SnoopLigase-cyclised PhyC retained solubility throughout heating, and even remained mostly soluble following 1 h at 100 °C. (c) SpyRing-cyclised PhyC was more resilient to aggregation than wild-type PhyC, but aggregated completely following 1 h at 100 °C.

Previously, the SpyRing has been reported to confer solubility to PhyC by Chris Schoene (Schoene et al., 2016a). To better distinguish the superior cyclisation strategy for imparting thermal resilience to PhyC, constructs were heated for longer periods of time before assaying for soluble fraction remaining (Figure 3.14). Wild-type PhyC completely aggregated at all three temperatures, whereas both cyclisation methods resulted in the retention of soluble PhyC, demonstrating the effectiveness of both cyclisation strategies.

However, SpyRing-cyclised PhyC aggregated more than its SnoopLigase-cyclised counterpart. SpyRing-cyclised PhyC retained 27%, 22% and 2.5% solubility following 1 h at 75, 90 and 100 °C. On the other hand, SnoopLigase-cyclised PhyC retained 89%, 86% and 74% solubility following an hour at 75, 90 and 100 °C, respectively. This demonstrates the exceptional thermal resilience to heat-induced aggregation conferred by SnoopLigase cyclisation, which greatly outperforms that conferred by the SpyRing.

3.2.6 Thermal Resilience in Dialysed Cleared Lysate

A long-term goal of enzyme stabilisation is to allow for its effective application to industry. In engineering and selecting enzyme candidates for industrial use, many process design criteria are evaluated, including increased thermostability, selectivity and/or stability in organic solvents (Bornscheuer et al., 2012). Of all process design criteria, often the most desired is thermal stability since biocatalysts must be able to withstand large-scale reactor environments and a wide range of reaction conditions without denaturation or inactivation.

This is particularly the case in engineering phytases for superdosing into animal feed. During formulation, the enzymes are exposed to a myriad of different substances and are subject to temperatures up to 95 °C during pelleting (Rebello et al., 2017). Most laboratory experiments measuring thermal resilience to aggregation and inactivation are conducted under conditions optimal for enzyme function. Often, only the enzyme, its substrate, cofactors and compounds necessary for assay readout are present in the optimal activity buffer. Such simple conditions do not faithfully replicate the industrial conditions to which the enzyme will be subjected.

To test the ability of SnoopLigase cyclisation to confer thermal resilience in reaction conditions closer to those found in the animal feed industry, cyclised PhyC constructs were assayed following heating in the presence of 0.2 % bovine serum albumin (BSA). BSA was supplemented to mimic the presence of extraneous proteins during the pelleting of animal feed. Heating SpyRing-cyclised constructs in the presence of 0.2% BSA produced a dramatic reduction in thermal resilience, and the observed resilience was now more comparable to wild-type PhyC (Figure 3.15). As a result, in the presence of 0.2% BSA, SpyRing cyclisation was ineffective at imparting thermal resilience to PhyC.

The thermal resilience of SnoopLigase-cyclised PhyC was also slightly compromised following heating in the presence of 0.2% BSA, but PhyC still remained active following incubation at all temperatures. Even in the presence of BSA, SnoopLigase-cyclised PhyC demonstrated a degree of thermal resilience that was significantly improved over its wild-type counterpart (Figure 3.15). This suggests that SnoopLigase cyclisation is a more robust strategy whose stabilising effects are better able to withstand heating in the presence of extraneous proteins.

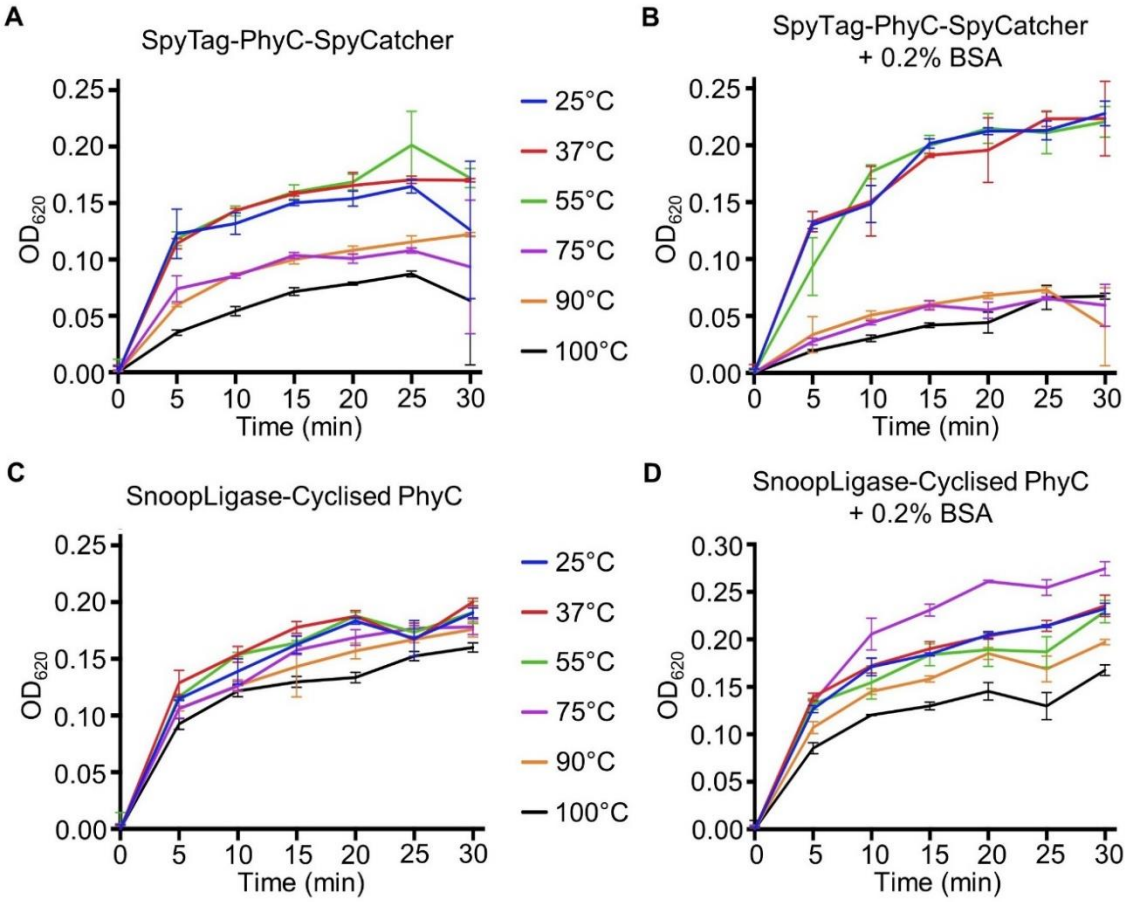

Figure 3.15 Thermal resilience conferred by SnoopLigase cyclisation is more robust during heating with BSA. PhyC constructs were heated with and without 0.2% BSA at the above indicated temperatures before use in a colorimetric assay to quantify phosphate release from phytic acid hydrolysis. All are mean of triplicate ± 1 SD. (a) SpyRing-cyclised PhyC exhibited improvements in thermal resilience and resisted complete inactivation following incubation at all temperatures. (b) SpyRing-cyclised PhyC lost all improvements in thermal resilience over the wild-type enzyme in the presence of 0.2% BSA. (c) SnoopLigase cyclised-PhyC demonstrated improvements in thermal resilience and retained full activity throughout heating at all temperatures. (d) SnoopLigase cyclised-PhyC retained improvements in thermal resilience even in the presence of 0.2% BSA and resisted inactivation at all temperatures.

However, it has been shown that the inherent “stickiness” of BSA leads BSA to complex with stressed proteins to reduce aggregation during heat stress (Finn et al., 2012). The observed anti-aggregation activity of BSA is not conducive to recreating the additional stress placed on phytase by the presence of extraneous proteins during pelleting at 95 °C. Therefore, the stress placed on PhyC during heating in previous assays by BLA (figure 3.15) was too little to mimic real-life conditions.

To better replicate real-life conditions of industrial pelleting, PhyC constructs were heated in dialysed cleared lysate (DCL) and assayed for activity (Chapter 2.6.6). Since phytases are expressed by yeast in the animal feed industry and are therefore secreted into the media in the presence of many extraneous proteins and compounds, *E. coli* cleared lysate was chosen to mimic such reaction conditions. The lysate was dialysed prior to use in phytase assays to remove free phosphates that would affect the readout of the assays.

As observed in the presence of 0.2% BSA (Figure 3.15), the thermal resilience to inactivation of SpyRing-cyclised PhyC was greatly compromised upon heating in DCL (Figure 3.16). SpyRing-cyclised PhyC was inactive following incubation with DCL at temperatures above 55 °C, demonstrating no improvement in thermal resilience over the wild-type enzyme. SnoopLigase-cyclised PhyC, on the other hand, retained thermal resilience and remained active following incubation with DCL at all temperatures. SnoopLigase-cyclised PhyC only exhibited a slight compromise in activity following boiling in DCL for 10 min, demonstrating its robustness (Figure 3.16).

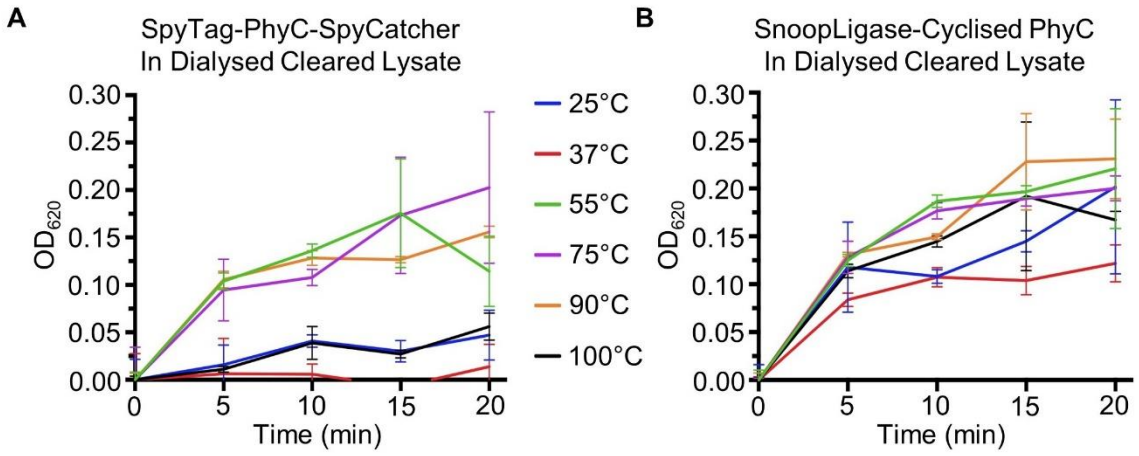

Figure 3.16 Thermal resilience conferred by SnoopLigase cyclisation is robust during heating in DCL. SpyRing and SnoopLigase-cyclised PhyC was heated in 5 mg/mL dialysed cleared lysate to the temperatures indicated above before use in a colorimetric assay to quantify phosphate release from phytic acid hydrolysis. All are mean of triplicate ± 1 SD.

3.3 Discussion

Enzyme stabilisation is most often a requirement prior to application in industry due to the rigors of biotechnological processing. Head-to-tail cyclisation presents an industrially viable method for the thermal stabilisation of enzymes because solid supports are not required, since they are often too expensive for large-scale manufacturing (DiCosimo et al., 2013). Limitations of currently available cyclisation approaches include long incubation times, low cyclisation efficiency and inability to separate uncyclized substrate from cyclised enzyme (Antos et al., 2009a, 2009b; Tarasava and Freisinger, 2014). As a result, there is a need for highly efficient cyclisation systems that confer exceptional improvements in thermal resilience to a wide range of enzymes.

The SnoopLigase platform, developed by Can Buldun, is a protein conjugation system derived through tripartite splitting of the RrgA C-terminal domain. SnoopTagJr and DogTag are covalently ligated upon incubation with SnoopLigase, effectively recreating the parent domain (Buldun et al., 2018). SnoopTagJr and DogTag were placed on the N- and C-termini, respectively, of mesophilic enzymes BLA and PhyC. SnoopTag and DogTag-flanked BLA and PhyC were efficiently cyclised by SnoopLigase to produce monomeric cyclised enzyme species.

SnoopLigase cyclisation imparted BLA and PhyC with exceptional thermal resilience to heat-induced aggregation and deactivation. The conjugation of peptide tags alone was solubilising and enabled BLA to resist aggregation to a limited degree, but cyclisation was necessary to exploit full thermal resilience. SnoopLigase-cyclised BLA and PhyC were able to resist aggregation and retain catalytic activity even after boiling for 10 min, demonstrating dramatic improvements in thermal resilience compared to their wild-type counterparts.

In testing the thermal resilience of BLA constructs, both solubility and activity were most compromised following incubation at 37 °C. This suggests that in the protein folding landscape of BLA, there exists an energetic trap such that around 37 °C, there is just enough energy in the system to be permissive for irreversible aggregation and subsequent deactivation, but insufficient energy to be permissive for leaving this energetic trap. Therefore, at higher temperatures, the presence of more thermal energy would increase the ability of constructs to more freely navigate the folding landscape to escape the energetic trap and therefore not become insoluble to account for the observed increase in soluble fraction.

SnoopLigase cyclisation proved superior to SpyRing cyclisation not only during longer incubations at high temperatures, but also during heating in the presence of extraneous proteins. PhyC constructs were heated in dialysed cleared lysate to mimic fermentation formulation and pelleting conditions employed in the animal feed industry. Under such conditions, SnoopLigase-cyclised phytase was able to retain thermal resilience, whereas SpyRing-cyclised phytase lost thermal resilience and performed similarly to the wild-type enzyme.

Mechanism of Thermal Stabilisation in SnoopLigase Cyclisation

Gaining a better understanding of the mechanism through which SnoopLigase cyclisation confers thermal resilience is important in understanding how the system can be improved, and for predicting the enzymes that can be effectively stabilised using SnoopLigase. SnoopLigase cyclisation effectively conferred resilience to BLA and PhyC, enzymes that were previously improved by SpyRing, an alternate isopeptide-mediated cyclisation strategy (Schoene et al., 2016a). SpyRing-cyclised enzymes showed comparatively small increases in T_m, but instead conferred thermal resilience by increasing the reversibility of heat-induced unfolding (Schoene et al., 2016a). This reversibility could be due to the isopeptide bond, which may serve as a point of reference for protein refolding. This has been observed in covalent multipoint attachment of enzymes or stabilisation, in which the attachment loci serve to facilitate the recovery of proper folding and activity (Miranda et al., 2011).

If SnoopLigase and SpyRing cyclisation both confer thermal resilience through the shared mechanism of increasing the reversibility of heat-induced

unfolding, it is interesting that SnoopLigase-cyclised phytase was more robust following longer heating and heating in the presence of extraneous proteins. If the isopeptide bond serves as the reference point, it is also possible that the robustness and rigidity of the domains surrounding the isopeptide bond also contribute to the efficacy of the reference point in aiding refolding. It was originally demonstrated that SpyTag-SpyCatcher unfolds at 88 °C and SnoopTag-SnoopCatcher unfolds at 70 °C (Schoene et al., 2016b). However, SnoopLigase has undergone significant engineering, including β-turn stabilisation by proline and fold stabilisation by Rosetta-generated mutations (Buldun et al., 2018). As a result, it is possible that SnoopLigase is more structurally rigid than SpyTag-SpyCatcher, and therefore is better at bolstering isopeptide bond-mediated refolding. This rigidity and compactness of structure would also enable SnoopLigase to be less affected by extraneous aggregated proteins, as was evidenced.

In addition, though SnoopLigase remains stably associated with its conjugate product, it is not covalently bound to the cyclised enzyme. As a result, it is possible that at high temperatures, SnoopLigase dissociates from the cyclised enzyme to act as a free chaperone-like entity. By associating with multiple cyclised enzymes in this way, one SnoopLigase molecule may be able to reinforce the reversibility of denaturation in multiple enzymes to result in the superior robustness of thermal resilience observed.

Observed Advantages of SnoopLigase Cyclisation

This observed superior ability of SnoopLigase to confer thermal resilience to PhyC under mimicked reaction conditions is especially promising due to the

industrial and agricultural value of phytase. However, SnoopLigase-cyclised PhyC is not directly applicable to the animal feed industry due to the low specific activity (< 100 U/ mg) of PhyC (Gen Lei et al., 2012; Guerrero-Olazarán et al., 2010; Kerovuo et al., 1998; Rao et al., 2008). Phytases with low specific activities require more enzyme production to match the same degree of catalysis, thereby increasing manufacturing costs. As a result, phytases with higher specific activities are preferred for commercial application to animal feed, such as those from *Aspergillus niger*, *E. coli*, *Peniophora lycii* and *Citrobacter braakii* (Dersjant-Li et al., 2015). To produce a SnoopLigase-cyclised thermally resilient phytase that is more conducive to commercialisation, it should be applied on a phytase with high specific activity such as the *E. coli* AppA phytase or the *A. niger* PhyA phytase.

In addition to producing a promising platform for phytase stabilisation, SnoopLigase cyclisation also addressed critical limitations of previous cyclisation methods, such as the SpyRing. Other cyclisation methods including intein- or sortase-mediated head-to-tail cyclisation yield a mixture of linear and cyclic species that cannot be separated due to the small difference in molecular weight (Tarasava and Freisinger, 2014; Voloshchuk et al., 2017). However, the SnoopLigase system enabled the removal of SnoopLigase and uncyclized substrate following cyclisation to cleanly elute only cyclised enzyme and to enable ligase recycling (Buldun et al., 2018).

Furthermore, SnoopLigase cyclisation circumvented the fusion of a larger protein domain such as in SpyRing cyclisation to minimise the likelihood of hindered catalytic activity. In addition, the SnoopTag and DogTag-flanked enzymes can only be cyclised upon SnoopLigase addition, enabling temporal control over the cyclisation mechanism, unlike in other cyclisation technologies.

Future Work

Though SnoopLigase addressed the above limitations of currently available cyclisation strategies, SnoopLigase cyclisation was only trialled on BLA and PhyC, monomeric, mesophilic enzymes whose termini are in relative proximity (< 29 Å) and whose thermal resilience was previously improved by SpyRing cyclisation (Schoene et al., 2014, 2016a). To better understand the range of enzymes on which SnoopLigase cyclisation would confer thermal resilience, SnoopLigase cyclisation should be tested on enzymes that have not been successfully stabilised using other methods (including multimeric enzymes and enzymes whose termini are further apart).

Currently, the range of enzymes that can be stabilised by cyclisation is relatively small and is limited to monomeric enzymes whose termini are in relative proximity, located away from the active site (Schoene et al., 2016b). However, there exist many commercially coveted enzymes whose termini are located on opposite ends of the tertiary structure, such as many acid phosphatases (Guddat et al., 1999; Kostrewa et al., 1999). In the case of these enzymes, conjugation of the termini would be ineffective since it would contort and constrain the protein backbone excessively, and further potentially occlude the active site. In such cases, the ability of DogTag to maintain reactivity upon insertion into protein domains could be exploited to enable SnoopLigase-mediated intramolecular peptide-peptide locking (Buldun et al., 2018). This would extend the range of enzymes that could be effectively stabilised by isopeptide bond-forming conjugation systems.

Chapter 4: Cyclisation of Enzymes with Greater Distances Between Termini

Protein N- and C- termini are surface-exposed, flexible and often located in proximity to each (Thornton and Sibanda, 1983). Approximately 30% of all proteins have termini located within 20 Å of each other, and approximately 11% have termini located within 15 Å (Trabi and Craik, 2002). As a result, a wide range of enzymes are potential targets for stabilisation by head-to-tail cyclisation (Schoene et al., 2016b; Trabi & Craik, 2002). This is reflected in the many enzymes that have been successfully stabilised by cyclisation technologies, outlined in chapter 1, of which the greatest distance between termini was found in PhyC (29 Å).

In the previous chapter, I described two such successful cases: BLA and PhyC were flanked by an N-terminal SnoopTagJr and C-terminal DogTag, which led to cyclisation upon incubation with SnoopLigase. SnoopLigase cyclisation conferred dramatic improvements in thermal resilience, enabling both enzymes to retain solubility and activity after exposure to temperatures as high as 100 °C. Nevertheless, both BLA and PhyC are small (< 46 kDa) enzymes whose termini are no further apart than 29 Å (Schoene et al., 2014, 2016a).

However, there are also commercially and industrially valuable enzymes that require thermal stabilisation whose termini are not in close apposition (< 29 Å). One such enzyme is the AppA phytase from *E. coli* (1,700 U/ mg), which has been the basis for engineered phytase products from Danisco Animal Nutrition (Phyzyme XP), AB Vista (Quantum, Quantum Blue) and Huvepharma (OptiPhos) due to its high specific activity (Gen Lei et al., 2012; Speight, 2016). SnoopLigase-cyclised

Bacillus phytase exhibited greatly improved thermal resilience and remained active even after boiling in steam treatment-mimicking conditions (Buldun et al., 2018). Despite this, SnoopLigase-cyclised PhyC is not suitable for commercialisation due to the low specific activity (< 100 U/ mg) of PhyC (Guerrero-Olazarán et al., 2010; Kerovuo et al., 1998; Rao et al., 2008).

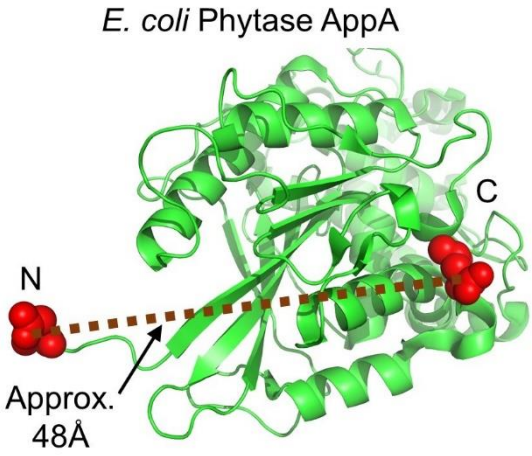

Figure 4.1 Distance between termini of AppA. The termini of the *E. coli* phytase AppA are located approximately 48 Å apart (PDB 1DKQ). The distance was measured from the amine group of the N-terminal glutamine to the amine group of the C-terminal leucine.

Consequently, a thermally stabilised, high specific activity phytase such as AppA would be highly coveted and directly applicable to the animal feed industry. However, the distance between the termini of AppA is 48 Å (based on PDB 1DKQ), which greatly exceeds the inter-termini distance (29 Å) of all enzymes stabilised by cyclisation (Figure 4,1). Therefore, the thermal stabilisation of AppA by head-to-tail cyclisation presents a novel challenge.

In this chapter, I describe the application of the SnoopLigase cyclisation system to AppA, in conjunction with a panel of structured linkers. The structured linkers were trialled to facilitate the bridging of the 48 Å distance between AppA termini for SnoopLigase cyclisation without causing excessive structural disruption.

4.1 Cyclisation of *Escherichia coli* phytase AppA

Locking of the N- and C-termini through cyclisation reduces the entropy of the denatured state and imbues rigidity to the protein backbone, thereby stabilising the native structure of the protein (Flory, 1956; Purkayastha and Kang, 2019). However, the demonstrated efficacy of SnoopLigase cyclisation has been limited to proteins whose termini are no further apart than 29 Å. Since the SnoopLigase system relies on the locking of genetically encoded peptide tags SnoopTagJr (12 residues) and DogTag (23 residues) by SnoopLigase for cyclisation, the peptides themselves do not contribute greatly to the physical bridging of the distance between the protein termini. Limiting enzyme flexibility has often been demonstrated to hinder both protein stability and function (Teilum et al., 2011).

To prevent these issues, suitable linkers must be used in conjunction with SnoopLigase cyclisation. There are three types of linkers: flexible, rigid and cleavable, of which the first two should be considered for such purposes (Chen et al., 2012). Cleavable linkers were not explored since enzyme stability conferred by cyclisation would be reversed upon cleavage. This reversibility of resilience introduced by cleavable linkers is not suited for the purposes of robust thermal resilience. Flexible (glycine and serine) linkers are unstructured and would exert no stabilising effects (Chen et al., 2012; Klein et al., 2014). Since highly structured,

well-folded protein domains have been shown to positively affect the stability and folding of neighbouring domains, rigid linkers are likely to be most effective (Batey and Clarke, 2006; Batey et al., 2008). Therefore, bridging the 48 Å gap with structured linkers would not only allow suitable enzyme mobility but also encourage the cooperative folding of enzyme domains to enhance thermal resilience (Batey and Clarke, 2006).

Linkers were assessed for their stability and scalability such that they would help the thermal stabilisation conferred by SnoopLigase cyclisation and be tunable to a range of distances between termini by altering the number of repeats. Three such candidates were identified: the L9 linker (Kuhlman et al., 1997), the consensus tetratricopeptide repeat (cTPR) linker (Main et al., 2003) and the leucine-rich repeat (LRR) linker (Park et al., 2015) (Figure 4.2).

Firstly, the L9 linker is a 34-residue α-helix from the *Bacillus stearothermophilus* ribosomal protein L9 (residues 41 – 74) (Kuhlman et al., 1997). It is ellipsoidal and spans around 50 Å, which should cover the distance between the termini of AppA (Kuhlman et al., 1997). The L9 helix is unusually stable for an isolated α-helix, and has been demonstrated to be 85% helical at 1 °C and 68% helical at 25 °C (Kuhlman et al., 1997). The L9 linker was shown to be effective in joining carbohydrate recognition domains and prevented their lateral movement with its rigidity (Earl et al., 2011). This demonstrated rigidity and stability shows promise for the application of L9 to the thermal stabilisation of AppA in conjunction with SnoopLigase cyclisation.

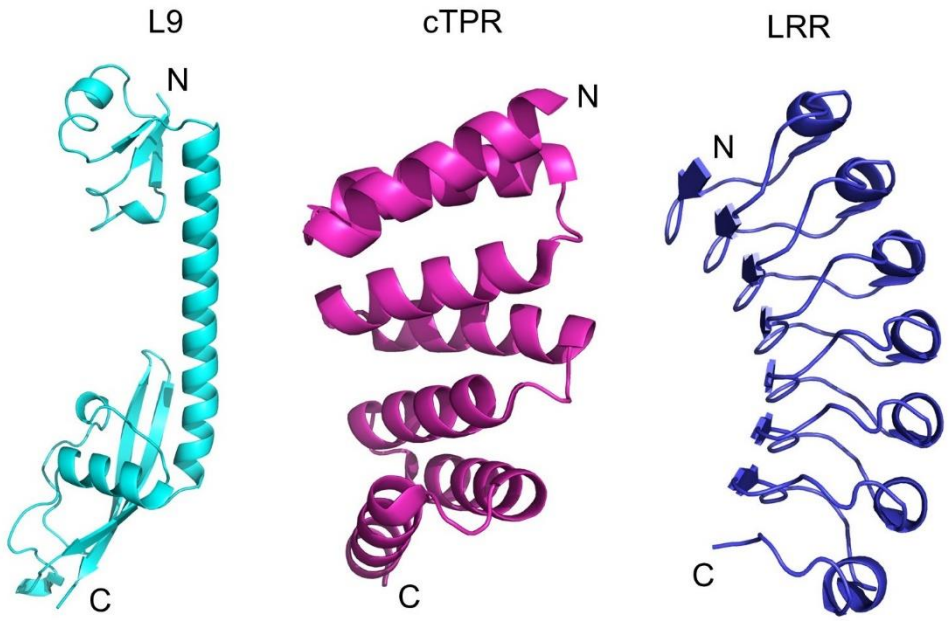

Figure 4.2 Structured linker candidates for SnoopLigase cyclisation of AppA. The L9 linker (PDB 1DIV) is a stable 34-residue helix from the ribosomal protein L9 (shown in cyan). The cTPR linker (PDB 1NA0) features stacked antiparallel α-helices that yield a superhelical structure resembling a spiral staircase. The LRR linker (PDB 4R58) has an inherently curved form, whose curvature is increased with each appended repeat.

Secondly, the cTPR linker is a 34-residue motif based on tetratricopeptide repeats, which acts as an important motif in mediating protein-protein interactions (Main et al., 2003). TPR modules are ancient motifs that play key roles in fundamental processes including the cell cycle and transcription (Blatch and Lässle, 1999; Sikorski et al., 1990) The cTPR linker adopts a “spiral staircase” formation in which two antiparallel α-helices constitute individual TPR motifs (Main et al., 2003). The cTPR linker is more stable than native counterparts and cTPR3 notably

exhibits cooperative thermal denaturation transitions that are 80 – 90% reversible at 83 °C (Main et al., 2003). The number of cTPR repeats was shown to predictably correlate with the distance bridged by the linker, demonstrating the scalability of the linker to different separation distances (Klein et al., 2014). The resilience to thermal denaturation and predictably scalability to different distances between enzyme termini makes the cTPR linker a favourable candidate for use in cyclisation.

Thirdly, the LRR linker is comprised of 20 to 30-residue repeats containing a β-strand on an α-helix that come together to form a horseshoe solenoid structure (Park et al., 2015; Parmeggiani et al., 2015). The Rosetta repeat protein idealisation method was applied to yield idealised leucine-rich repeat units, which were highly soluble and thermally stable (Park et al., 2015; Parmeggiani et al., 2015). The resulting DLRR repeats demonstrated constant curvature, which were predictably increased by increasing the number of repeats (Park et al., 2015). The precise predictability and curvature control of DLRR repeats was demonstrated through the successful assembly of a planar, closed circular molecule using LRR repeats, which required stringent control of the interaction geometry between repeats (Rämisch et al., 2014).

4.1.1 SpyRing Cyclisation of AppA

One potential long-term goal of thermal stabilisation of AppA by cyclisation is to improve upon commercially available phytases for use in the agricultural industry. For such application, the cyclisation strategy used must be amenable to cost-effective scaled-up production (Singh et al., 2016). In this regard, the SpyRing cyclisation platform is better suited to large-scale production than the SnoopLigase

system. SpyRing cyclisation is bipartite and spontaneous, resulting in cyclised enzyme species immediately following their expression. Conversely, SnoopLigase cyclisation is tripartite and requires the incubation of the peptide-tagged enzyme and SnoopLigase under specific conditions. The added prerequisite steps of SnoopLigase purification and incubation before cyclised enzyme production are barriers to industrial implementation.

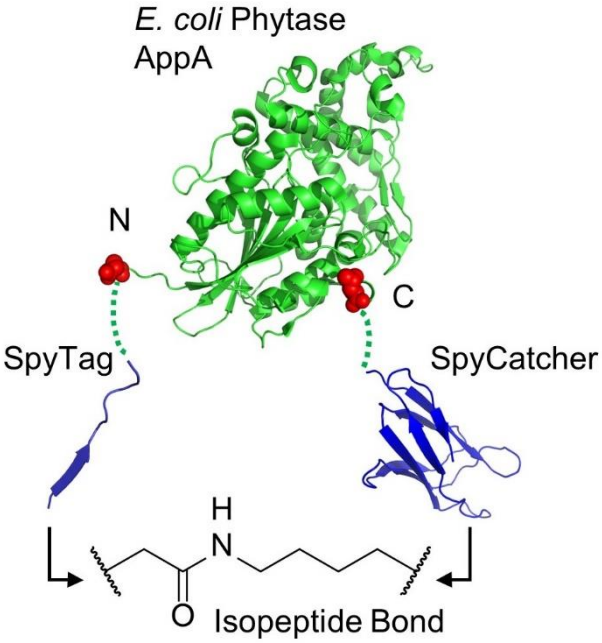

Figure 4.3 Design of AppA construct for SpyRing cyclisation. SpyTag (PDB 4MLI) was genetically encoded on the N-terminus and SpyCatcher (PDB 4MLI) on the C-terminus of AppA (PDB 1KDP) to enable spontaneous head-to-tail cyclisation. N- and C-termini of AppA are shown in red.

As a result, the SpyRing cyclisation system was trialled first on the cyclisation of AppA. Before trialling the SpyRing in conjunction with structured linkers, the SpyRing was tested alone to evaluate its efficacy in conferring thermal

resilience to AppA (Figure 4.3). The end-to-end length of the SpyTag-SpyCatcher complex (PDB 4MLI) is approximately 37 Å, whereas the distance between AppA termini is 48 Å. AppA was separated from SpyTag and SpyCatcher using a flexible $(GSG)_2$ linker on each end to aid in bridging the remaining distance and to allow for mobility of the adjoined SpyTag and SpyCatcher domains (Chen et al., 2012).

The thermal resilience activity assay of AppA showed that AppA is roughly as resilient as PhyC, remaining full activity following incubation at temperatures below 55 °C but losing all activity following incubation at > 75 °C (Figure 4.4). AppA also demonstrated markedly higher activity than PhyC. To reach similar levels of phosphate release after 20 min (A_{620} 0.3 – 0.35 using Biomol green) with 20 µM phytic acid substrate, 5-fold more PhyC (75 nM) was required compared to AppA (15 nM). This further demonstrates the commercial value of AppA, which has been reported to have the highest specific activity of characterised phytate-degrading enzymes (Gen Lei et al., 2012).

SpyRing cyclisation conferred minor improvements in thermal resilience to AppA, preventing complete inactivation following incubation at > 75 °C (Figure 4.4). The extent of improvement in thermal resilience of the SpyRing-cyclised enzyme was markedly compromised in AppA when compared to other SpyRing-cyclised enzymes. This highlights the novel challenge presented by AppA, a larger enzyme whose termini are much further apart. To test the specific improvement in thermal resilience imparted by the cyclisation itself, AppA was flanked by SpyTag and SpyCatcherEQ, an inactive SpyCatcher mutant. The inactive SpyRing AppA construct exhibited no improvement in resilience compared to AppA and was completely inactivated at temperatures above 75 °C (Figure 4.4). This shows that cyclisation has the potential to improve the thermal resilience of AppA.

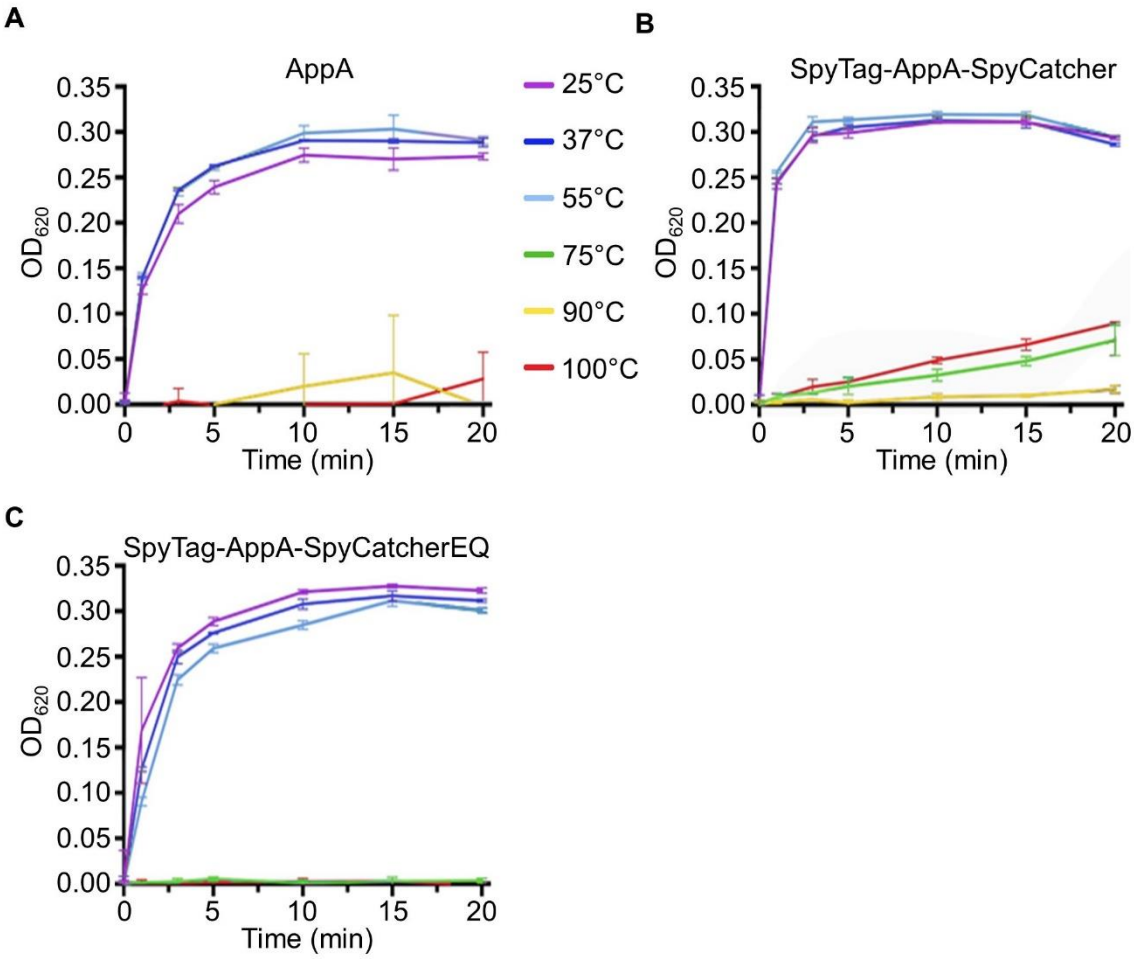

Figure 4.4 SpyRing cyclisation is insufficient to confer thermal resilience to AppA. AppA constructs were incubated at the temperatures indicated above for 10 min, cooled to 10 °C and used in a colorimetric assay to quantify phosphate release from phytic acid hydrolysis. All are mean of triplicate ± 1 SD. a) WT AppA loses activity following incubation at temperatures above 75 °C. b) SpyRing cyclisation only conferred minor improvements in AppA thermal resilience. c) Use of the inactive SpyCatcher mutant (SpyCatcherEQ) in AppA cyclisation abolished improvements in thermal resilience.

4.1.2 Positioning of Structured Linkers

Having validated the potential of cyclisation to confer thermal resilience to AppA, I tested structured linker placement to maximise improvements in resilience. The cTPR linker was placed at the N- or C-terminus of AppA within the SpyRing-cyclised AppA construct, before testing for thermal resilience to heat-induced deactivation (Figure 4.5). The enzymatic activity curves of the AppA constructs was not ideal, since the plots of the constructs incubated at lower temperatures (25, 37 and 55 °C) plateau within the first few time points (Figure 4.5). However, conclusions were drawn from the rates of phytic acid hydrolysis of constructs heated at higher temperatures (75, 90 and 100 °C), at which the rates of hydrolysis were lower (Figure 4.5). When the cTPR linker was placed at the N-terminus of AppA, no improvement in AppA thermal resilience could be observed, and AppA was mostly inactive following incubation at all temperatures above 75 °C (Figure 4.5).

Conversely, when the cTPR linker was placed on the C-terminus of AppA, AppA was not inactivated at temperatures above 75 °C (Figure 4.5). SpyTag-AppA-cTPR-SpyCatcher even retained catalytic activity following boiling for 10 min, presenting a notable improvement in thermal resilience compared to the wild-type enzyme (Figure 4.5). This demonstrated that C-terminal linker placement was better at maximising the increase in resilience imparted by cyclisation.

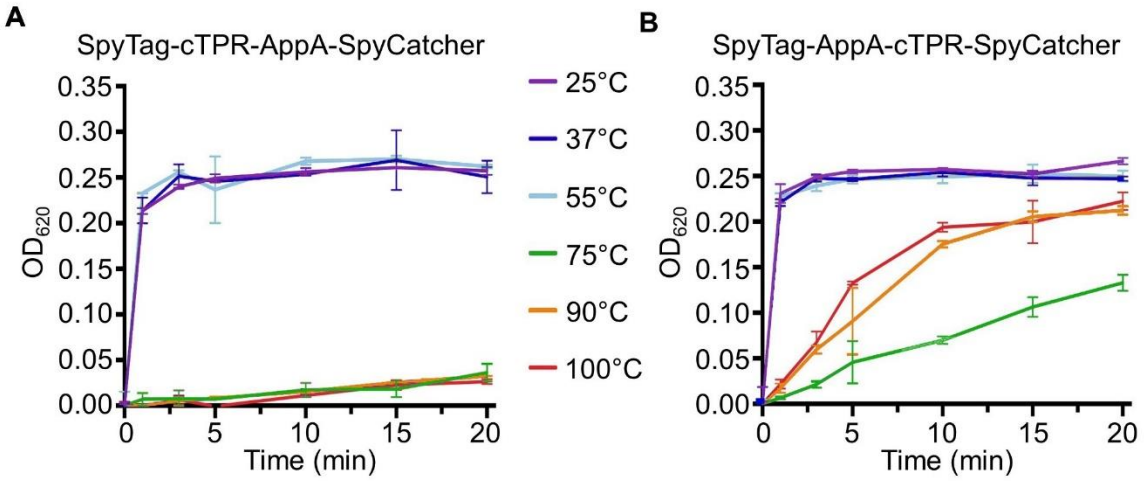

Figure 4.5 C-terminal linker placement for SpyRing cyclisation of AppA is superior for thermal resilience. SpyRing-cyclised AppA constructs with the cTPR linker were incubated for 10 min at the temperatures indicated above, cooled and used in a colorimetric assay to quantify phosphate release from phytic acid hydrolysis. All are mean of triplicate ± 1 SD. a) N-terminal placement of cTPR linker is ineffective at improving AppA thermal resilience. b) C-terminal cTPR linker placement improves AppA thermal resilience in conjunction with SypRing cyclisation.

4.1.3 Testing of cTPR, LRR and L9 Linkers

Since it was established that placing the structured linker on the C-terminus of AppA was better for improving thermal resilience, SpyRing constructs of AppA with LRR and L9 linkers were designed accordingly. The structured linkers were placed on the C-terminus of AppA, separated by a Gly-Ser-Gly linker at either end. Three such constructs are shown, each containing a cTPR, LRR or L9 linker.

For the SpyRing-cyclised AppA construct with the cTPR linker, three repeats of the tetratricopeptide repeat were used because each repeat is approximately 10 Å long and a minimum of 1.5 repeats is required (Main et al., 2003). N-terminal and C-terminal protein caps were preserved on each end of the cTPR3 linker to maintain the hydrophobicity of the repeats (Main et al., 2003). For the SpyRing-cyclised AppA construct with the LRR linker, the DLRR_A module was used. The DLRR_A module contains 6 repeats of the Rosetta-idealised L22 module (Park et al., 2015). The corresponding N-terminal and C-terminal protein caps were used to flank DLRR_A (Park et al., 2015). For the L9 linker-appended SpyRing-cyclised AppA construct, the L9 linker was used without any capping domains, as described (Kuhlman et al., 1997).

The produced structured linker constructs were tested for their resilience to heat-induced aggregation (Figure 4.6). Uncyclised, wild-type AppA was minimally resilient and formed insoluble aggregates following incubation at temperatures above 55 °C (Figure 4.6). The poor purity of the SpyTag-AppA-cTPR-SpyCatcher and SpyTag-AppA-LRR-SpyCatcher constructs can be observed via SDS-PAGE (Figure 4.6). This may be indicative of the negative impact of the cTPR and LRR linkers on protein soluble expression (Figure 4.6). As a result of the low purity, the relevant bands for the cTPR and LRR-appended SpyRing AppA constructs could not be confidently assigned by Coomassie staining (Figure 4.6).

The L9-appended SpyRing-cyclised AppA showed the clearest sign of expression and thermal resilience (Figure 4.6). SpyTag-AppA-L9-SpyCatcher retained solubility throughout heating at all temperatures, even following boiling for 10 min (Figure 4.6). As a result, The L9 linker was pursued in subsequent experiments.

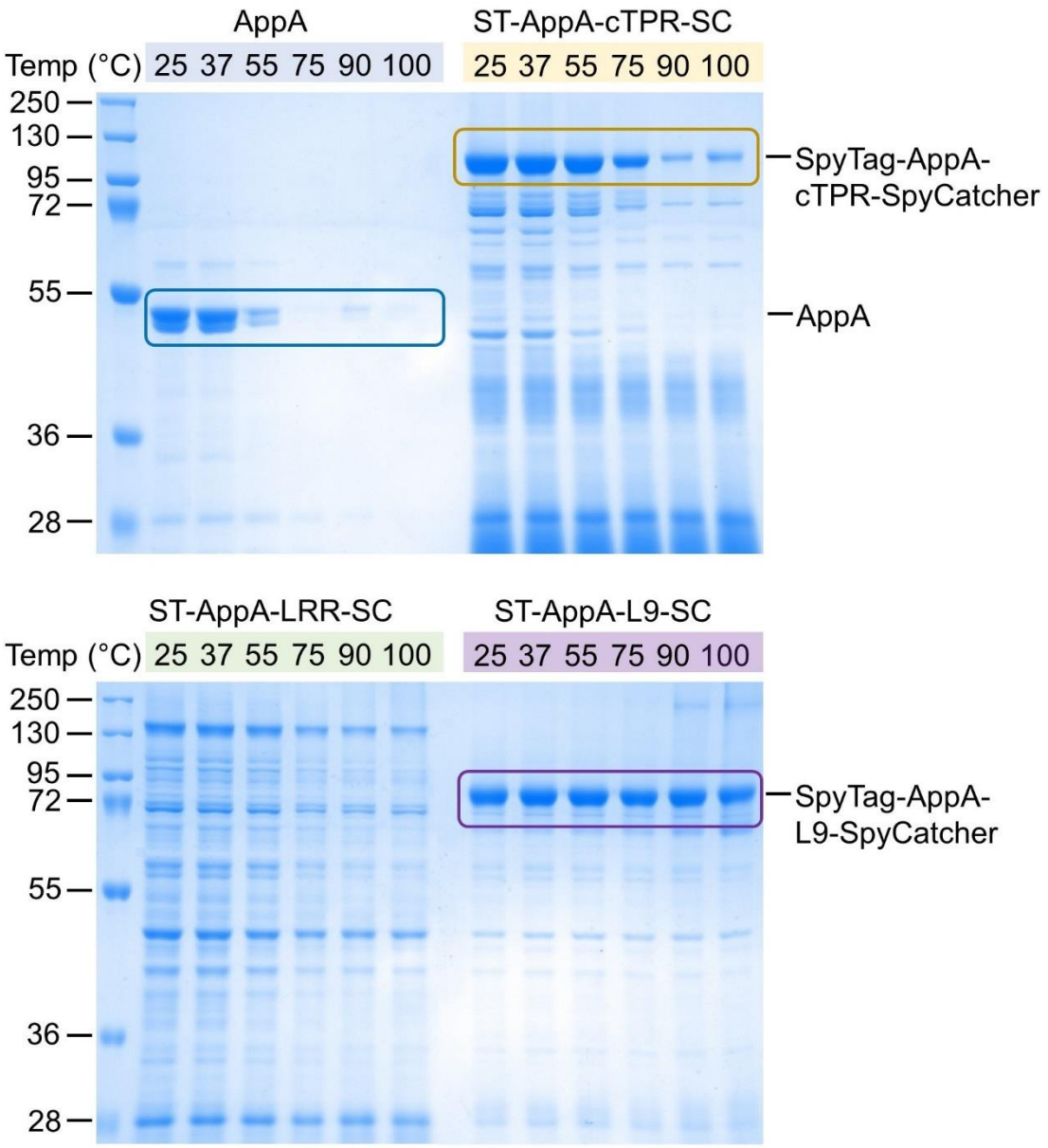

Figure 4.6 SpyRing cyclisation with L9 linker is most effective at improving AppA thermal resilience. Linker-appended SpyRing AppA constructs were expressed periplasmically using a periplasmic signal sequence and purified using the cold osmotic shock method. Purified constructs were incubated for 10 min at the temperatures indicated above, cooled to 10 °C, then centrifuged to remove insoluble aggregates. The soluble protein remaining in the supernatant was assayed via SDS-PAGE with Coomassie staining.

4.1.4 SpyRing-Cyclised AppA in Cleared Lysate

The L9-appended SpyRing-cyclised AppA demonstrated the greatest degree of soluble protein expression and resilience to heat-induced aggregation, and therefore showed the most promise for industrial application (Figure 4.6). As discussed in 3.2.6, superdosed phytases in animal feed must withstand steam treatment during pelleting while exposed to a wide range of sub-optimal reaction conditions. Since the thermal resilience assay experiments are conducted in optimal conditions for enzyme function and stability, the results do not necessarily translate to resilience following industrial implementation.

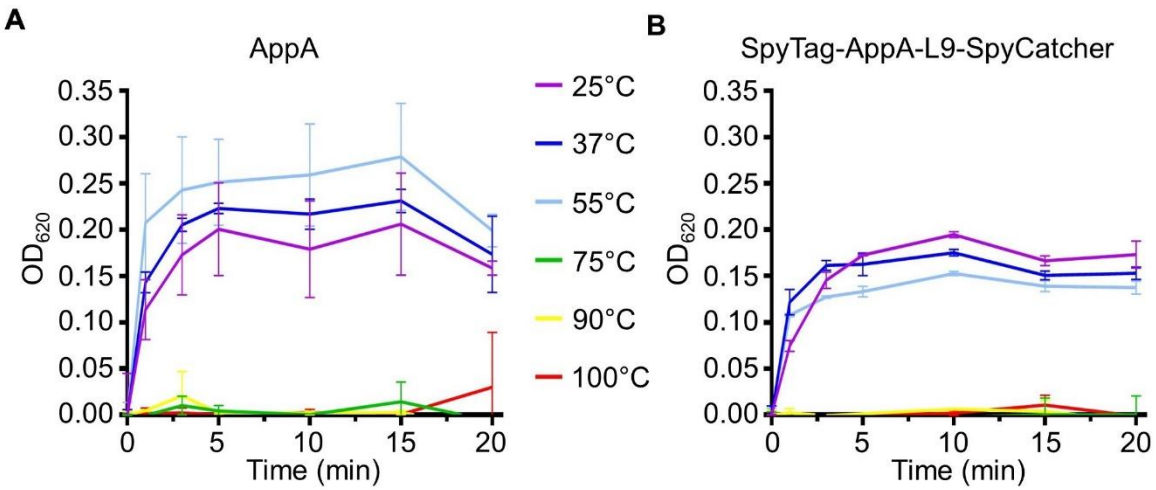

Figure 4.7 L9-appended SpyRing cyclisation does not improve AppA thermal resilience in dialysed cleared lysate. AppA constructs were heated in 5 mg/mL dialysed cleared lysate to the temperatures indicated above before use in a colorimetric assay to quantify phosphate release from phytic acid hydrolysis. All are mean of triplicate ± 1 SD. a) The thermal resilience of AppA was unchanged in dialysed cleared lysate. b) SpyRing cyclisation with the L9 linker was ineffective at conferring improvements in AppA thermal resilience in dialysed cleared lysate.

To better gauge the increase in thermal resilience imparted by the L9 linker and SpyRing cyclisation to AppA, thermal resilience activity assays were conducted in dialysed cleared *E. coli* lysate (Figure 4.7). *E. coli* lysate was chosen to mimic industrial conditions because it contains a wide range of proteins, since superdosed phytases are exposed to high concentrations of proteins and other exogenous matter during feed formulation and steam treatment.

The thermal stability of wild-type AppA was unchanged, and AppA was deactivated following incubation at temperatures above 75 °C (Figure 4.7). SpyRing-cyclised, L9-appended AppA, however, lost all improvements in thermal resilience in cleared lysate (Figure 4.7). This is in line with previous thermal resilience assays of SpyRing and SnoopLigase-cyclised PhyC in cleared lysate (Figure 3.16), which showed that SpyRing-mediated thermal resilience is not robust in cleared lysate.

4.1.5 SnoopLigase Cyclisation of L9-Appended Constructs

Though SpyTag-AppA-L9-SpyCatcher was initially promising and improved the thermal resilience of AppA, such improvements were lost in the presence of cleared lysate. Thermal resilience conferred by SnoopLigase cyclisation was previously demonstrated to be more robust (Figure 3.16). As a result, SnoopLigase cyclisation with the L9 linker was applied to AppA to produce a construct with improved thermal resilience that would persist in cleared lysate, designed to partly mimic industrial conditions.

For SnoopLigase cyclisation, AppA was flanked with SnoopTagJr and DogTag, and the L9 linker was placed at the N- or C-terminus of AppA. Upon

incubation with an equimolar quantity with SnoopLigase in the cyclisation buffer, SnoopLigase efficiently cyclised SnoopTagJr-AppA-L9-DogTag, as indicated by the decrease in electrophoretic mobility (Figure 4.8). Most of the enzyme had been cyclised after 6 hours, though the cyclisation reaction continued up to 24 hours (Figure 4.8). A secondary band below the monomeric SnoopTagJr-AppA-L9-DogTag was visible throughout but was not cyclised by SnoopLigase (Figure 4.8). Higher molecular weight bands could also be observed at low concentrations, corresponding to AppA dimers (~110 kDa) and trimers formed by intermolecular locking by SnoopLigase (Figure 4.8). The band corresponding to SnoopLigase was not visible due to the lower acrylamide concentration in the resolving gel but would present at around 14 kDa.

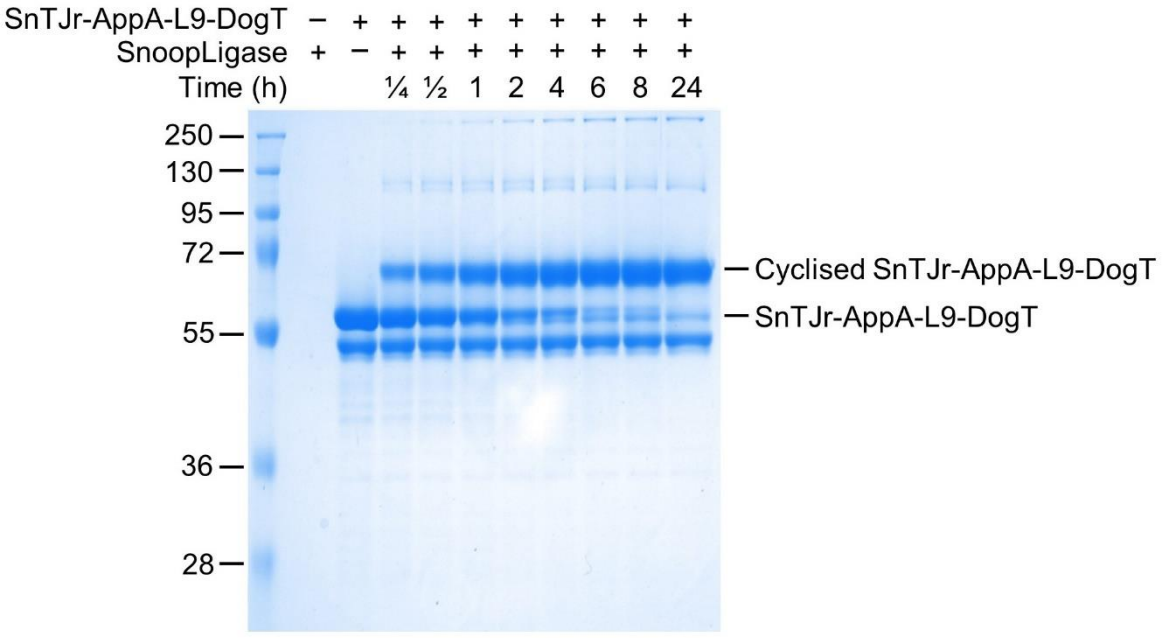

Figure 4.8 SnoopLigase cyclises SnoopTagJr-AppA-L9-DogTag. Equimolar quantities (10 µM) of SnoopLigase and SnoopTagJr-AppA-L9-DogTag were incubated at 4 °C for 0.25 – 24 h, prior to SDS-PAGE with Coomassie staining.

Having validated the successful SnoopLigase cyclisation of SnoopTagJr-AppA-L9-DogTag (Figure 4.8), cyclised AppA was tested for thermal resilience to heat-induced aggregation and inactivation. Solubility assays showed that SnoopTagJr-AppA-L9-DogTag was more resistant to heat-induced aggregation than SnoopTagJr-L9-AppA-DogTag prior to SnoopLigase cyclisation (Figure 4.9). However, following SnoopLigase cyclisation, cyclised SnoopTagJr-L9-AppA-DogTag was more soluble following incubation at 75 and 90 °C (Figure 4.9). A secondary band below the monomeric SnoopTagJr-AppA-L9-DogTag band could be observed before and after cyclisation (Figure 4.9). This secondary band followed the pattern of thermal resilience of the SnoopTagJr-AppA-L9-DogTag construct, aggregating after incubation at 75 and 90 °C after SnoopLigase cyclisation (Figure 4.9). Following SnoopLigase cyclisation of both constructs, higher molecular weight dimer (~110 kDa) and trimer bands were visible from intermolecular locking by SnoopLigase (Figure 4.9).

Though N-terminal L9 linker placement led to greater resilience to heat-induced aggregation (Figure 4.9), C-terminal L9 linker placement demonstrated very good thermal resilience of activity (Chapter 2.6.4) for SnoopLigase-cyclised AppA (Figure 4.10). SnoopLigase-cyclised SnoopTagJr-AppA-L9-DogTag retained high catalytic activity following incubation at all temperatures, and activity was only slightly compromised following incubation at 75 °C for 10 min (Figure 4.10).

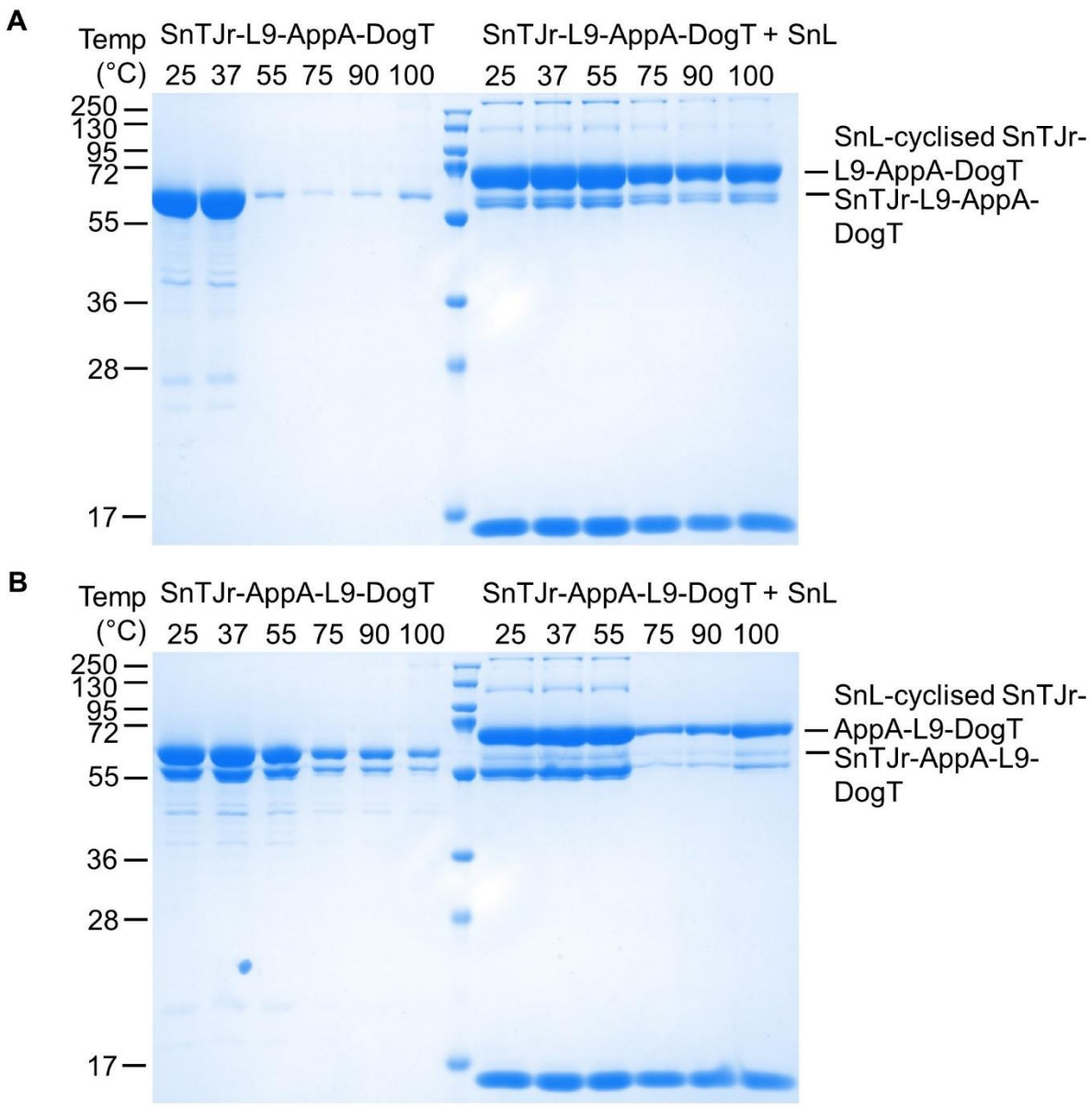

Figure 4.9 SnoopLigase cyclisation with L9 linker improved AppA resilience to heat-induced aggregation. AppA constructs for cyclisation were incubated with equimolar quantities of SnoopLigase overnight at 4 °C in SnoopLigase cyclisation buffer. Constructs were incubated at the temperatures indicated above, cooled and centrifuged to remove insoluble aggregates. Soluble protein remaining in the supernatant was assayed by SDS-PAGE with Coomassie staining.

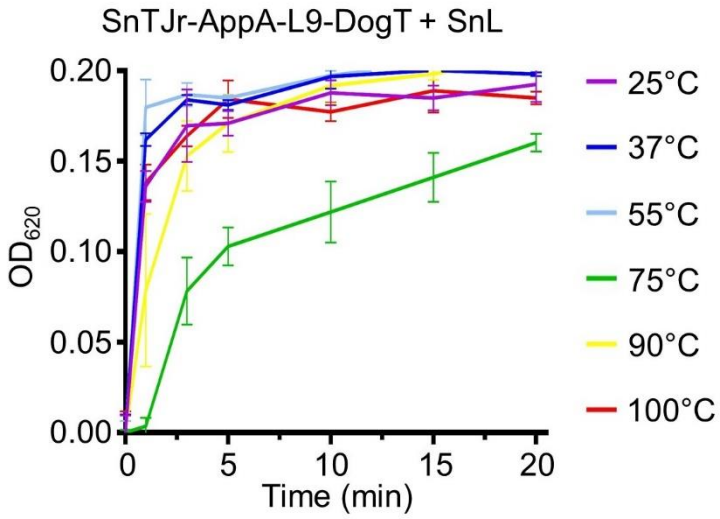

Figure 4.10 SnoopLigase-cyclised SnoopTagJr-AppA-L9-DogTag is thermally resilient. For SnoopLigase cyclisation, SnoopTagJr-AppA-L9-DogTag was incubated with equimolar quantities of SnoopLigase overnight at 4 °C. Following cyclisation, SnoopTagJr-AppA-L9-DogTag was incubated at the above indicated temperatures for 10 min, cooled, then used in a colorimetric assay to quantify phosphate release from phytic acid hydrolysis. All are mean of triplicate ± 1 SD.

4.1.6 SnoopLigase-Cyclised AppA in Cleared Lysate

Regardless of L9 linker placement, the thermal resilience of both L9 linker-appended AppA constructs was greatly enhanced following SnoopLigase cyclisation (Figure 4.10). To test whether this observed improvement in resilience would be preserved under industrial processing-mimicking conditions, SnoopLigase-cyclised SnoopTagJr-AppA-L9-DogTag was tested in cleared lysate (Figure 4.11). SnoopLigase-cyclised AppA was unable to retain improvements in cleared lysate and reverted to similar levels of thermal resilience as wild-type AppA

(Figure 4.11). Though SnoopLigase-cyclised SnoopTagJr-AppA-L9-DogTag remained substantially active following exposure to all temperatures up to 90 °C under optimal enzyme conditions (Figure 4.10), it was fully deactivated following incubation at temperatures above 75 °C in cleared lysate (Figure 4.11).

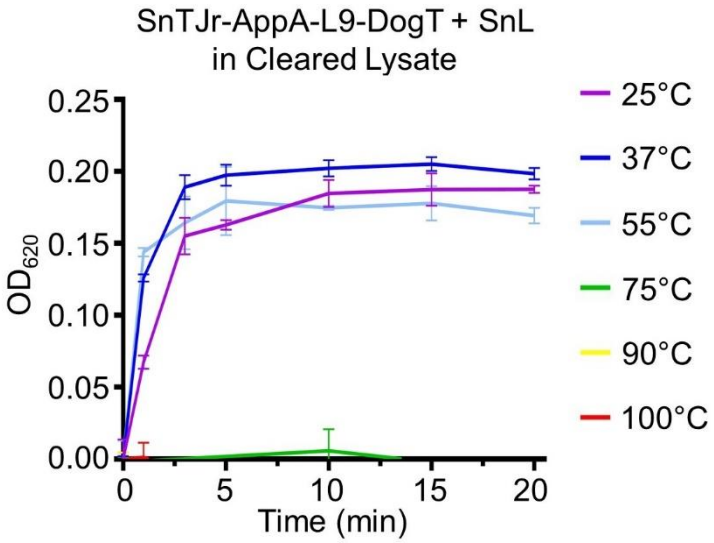

Figure 4.11 SnoopLigase-cyclised SnoopTagJr-AppA-L9-DogTag is not thermally resilient in cleared lysate. For cyclisation, SnoopTagJr-AppA-L9-DogTag was incubated with an equimolar quantity of SnoopLigase at 4 °C overnight. The cyclised enzyme was heated in 5 mg/mL dialysed cleared lysate to the temperatures indicated above before use in a colorimetric assay to quantify phosphate release from phytic acid hydrolysis. All are mean of triplicate ± 1 SD.

4.1.7 SnoopLigase Depletion Following AppA Cyclisation

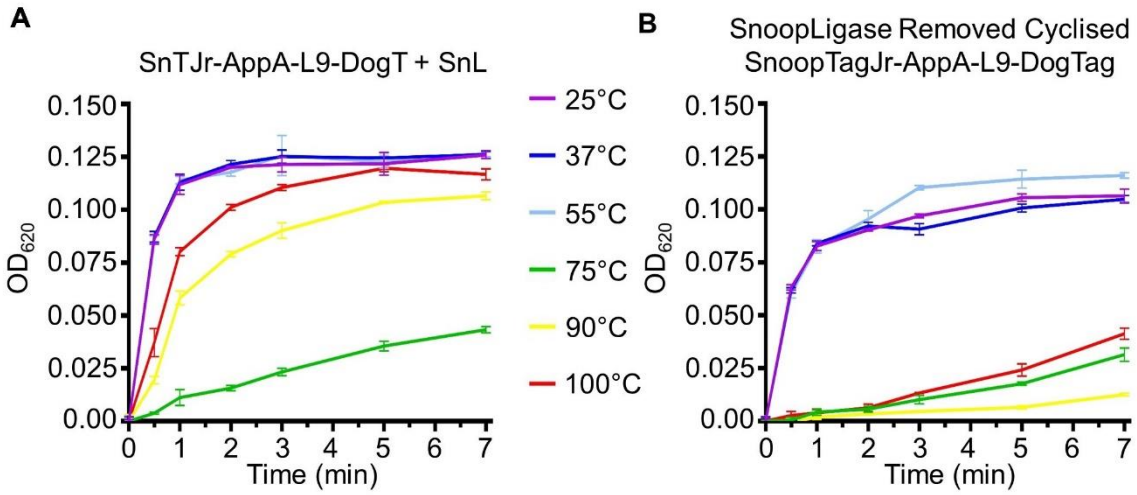

Figure 4.12 SnoopLigase association with cyclised SnoopTagJr-AppA-L9-DogTag is required for thermal resilience. Cyclized SnoopTagJr-AppA-L9-DogTag before and after SnoopLigase removal was incubated for 10 min at indicated temperatures. SnoopLigase was removed following SnoopTagJr-AppA-L9-DogTag cyclisation using the imidazole elution method. Constructs were then used in a colorimetric assay to quantify phosphate release from phytic acid hydrolysis. All are mean of triplicate ± 1 SD. a) L9-appended, SnoopLigase-cyclised AppA resisted deactivation following incubation at all temperatures. b) SnoopLigase removal abolished all improvements in thermal resilience.

Since SnoopLigase remains stably bound to its conjugate following cyclisation, the observed improvement in thermal resilience of SnoopLigase-cyclised SnoopTagJr-AppA-L9-DogTag could be attributed to the cyclisation and to the bound SnoopLigase (Buldun et al., 2018). To better understand the stabilising effects of the cyclisation action itself and of the continued association of SnoopLigase following cyclisation, SnoopLigase was depleted following AppA

cyclisation using the imidazole elution method (Chapter 2.5.2.2) following the solid-phase immobilisation of biotinylated SnoopLigase (Figure 4.12).

SnoopLigase-cyclised SnoopTagJr-AppA-L9-DogTag demonstrated a notable increase in thermal resilience compared to wild-type AppA, resisting deactivation following incubation at all temperatures (Figure 4.12). The activity was most compromised following incubation at 75 °C but was much less changed following incubation at all other temperatures (Figure 4.12). However, SnoopLigase depletion following cyclisation removed all improvements in resilience, rendering the cyclised enzyme mostly inactive after incubation at temperatures over 75 °C (Figure 4.12). SnoopLigase depletion following cyclisation removed much of the conferred improvements in thermal resilience, highlighting the stabilising effect of the bound SnoopLigase (Figure 4.12).

4.2 SnoopLigase Cyclisation of Quantum Blue

4.2.1 Quantum Blue

Quantum Blue™, an engineered *E. coli* AppA phytase with enhanced thermostability, is the current phytase product marketed by AB Vista. Quantum Blue™ is an improved version of its predecessor, Quantum™. Quantum™ was generated through systematic mutagenesis of AppA through gene site saturation mutagenesis (GSSM), followed by high-throughput screening of variants for most residual activity after heat treatment (Garrett et al., 2004; Gen Lei et al., 2012). The selected mutations were further analysed to maximise the additive synergy of combined mutations using a recursive addition protocol (Garrett et al., 2004). This protocol tested all possible combinations of mutations at each step before the

addition of another mutation to produce the most thermostable daughter construct, dubbed Phy9X (later known as Quantum™) (Garrett et al., 2004). Phy9X contained eight total mutations and exhibited a 12 °C increase in Tm, as well as 3.5× increase in half-life in simulated gastric fluid without change in specific activity when compared to the parental AppA enzyme (Garrett et al., 2004).

I expressed Quantum Blue periplasmically *in E. coli* and purified QB in the same manner as AppA. The two enzymes were compared for their thermal resilience to heat-induced aggregation and inactivation (Figure 4.13). QB was notably more heat-resilient than the parental enzyme AppA and retained full solubility throughout heating at all temperatures (Figure 4.13). Whereas AppA mostly aggregated following incubation at 55 °C, QB remained soluble even after boiling for 10 min (Figure 4.13).

AppA remained fully active following incubation at all temperatures up to (and including) 55 °C but was completely inactivated at temperatures above 75 °C (Figure 4.13). Conversely, QB retained high activity after exposure to all temperatures up to 75 °C was only lost the majority of activity following incubation at 90 and 100 °C (Figure 4.13). Previously, SnoopLigase cyclisation with the L9 structured linker was shown to confer exceptional thermal resilience to AppA, enabling the retention of activity even after boiling for 10 min (Figure 4.10). Given this degree of resilience exceeded that of QB, which was inactivated after exposure to 90 and 100 °C (Figure 4.13), SnoopLigase cyclisation with the L9 linker was applied to QB to test if it further improved thermal resilience.

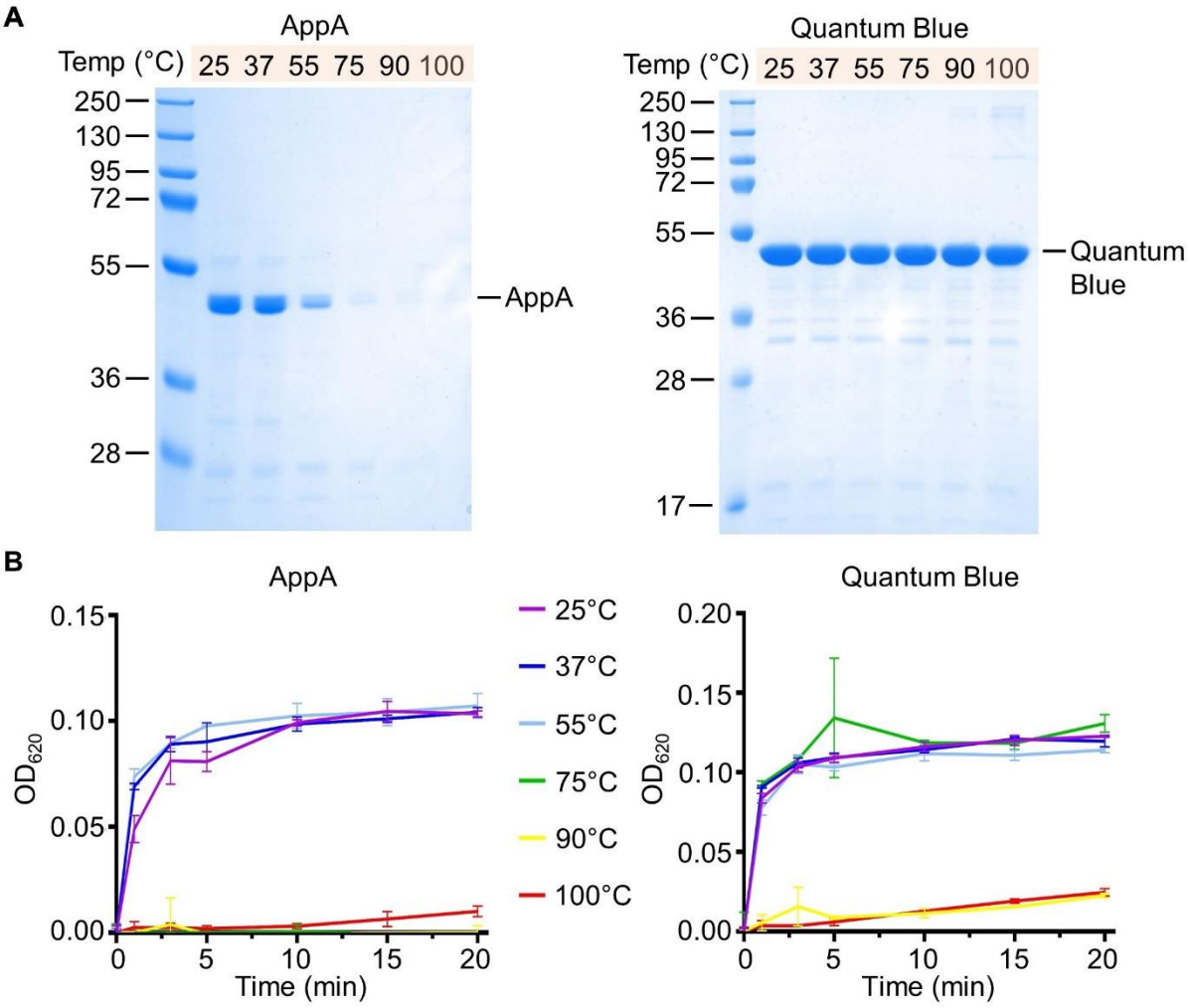

Figure 4.13 Quantum Blue is more thermally resilient than AppA. a) Phytase constructs were incubated at the temperatures indicated above for 10 min then centrifuged to remove insoluble aggregates. Soluble enzyme remaining in the supernatant was assayed via SDS-PAGE with Coomassie staining. b) Constructs were incubated at the indicated temperatures for 10 min, cooled, then used in a colorimetric assay to quantify phosphate release from phytic acid hydrolysis. All are mean of triplicate ± 1 SD.

4.2.2 SnoopLigase Cyclisation of L9-Appended Quantum Blue

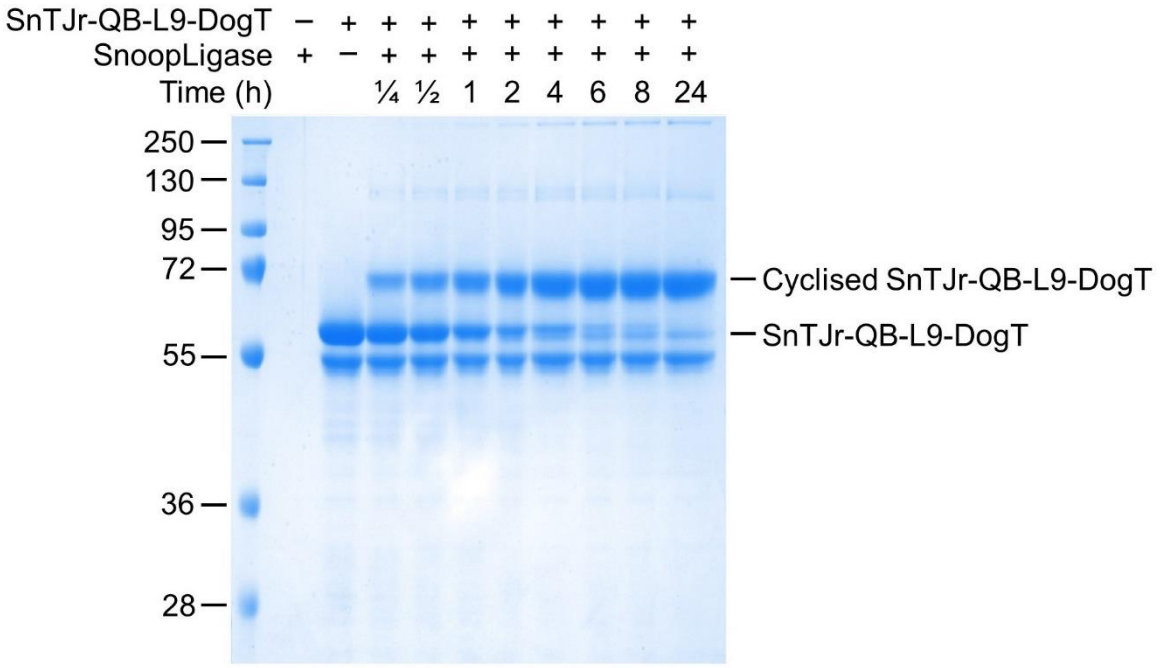

Figure 4.14 SnoopLigase cyclises SnoopTagJr-QB-L9-DogTag. Equimolar quantities (10 µM) of SnoopLigase and SnoopTagJr-QB-L9-DogTag were incubated at 4 °C for 0.25 – 24 h, prior to SDS-PAGE with Coomassie staining. Higher molecular weight dimer (~ 110 kDa) and trimer (top of gel) bands are visible at low concentrations due to intermolecular locking by SnoopLigase. A secondary band pertaining to the monomeric QB enzyme can be seen below the SnoopTagJr-QB-L9-DogTag band but the secondary band is not cyclised by SnoopLigase.

To enable L9 linker-appended cyclisation just as in the case of AppA, I then created the SnoopTagJr-QB-L9-DogTag construct. SnoopTagJr-QB-L9-DogTag was then incubated with an equimolar quantity of SnoopLigase under optimal cyclisation conditions and assayed via SDS-PAGE to verify successful cyclisation (Figure 4.14). SnoopLigase efficiently cyclised SnoopTagJr-QB-L9-DogTag, as

indicated by the decrease in electrophoretic mobility on the SDS-PAGE gel (Figure 4.14). Most of the QB was cyclised after 6 hours, though the cyclisation reaction continued up until 24 hours (Figure 4.14).

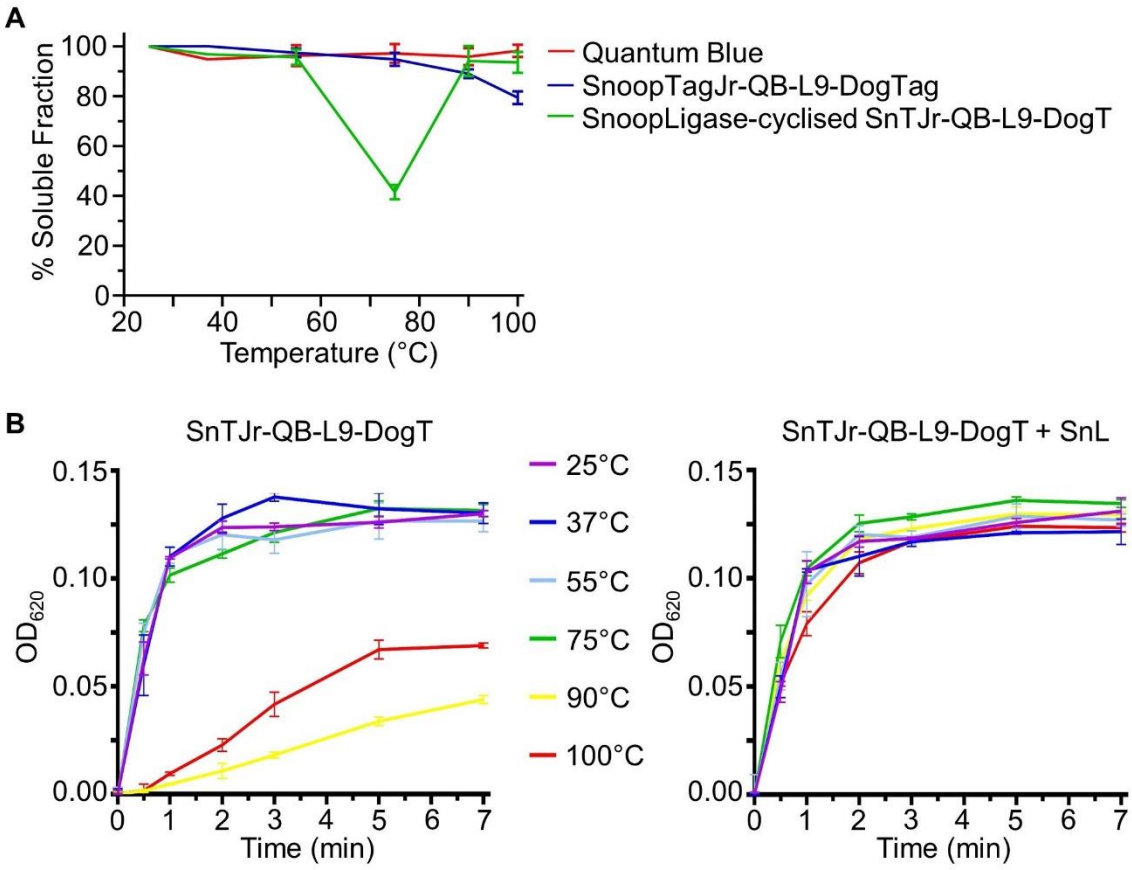

Figure 4.15 SnoopLigase cyclisation with the L9 linker improves the thermal resilience of Quantum Blue. a) QB constructs were incubated at the temperatures indicated above for 10 min, cooled, then centrifuged to remove insoluble aggregates. Soluble enzyme remaining in the supernatant was assayed via SDS-PAGE with Coomassie staining. All are mean of triplicate ± 1 SD. b) SnoopTagJr-QB-L9-DogTag before and after SnoopLigase cyclisation was incubated at the temperatures indicated for 10 min, cooled and used in a colorimetric activity assay to quantify phosphate release from phytic acid hydrolysis. All are mean of triplicate ± 1 SD.

Having verified the SnoopLigase cyclisation of QB, the cyclised enzyme was assayed for resilience to aggregation and inactivation. QB prior to cyclisation was extremely heat-resilient, and resisted aggregation throughout heating at all temperatures (Figure 4.15a). Following the conjugation of SnoopTagJr on the N-terminus and the L9 structured linker and DogTag on the C-terminus, the solubility of QB was largely unaffected, and remained mostly soluble following heating at all temperatures (Figure 4.15a). However, SnoopLigase cyclisation of SnoopTagJr-QB-L9-DogTag compromised the solubility of the enzyme after incubation at 75 °C, at which point only 41.5% enzyme remained soluble (Figure 4.15a).

Though SnoopLigase cyclisation appeared to negatively affect the resilience to aggregation of SnoopTagJr-QB-L9-DogTag, it improved the thermal resilience to loss of catalytic activity (Figure 4.15b). Uncyclised SnoopTagJr-QB-L9-DogTag was marginally more thermally resilient than QB, and exhibited compromised activity following incubation at 90 and 100 °C (Figure 4.15b). SnoopLigase-cyclised SnoopTagJr-QB-L9-DogTag exhibited improvements in resilience, retaining largely unchanged activity after incubation at all temperatures (Figure 4.15b). Whereas QB and SnoopTagJr-QB-L9-DogTag had shown little or no activity after incubation at temperatures above 90 °C, SnoopLigase cyclisation enabled QB to retain almost full activity at all temperatures, presenting an improvement in thermal resilience to an already exceptionally resilient enzyme.

4.2.3 SnoopLigase-Cyclised Quantum Blue in Cleared Lysate

SnoopLigase cyclisation with the L9 linker was shown to improve the thermal resilience of QB, enabling cyclised QB to remain active following incubation at all

temperatures, even after boiling for 10 min. To test whether such improvements would be sustained under mimicked industrial processing conditions for phytase superdosed into animal feed, SnoopLigase-cyclised SnoopTagJr-QB-L9-DogTag was assayed for thermal resilience in the presence of cleared lysate.

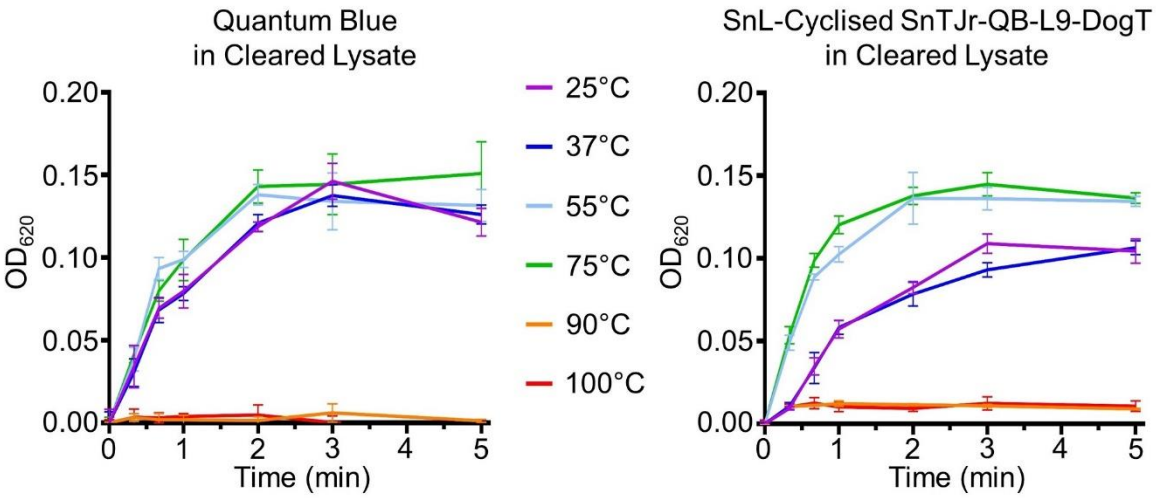

Figure 4.16 SnoopLigase-cyclised SnoopTagJr-QB-L9-DogTag is not thermally resilient in cleared lysate. QB constructs were incubated at the above indicated temperatures in 9 mg/ mL *E. coli* cleared lysate, cooled and used in a colorimetric activity assay to quantify phosphate release upon hydrolysis of phytic acid. All are mean of triplicate ± 1 SD. a) The thermal resilience of QB is unchanged in dialysed cleared lysate. b) SnoopLigase cyclisation ins ineffective at improving the thermal resilience of QB in dialysed cleared lysate.

Quantum Blue and SnoopLigase-cyclised SnoopTagJr-QB-L9-DogTag were incubated at a range of temperatures in 9 mg/ mL *E. coli* cleared lysate. The thermal resilience profile of QB was unchanged in cleared lysate, and QB was inactivated following incubation at temperatures above 90 °C (Figure 4.16). SnoopLigase-

cyclised QB, however, exhibited a similar degree of thermal resilience to QB in lysate, and had lost the improvements in resilience previously conferred by SnoopLigase cyclisation (Figure 4.16). Since the QB constructs were heated in the presence of a high concentration of extraneous proteins (9 mg/ mL), the challenge posed could have been too harsh.

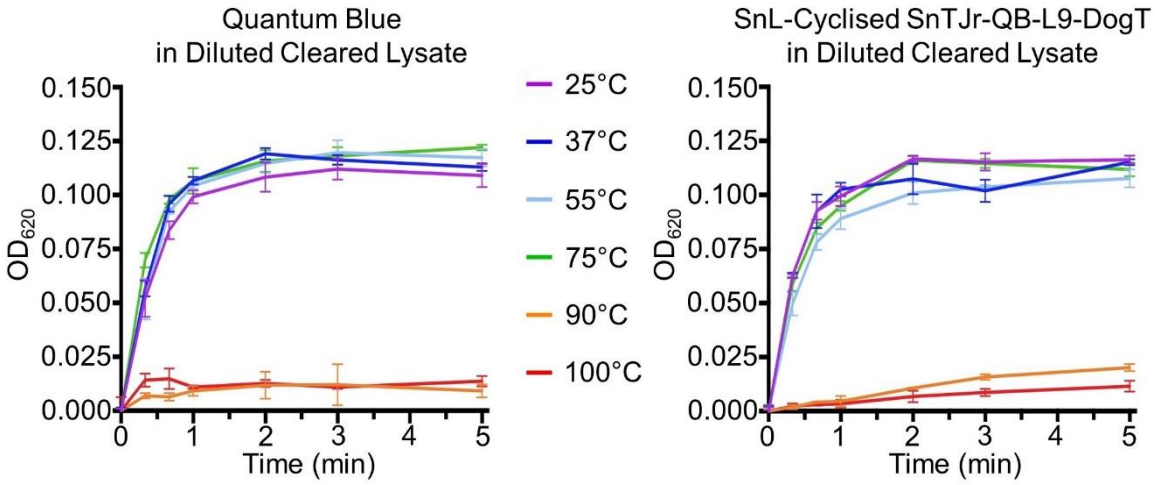

Figure 4.17 SnoopLigase cyclisation is ineffective at improving the thermal resilience of QB even at lower concentrations of cleared lysate. QB constructs were incubated at the above indicated temperatures in 0.5 mg/ mL *E. coli* cleared lysate, cooled and used in a colorimetric activity assay to quantify phosphate release upon hydrolysis of phytic acid. All are mean of triplicate ± 1 SD.

The constructs were therefore heated in much lower concentration of cleared lysate (0.5 mg/ mL) prior to activity assays to determine whether improvements in SnoopLigase-cyclised QB could be sustained. Even at a lower concentration of cleared lysate, SnoopLigase-cyclised QB lost all improvements and was reverted to the same degree of resilience as QB (Figure 4.17). This

showed that improvement conferred by SnoopLigase cyclisation with the L9 linker to QB is not robust in the presence of extraneous proteins and may not be sustained under steam treatment conditions of animal feed.

4.2.4 SnoopLigase Depletion Following QB Cyclisation

SnoopLigase-cyclised SnoopTagJr-QB-L9-DogTag was shown to be markedly more thermally resilient than QB, remaining active following incubation at all temperatures and avoiding heat-induced inactivation (Figure 4.15). To separate the individual contributions of the cyclisation action and the binding of the SnoopLigase to the observed improvement in thermal resilience, SnoopLigase was depleted following cyclisation of SnoopTagJr-QB-L9-DogTag using the imidazole elution method (Chapter 2.5.2.2).

SnoopLigase depletion following cyclisation compromised the improvement in resilience previously conferred (Figure 4.18). When SnoopLigase remained stably associated with the cyclised QB construct, the enzyme retained activity following incubation at all temperatures, even after boiling for 10 min (Figure 4.18a). SnoopLigase removal led to an overall decrease in activity in the cyclised QB construct, even following incubation at lower temperatures (Figure 4.18b). Furthermore, the SnoopLigase-removed cyclised QB exhibited even lower levels of catalytic activity following incubation at 90 and 100 °C (Figure 4.18b).

This suggests that the SnoopLigase removal process compromises the enzyme, potentially through conformational distortion. In addition, this showed that the association of SnoopLigase is a major contributor to the improvements in thermal resilience observed following SnoopLigase cyclisation. Therefore, the

maintenance of SnoopLigase binding to its cyclisation product is critical for maximum thermal resilience.

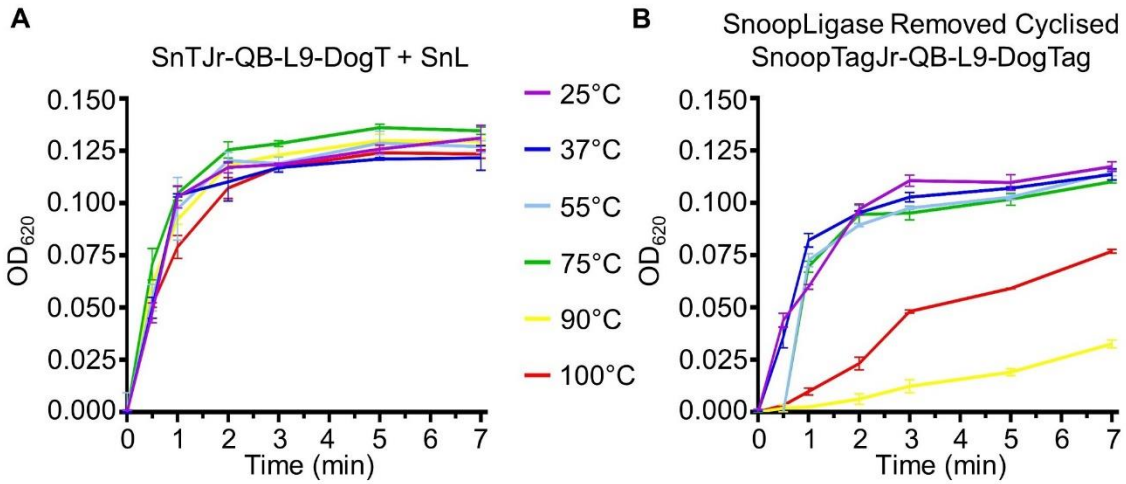

Figure 4.18 SnoopLigase depletion following cyclisation compromises the thermal resilience of Quantum Blue. SnoopLigase-cyclised SnoopTagJr-QB-L9-DogTag before and after SnoopLigase depletion were incubated at the temperatures above indicated for 10 min. SnoopLigase was removed following SnoopTagJr-QB-L9-DogTag cyclisation using the imidazole elution method Constructs were then cooled and used in a colorimetric assay to quantify phosphate release from phytic acid hydrolysis. All are mean of triplicate ± 1 SD. a) Figure 4.18a is as shown in figure 4.15b. L9-appended, SnoopLigase-cyclised QB is thermally resilient and retains full activity following incubation at all temperatures. b) SnoopLigase removal led to an overall decrease in activity and compromised the thermal resilience.

4.2.5 SnoopLigase Titration Following Depletion

Results from sections 3.1.5, 3.2.4, 4.1.7 and 4.2.4 showed that SnoopLigase depletion following cyclisation of BLA, PhyC, AppA and QB compromised the

improvement in thermal resilience observed when SnoopLigase remained stably associated with the cyclisation product. This suggested that the increase in resilience upon SnoopLigase cyclisation is conferred only in part by the conjugation action itself and is rather mainly conferred by the stable association of the SnoopLigase. SnoopLigase acts as a thermostable partner for the cyclised enzyme construct to enhance overall thermostability and aid refolding following unfolding at high temperatures.

To better understand the extent to which the thermal resilience of SnoopLigase-cyclised SnoopTagJr-QB-L9-DogTag is dependent on the presence and association of SnoopLigase, SnoopLigase was titrated back into SnoopLigase-depleted, cyclised enzyme. The removal of SnoopLigase following cyclisation of QB was shown to compromise the thermal resilience and the overall activity of the enzyme, potentially through conformational disruption (Figure 4.18). Re-introduction of SnoopLigase to SnoopLigase-removed, cyclised QB would show whether SnoopLigase removal-induced enzyme misfolding is permanent. Should the catalytic activity and improvements in thermal resilience in SnoopLigase-removed, cyclised QB be restored upon re-introduction of SnoopLigase, then the removal-induced misfolding can be deemed reversible. SnoopTagJr-QB-L9-DogTag was cyclised with equimolar ratios of SnoopLigase, then depleted of SnoopLigase using the imidazole elution method (Chapter 2.5.2.2). SnoopLigase was titrated back into the SnoopLigase-depleted, cyclised QB and used in thermal resilience activity assays (Figure 4.19).

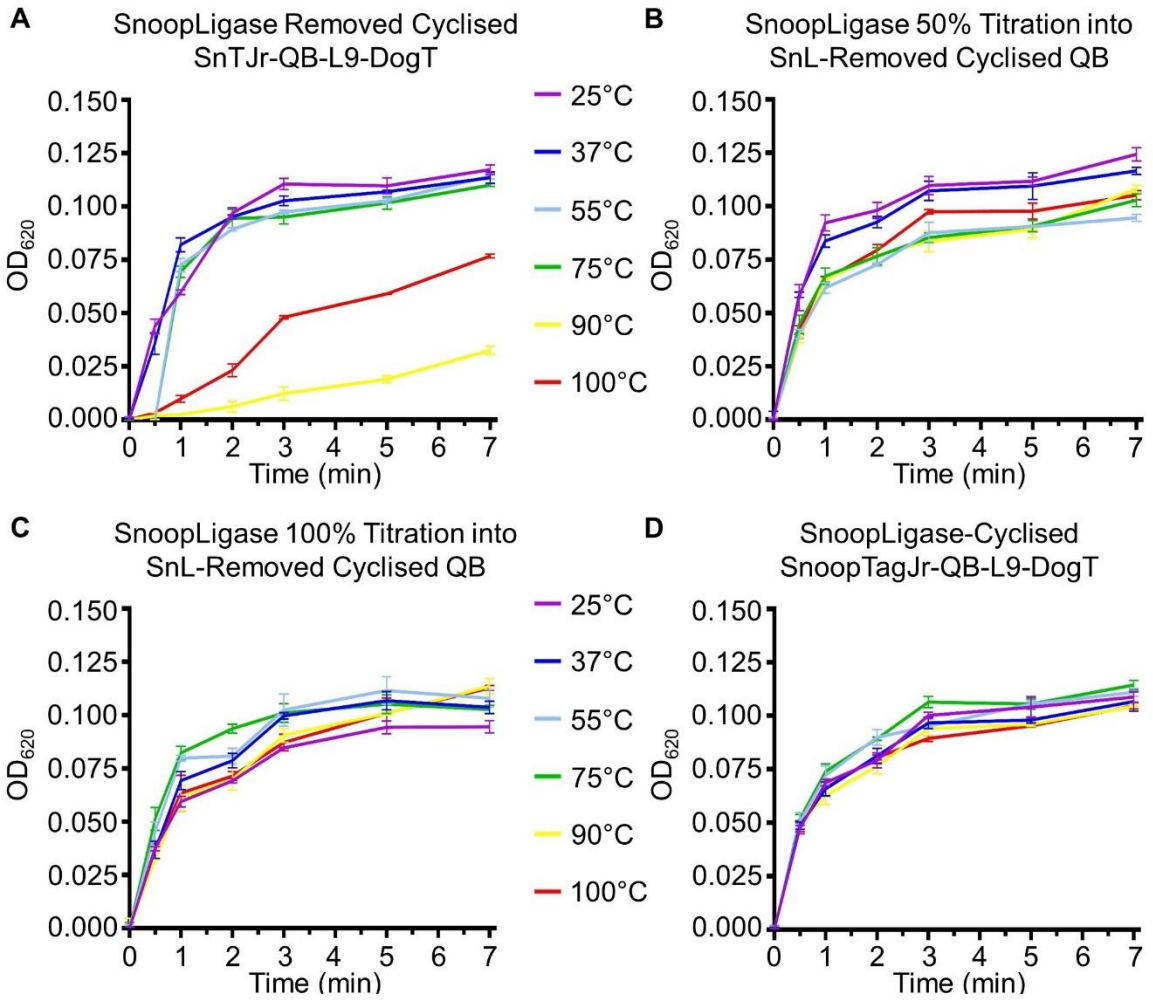

Figure 4.19 Titration of SnoopLigase into SnoopLigase-depleted cyclised SnoopTagJr-QB-L9-DogTag restores improvements in thermal resilience. SnoopLigase-cyclised SnoopTagJr-QB-L9-DogTag was depleted of SnoopLigase using the imidazole elution method. SnoopLigase was titrated back into the depleted, cyclised construct and incubated overnight at 4 °C under optimal SnoopLigase reaction conditions. Constructs were incubated at the temperatures indicated above for 10 min, cooled and used in a colorimetric activity assay to quantify phosphate release upon phytic acid hydrolysis. All are mean of triplicate ± 1 SD. (a) Figure 4.19a as shown in figure 4.18b. (b) SnoopLigase was titrated into cyclised, SnoopLigase-depleted enzyme at a 2:1 enzyme to SnoopLigase molar

ratio. (c) SnoopLigase was titrated into cyclised, SnoopLigase-depleted enzyme at a 1:1 enzyme to SnoopLigase molar ratio. (d) SnoopLigase-cyclised SnoopTagJr-QB-L9-DogTag control prior to SnoopLigase depletion.

Upon SnoopLigase depletion, cyclised QB incubated at 90 and 100 °C exhibited compromised activity compared to the cyclised construct with SnoopLigase unremoved (Figure 4.19). When the SnL-depleted cyclised enzyme was incubated with SnoopLigase at a 1:1 molar ratio, the full increase in thermal resilience could be observed (Figure 4.19c). Even when 50% SnoopLigase was titrated in (Figure 4.19b), the enzyme was as thermally resilient as SnoopLigase-cyclised QB (4.19d).

Figure 4.19 showed that the full increase in thermal resilience could be re-achieved when 50% SnoopLigase was titrated back into cyclised, SnoopLigase-depleted enzyme. Instead of titrating SnoopLigase into cyclised, SnoopLigase-depleted enzyme constructs, SnoopLigase cyclisation reactions with SnoopTagJr-QB-L9-DogTag were set up at varying enzyme to SnoopLigase ratios. When SnoopTagJr-QB-L9-DogTag was cyclised with an equimolar quantity (100%) of SnoopLigase, QB remained fully active following incubation at all temperatures with no decreases in activity (Figure 4.20d). Interestingly, the same could be observed when SnoopTagJr-QB-L9-DogTag was cyclised with 25% and 50% SnoopLigase (Figure 4.20b, c).

SnoopTagJr-QB-L9-DogTag cyclised with 10% SnoopLigase exhibited a comparable degree of thermal resilience to constructs cyclised with 25, 50 and 100% SnoopLigase (Figure 4.20a). This could be indicative of SnoopLigase acting as a

mobile chaperone between multiple enzymes to confer the heightened degree of thermal resilience observed despite being present in low molar quantities. However, QB cyclised with 10% SnoopLigase was less active following incubation at 90 and 100 °C, suggesting that the amount of SnoopLigase present was insufficient to fully stabilise enzymes at higher temperatures (Figure 4.20a).

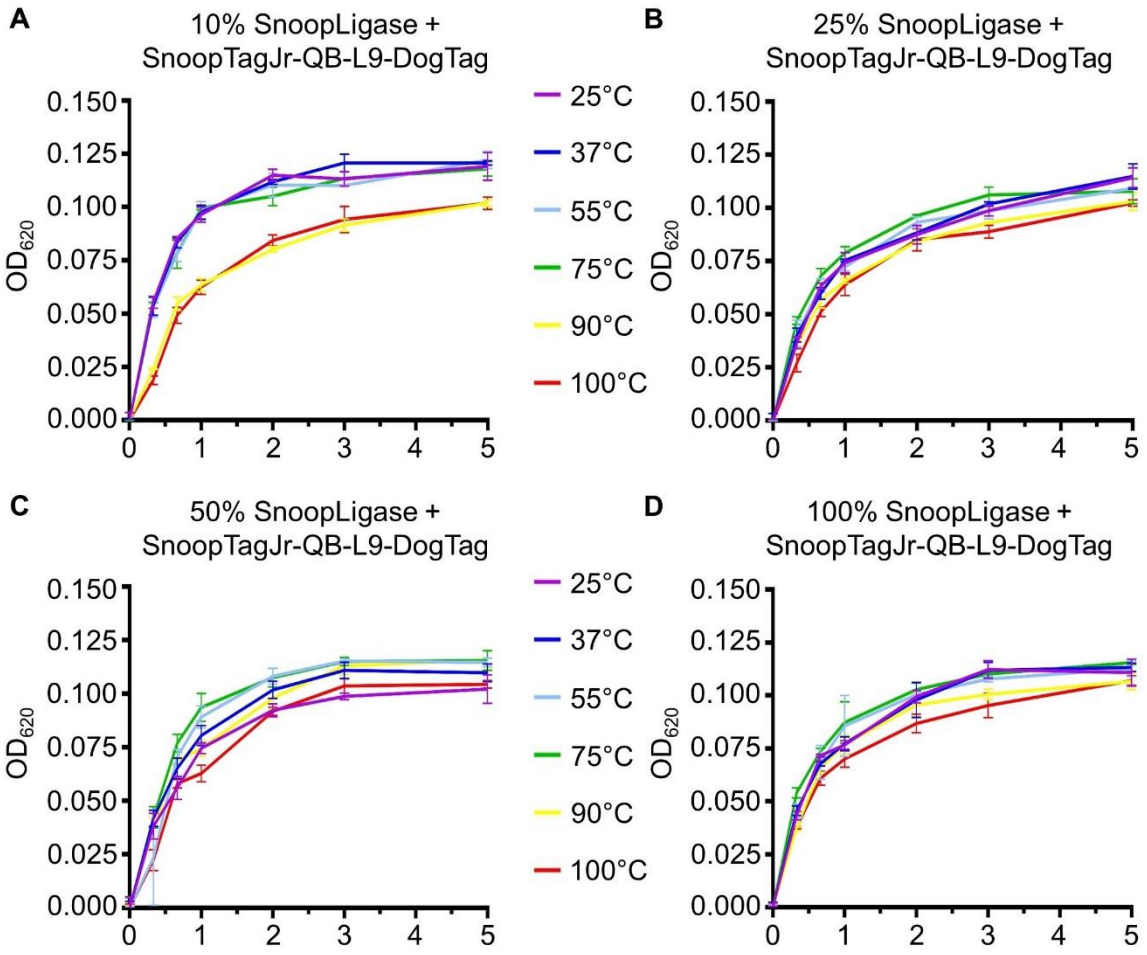

Figure 4.20 SnoopLigase cyclisation of SnoopTagJr-QB-L9-DogTag at varying molar ratios. SnoopTagJr-QB-L9-DogTag was incubated with 10%, 25%, 50% and 100% molar quantities of SnoopLigase in optimal SnoopLigase cyclisation buffer [50 mM TB pH 7.25 + 15% (v/v) glycerol] overnight at 4 °C. Cyclised QB constructs were then incubated at the temperatures indicated above for 10 min,

cooled and used in a colorimetric activity assay to quantify the release of phosphate upon hydrolysis of phytic acid. All are mean of triplicate ± 1 SD.

The marked improvement in thermal resilience of SnoopLigase-removed cyclised QB upon titration of 50% SnoopLigase (Figure 4.19b) and the thermal resilience of QB cyclised with 10% SnoopLigase (Figure 4.20a) could be associated with the presence of glycerol during heating. SnoopLigase-removed cyclised QB was dialysed into and heated in the optimal buffer for its mother construct, AppA (0.1 M sodium acetate pH 4.5). Contrastingly, SnoopLigase-removed, cyclised QB titrated with 50% SnoopLigase and QB constructs cyclised at any SnoopLigase ratio were heated in the optimal SnoopLigase reaction buffer [50 mM TB pH 7.25 + 15% (v/v) glycerol].

Glycerol is a widely used cosolvent known to stabilise protein native structures and prevent aggregation during refolding (Gekko and Timasheff, 1981; Vagenende et al., 2009). Glycerol stabilises the protein by pushing the native structure towards more ordered and compact conformations through exclusion of glycerol by electrostatic interactions at the protein surface (Vagenende et al., 2009). Furthermore, glycerol acts as an amphiphilic interface between polar solvent molecules and areas of contiguous surface hydrophobicity, which preferentially interact with glycerol and exclude water (Vagenende et al., 2009). As a result, glycerol stabilises partially unfolded intermediates and prevents their aggregation by inhibiting the exposure of aggregation-prone hydrophobic patches (Mishra et al., 2007; Vagenende et al., 2009; Wu et al., 2008a).

Through these mechanisms, glycerol has been shown to inhibit heat-induced aggregation and inactivation in enzymes including creatine kinase (CK) and citrate synthase (CS) (Meng et al., 2004; Mishra et al., 2005). At 25% glycerol, the aggregation of CK was completely inhibited following incubation at 50 °C for 90 min (Meng et al., 2004). Heat-induced inactivation of CK was similarly inhibited in a concentration-dependent manner until 25% and 30% glycerol, which presented similar degrees of protection (Meng et al., 2004). Concentration-dependent increases in the refolding yield of CS were also shown, with the greatest refolding yield of 83% in 7 M glycerol (≈ 51% v/v) (Mishra et al., 2005). Such stabilising and protective effects of glycerol at high temperatures have also previously been demonstrated on the *Aspergillus niger* phytase (Rodríguez-Fernández et al., 2013).

During heating of SnoopLigase-cyclised QB constructs, glycerol was present at 15% (v/v). This concentration is far from the reported glycerol concentrations required for maximal protective effects from heat-induced aggregation and inactivation, which range from 30% (v/v) to 7 M (≈ 51% v/v) (Meng et al., 2004; Mishra et al., 2005). Nevertheless, protective effects were demonstrated at 15% glycerol, reducing the heat-induced aggregation and inactivation of CK (Meng et al., 2004). Similarly, CS exhibited a refolding yield of 36% with no glycerol, but the refolding yield was improved to 56% at 2 M (≈ 15% v/v) glycerol and 83% at 7 M (≈ 51% v/v) glycerol (Mishra et al., 2005). This shows that some of the marked improvements demonstrated upon titration of 50% SnoopLigase into SnoopLigase-removed cyclised QB (Figure 4.19b) and upon cyclisation of QB with 10% SnoopLigase (Figure 4.20a) can be attributed to the presence of glycerol.

To better discern the contributions of glycerol and SnoopLigase cyclisation on the thermal resilience of QB, SnoopTagJr-QB-L9-DogTag was cyclised with varying molar ratios of SnoopLigase in the absence of glycerol. The cyclised constructs were then incubated at varying temperatures in the absence of glycerol and assayed for their activity (Figure 4.21). When cyclised and heated in the presence of glycerol with 10% SnoopLigase, QB appeared remarkably thermally resilient and was mostly active following incubation at 90 and 100 °C (Figure 4.20a).

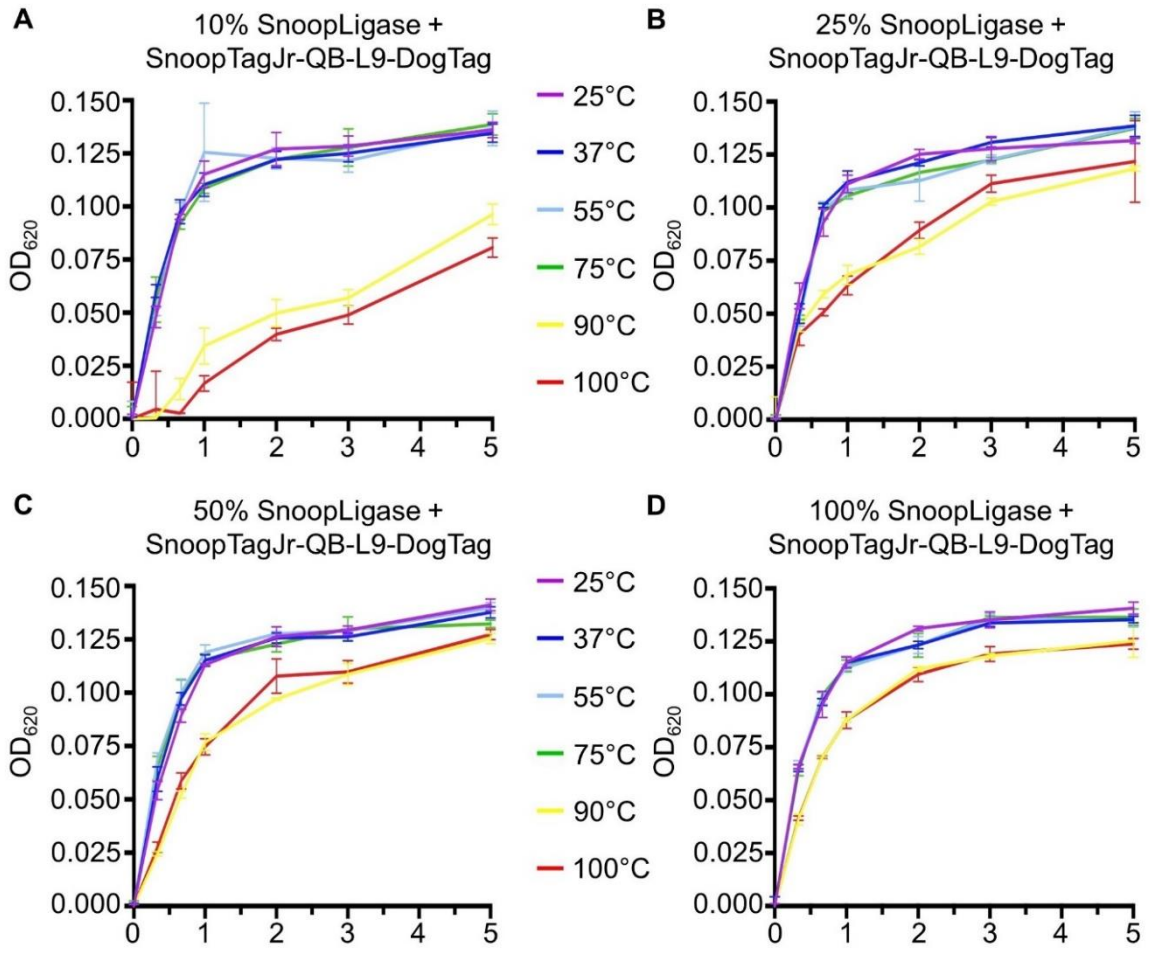

Figure 4.21 SnoopLigase cyclisation of SnoopTagJr-QB-L9-DogTag at varying molar ratios with no glycerol. SnoopTagJr-QB-L9-DogTag was incubated with 10%, 25%, 50% and 100% molar quantities of SnoopLigase in optimal SnoopLigase cyclisation buffer (50 mM TB pH 7.25) overnight at 4 °C.

Cyclised QB constructs were then incubated at the temperatures indicated above for 10 min, cooled and used in a colorimetric activity assay to quantify the release of phosphate upon hydrolysis of phytic acid. All are mean of triplicate ± 1 SD.

In the absence of glycerol, QB cyclised with 10% SnoopLigase (Figure 4.21a) appeared only similarly thermally resilient to uncyclised SnoopTagJr-QB-L9-DogTag (Figure 4.15b). However, when cyclised with 25% and 50% SnoopLigase without glycerol, clear improvements in the thermal resilience of QB could be observed (Figure 4.21). Upon cyclisation at a QB to SnoopLigase molar ratio of 2:1, the thermal resilience of QB was comparable to that of QB cyclised with an equimolar quantity of SnoopLigase (Figure 4.21).

When QB was cyclised with an equimolar quantity of SnoopLigase in the absence of glycerol (Figure 4.21d), the activity of the cyclised QB following incubation at 90 and 100 °C was slightly lower than that previously observed in QB cyclised and heated with glycerol (Figure 4.15b). This could be attributed to the additional stabilisation by glycerol during heat incubation. Furthermore, this demonstrates that even in the absence of glycerol, SnoopLigase cyclisation is effective at conferring exceptional thermal resilience to an already thermostable enzyme.

4.3 Discussion

Previously, SnoopLigase cyclisation was shown to be effective at conferring thermal resilience to mesophilic enzymes BLA and PhyC, whose termini were in relative proximity. The efficacy of SnoopLigase cyclisation despite the range of

distances bridged (7 – 29 Å) and in sizes of enzymes stabilised (29 – 39 kDa) suggested that the SnoopLigase system is adaptable. To test the limits of the system and to better characterise the range of enzymes for which SnoopLigase cyclisation would be effective, SnoopLigase cyclisation was applied to the industrially relevant *E. coli* phytase AppA, and its commercially available thermostable variant, Quantum Blue™.

AppA is inherently thermostable, and has a temperature optimum of 55 °C and T_m of 63.7 °C (Gen Lei et al., 2012). Quantum Blue demonstrates a superior level of thermostability since it is the product of further improvement on Phy9X, which retained all activity after 1 h at 62 °C and had a Tm of 75.7 °C (Garrett et al., 2004). Both AppA and QB are thermostable enzymes whose termini are 48 Å apart, and therefore present a novel challenge for SnoopLigase cyclisation.

Structured Linkers in Enzyme Cyclisation

To bridge the greater distance between the termini of AppA constructs, structured linkers (L9, cTPR and LRR) were trialled. The LRR linker was ineffective and compromised the stability of the enzymes. Conversely, the cTPR linker was moderately effective and improved the thermal resilience against heat-induced aggregation. However, the most improvement could be witnessed when the L9 linker was implemented, so it was taken forward.

Given that tertiary structures of enzymes vary widely, it may be difficult for structured linkers of defined curvatures to function as part of a generic cyclisation platform that is applicable to many enzymes. The observed reduction in soluble protein expression of SpyTag-AppA-LRR-SpyCatcher could be attributed to

incompatibility between the defined curvature of the idealised LRR linkers and the gap between the termini of AppA (Figure 4.6). The idealised LRR repeats were developed using the Rosetta repeat protein idealisation method (Parmeggiani et al., 2015). In this protocol, Rosetta *de novo* protein structure generation calculations were combined with available sequences and structural information from the repeat protein family (Parmeggiani et al., 2015). Naturally occurring LRR proteins were studied for their module organisation, and a suite of building blocks and junction modules were identified and idealised (Park et al., 2015; Parmeggiani et al., 2015).

The resulting idealised building blocks and junction modules could be accurately assembled to create proteins of predefined geometries due to the high degree of control over protein curvature (Park et al., 2015). In the case of enzymes whose structures have been resolved, it may be possible to use appropriate combinations of linkers and junction modules to create optimal linkers that accurately fit the gap between the termini for thermal stabilisation by head-to-tail cyclisation. However, this would require individual linker engineering per enzyme for stabilisation despite the modularity of the linkers and would not be conducive to functioning as a generic, widely applicable platform.

Structured linkers, as opposed to unstructured glycine and serine linkers, were explored since the highly structured nature of the linker domain would potentially aid enzyme refolding at high temperatures. However, there is room for improvement. If the primary mechanism by which cyclisation confers thermal resilience is through providing points of reference for enzyme refolding following unfolding at high temperatures, then the optimal linker to reinforce such effects would be an inherently structured and thermostable linker. Alternately, if the mechanism relies more upon the solubilisation of the enzyme to prevent

aggregation at high temperatures to facilitate recovery of activity upon cooling, the optimal linker would be designed to enhance solubility. In this instance, known solubility-enhancing protein tags, such as the Fh8 fusion system and polyionic tags, could be employed as linkers to aid in enzyme stabilisation by solubilisation (Costa et al., 2014; Paraskevopoulou and Falcone, 2018).

In developing such improved linkers, directed evolution could be used to select for optimised linker variants that best aid thermal stabilisation. Thermophilic protein fusion has been shown to be a potent solubility enhancement and kinetic stabilisation strategy (Fox et al., 2003; Kim et al., 2009a). Specifically, the maltodextrin-binding protein from *Pyrococcus furiosus* has been shown to be an effective thermostable fusion partner for improving solubility (Kim et al., 2009a; Luke et al., 2011). Similarly, thermostable domains of stable proteins from thermophilic organisms could be engineered into stabilising linkers, which could then be used in conjunction with cyclisation systems.

SnoopLigase Cyclisation of AppA and QB

SnoopLigase cyclisation, in conjunction with the C-terminal fusion of a structured L9 linker, was effective in conferring exceptional thermal resilience to AppA and QB. SnoopLigase cyclisation of AppA and QB flanked by N-terminal SnoopTagJr and C-terminal L9-DogTag enabled both enzymes to retain activity following boiling for 10 min, conferring a marked improvement in thermal resilience in both instances. This showed that SnoopLigase cyclisation can effectively improve the thermal resilience of enzymes that are inherently thermostable, and that the efficacy of cyclisation is not limited to mesophilic enzymes. All published

literature on cyclised enzymes report improvement on enzymes whose termini are no further apart than 29 Å apart. Therefore, this is the first instance in which the thermal resilience of enzymes with termini 48 Å as far as apart was improved.

Despite the marked improvement in thermal resilience in AppA and QB following SnoopLigase cyclisation with the L9 linker, the robustness of the increase in thermal resilience was not sustained in cleared lysate. Even when the concentration of cleared lysate during heating was lowered to 0.5 mg/mL, the improvements in thermal resilience were ablated. It is possible that the extraneous proteins, which aggregated during incubation at high temperatures, precipitated the aggregation of the SnoopLigase-cyclised enzyme constructs. Previously, SnoopLigase-cyclised SnoopTagJr-PhyC-DogTag retained its thermal resilience in cleared lysate, whereas SnoopTagJr-AppA-L9-DogTag and SnoopTagJr-QB-L9-DogTag both lost increases in thermal resilience in cleared lysate.

The decrease in robustness of the improvements conferred could be attributed to the introduction of the L9 structured linker, which could be precipitating aggregation in cleared lysate to produce the observed decrease in thermal resilience. If this is the case, then the replacement of the L9 linker with a solubilising linker would be effective in restoring the robustness of the thermal resilience conferred by SnoopLigase cyclisation. This observed reduction in thermal resilience in cleared lysate could also be attributed to the impaired reassociation of SnoopLigase with the cyclised enzyme conjugate in cleared lysate. Materials present in cell lysate such as nucleic acids and reducing agents could disrupt the interaction between SnoopLigase and the cyclised enzyme to abolish improvements in thermal resilience conferred by association with SnoopLigase.

E. coli cleared lysate was chosen since it contains a diverse range of extraneous proteins, nucleic acids and other materials. Nevertheless, it is insufficient to accurately replicate the steam treatment step during animal feed pelleting. As reported by the Food and Agriculture Organization of the United Nations (FAO), the steam treatment is conducted at 15 – 16% moisture at 80 – 90 °C, reaching a final high temperature of approximately 92 °C (varies by company, up to 104 °C) during extrusion through a ring die (Rebello et al., 2017). To better replicate pelleting conditions, future work could be conducted in similarly pressurised, low-moisture conditions in the presence of materials found in animal feed, such as wheat bran. This would allow for more accurate prediction of field performance of stabilised phytase constructs before conducting larger-scale field trials.

SnoopLigase Depletion Following Enzyme Cyclisation

The improvements in thermal resilience were also greatly compromised upon depletion of the SnoopLigase following cyclisation. SnoopLigase depletion following cyclisation of BLA and PhyC compromised the thermal resilience of the cyclised enzymes, but the SnoopLigase-depleted, cyclised enzymes remained more resilient than their wild-type counterparts. However, in the case of SnoopLigase depletion following cyclisation of AppA and QB, the compromise in thermal resilience was more notable and reverted the cyclised enzyme to a comparable degree of resilience to their uncyclised counterparts. This suggests that SnoopLigase association is of increased importance in the thermal resilience of cyclised *E. coli* phytase constructs. This was corroborated by the complete re-

establishment of thermal resilience upon titration of 50% SnoopLigase following initial SnoopLigase depletion. This increased importance of SnoopLigase association in *E. coli* phytase cyclisation compared to BLA and PhyC cyclisation could be linked to the increased difficulty of thermal stabilisation of AppA constructs.

The compromised thermal resilience of AppA constructs following SnoopLigase depletion could also be attributed to the SnoopLigase removal process. SnoopLigase was removed from cyclised AppA and QB constructs using the imidazole method, in which cyclised enzyme bound to immobilised SnoopLigase was eluted using 2.5 M imidazole. Imidazole constitutes the side chain of His and enables molecular interactions with charged or aromatic amino acids (Liao et al., 2013). As a result, high concentrations of imidazole could compete with or disrupt His residue interactions to alter protein structure, compromise stability and hinder enzyme function. Exposure of AppA constructs to high imidazole concentrations during SnoopLigase removal may have contributed to the loss of thermal resilience. Development of a SnoopLigase with catalytic turnover would enable circumvention of enzyme exposure to high concentrations of imidazole to facilitate SnoopLigase removal without disrupting enzyme function and stability.

SnoopLigase Association with its Cyclised Enzyme Conjugate

To better understand the role of SnoopLigase association in the thermal resilience of cyclised enzyme constructs, varying SnoopLigase: enzyme ratios were tested for the cyclisation reaction. The findings showed that the SnoopLigase need not be present in equimolar quantities to reap the full improvements in enzyme

thermal resilience. Even when cyclisation reactions were set up using a 1:2 ratio of SnoopLigase to QB, marked improvements in resilience to heat-induced inactivation could be seen on an already thermostable enzyme.

The increase in cyclised enzyme thermal resilience is not proportionate to the amount of SnoopLigase present, which suggests that SnoopLigase need not be associated with every cyclised enzyme molecule to produce the observed overall stabilisation. A possibility is that SnoopLigase acts as a mobile chaperone, aiding the refolding of multiple enzyme molecules and preventing aggregation through fleeting associations at higher temperatures. At higher temperatures, SnoopLigase may be able to associate with multiple cyclised enzyme species since its binding to its conjugate product through parental domain reconstitution would be weakened.

However, the observed improvements in thermal resilience when cyclisation reactions were set up using lower molar ratios of SnoopLigase to enzyme could also be attributed the use of non-limiting amounts of enzyme in the thermal resilience activity assays. This explanation could account for the discrepancy between the observed lower resilience to heat-induced aggregation of SnoopLigase-cyclised QB and its exceptional thermal resilience to inactivation.

Given such findings, the most important concepts for future exploration and characterisation include a better understanding of the mechanism through which SnoopLigase cyclisation confers thermal resilience and the effects of various linker types on the effectiveness of the SnoopLigase platform. Deeper insights into both areas would enable better predictive capabilities for ascertaining for which enzymes SnoopLigase cyclisation carries the potential be effective.

Chapter 5: Summary and General Discussion

Enzyme head-to-tail cyclisation carries the potential to function as a generic platform for stabilisation (Schoene et al., 2016b). The SpyRing, a cyclisation platform using spontaneous isopeptide bond-forming protein partners, has been demonstrated to be effective at improving the thermal resilience of a range of enzymes (Purkayastha and Kang, 2019; Schoene et al., 2016c; Wang et al., 2020). However, SpyRing cyclisation requires the fusion of a larger protein partner domain and its efficacy has only been validated on mesophilic enzymes whose termini are in relative proximity (Schoene et al., 2016a).

In this thesis, I have applied the SnoopLigase tripartite conjugation system to enzyme cyclisation. SnoopLigase cyclisation enables the isopeptide bond-locking of enzyme termini to confer thermal resilience while bypassing the fusion of a larger protein domain. SnoopLigase cyclisation further enables cyclised enzyme purification away from unreacted, uncyclised enzyme species and from SnoopLigase.

In Chapter 3, I cyclised mesophilic enzymes BLA and PhyC using the SnoopLigase platform. SnoopLigase cyclisation proceeded to high yield and conferred substantial improvements in thermal resilience that were comparable to those imparted by SpyRing cyclisation. Both SnoopLigase-cyclised enzymes were able to withstand aggregation and inactivation following heating at 100 °C. Cyclised enzymes could be cleanly purified from uncyclised enzyme and SnoopLigase using solid-phase immobilisation. SnoopLigase depletion had a marginal effect on the thermal resilience of cyclised enzymes.

SnoopLigase cyclisation was superior to the SpyRing at conferring lasting thermal resilience during longer heat challenges. To simulate the heating conditions enzymes are subjected to in industrial catalysis, cyclised enzymes were heated in cleared lysate. Compared to the improvements conferred by the SpyRing, the thermal resilience imparted by SnoopLigase cyclisation was more robust during heating in the presence of extraneous proteins.

In Chapter 4, I cyclised the *E. coli* phytase AppA using SnoopLigase cyclisation. The maximum reported distance conjugated by head-to-tail cyclisation was 29 Å, so the cyclisation of AppA (termini 48 Å apart) presented a novel challenge. Structured linkers were tested in conjunction with SnoopLigase cyclisation to facilitate physical bridging of the distance between termini while allowing for backbone rigidification. Of the tested linker constructs, SnoopLigase-cyclised SnoopTagJr-AppA-L9-DogTag exhibited the greatest improvement in thermal resilience. However, the improvements were not sustained in cleared lysate and were abolished upon SnoopLigase depletion.

Quantum Blue™ (QB), a commercially available, stabilised variant of AppA, was also cyclised using SnoopLigase in conjunction with the L9 linker. The cyclisation of QB presented a complex challenge since it was the first instance of cyclising an already thermostable enzyme with a large distance between termini. SnoopLigase-cyclised SnoopTagJr-QB-L9-DogTag exhibited improvements in thermal resilience, withstanding aggregation and inactivation even at 100 °C. However, these improvements were also not sustained in cleared lysate and were mostly abolished following removal of SnoopLigase. The improvements in thermal resilience abolished by SnoopLigase depletion could be re-established through the addition of 50% SnoopLigase.

Overall, the work presented in this thesis demonstrates the potential of SnoopLigase cyclisation as a generic strategy to substantially improve the thermal resilience of enzymes for industrial application. In addition, the work outlined in Chapter 4 showed the potential to broaden the range of enzymes suitable for stabilisation by cyclisation to include those with greater distances between termini. However, SnoopLigase cyclisation has only been tested on four enzymes in this thesis. Validation of the beneficial effects of SnoopLigase cyclisation on additional industrially important enzymes and testing of SnoopLigase-cyclised enzymes under more accurate field conditions is important to better assess the utility of SnoopLigase cyclisation.

The presented work brought up many questions, especially those relating to the mechanism by which SnoopLigase cyclisation confers thermal resilience. Head-to-tail cyclisation has been theorised to increase enzyme stability by reducing the entropy of the unfolded state; cyclisation locks the termini together to inhibit the unfolding of terminal secondary structures and rigidifies the protein backbone (Iwai et al., 2001; Schumann et al., 2015). Cyclisation may also help to reduce the entropy cost of bringing distant residues in the primary sequence into proximity during protein refolding, thereby facilitating protein refolding following denaturation (Iwai et al., 2001; Takahashi et al., 2007). This cyclisation-induced increase in the reversibility of the denatured, unfolded state was hypothesised to be the mechanism for thermal stabilisation by the SpyRing since the marginal increases in T_m did not account for the observed improvements in thermal resilience of cyclised constructs (Schoene et al., 2016a).

Beyond this project, experimental techniques that have the potential to give the best insight into the effects of SnoopLigase cyclisation on enzyme resilience

are hydrogen deuterium exchange mass spectrometry (HDX-MS) and small-angle X-ray scattering (SAXS). HDX-MS has been used to map the kinetic refolding of proteins such as maltose-binding protein (MBP) and the thermal transitions of capsid proteins at temperatures up to 60 °C (Walters et al., 2013; van de Waterbeemd et al., 2017). Therefore, HDX-MS could be used to probe the differences in refolding dynamics between cyclised enzymes and uncyclised controls and between SnoopLigase-bound and SnoopLigase-removed cyclised enzymes (Masson et al., 2019; Walters et al., 2013). SAXS has previously been used to characterise the thermal collapse of the intrinsically disordered tau protein at temperatures up to 60 °C (Ciasca et al., 2012). In conjunction with molecular dynamics simulations, SAXS could also be used to yield information on the tertiary structures of cyclised enzymes during thermal denaturation and refolding to better understand the effects of SnoopLigase cyclisation on refolding kinetics (Bianconi et al., 2012; Ciasca et al., 2012).

Another topic that requires further investigation is the role of linkers in enzyme cyclisation. The length and properties of linkers have been shown to affect the folding, stability, yield and activity of fusion proteins (Chen et al., 2013; Yu et al., 2015). In Chapter 4, I also showed that structured linkers had varying effects on the expression and thermal stability of cyclised enzymes. Consequently, there is a need for an optimised linker for conferring thermal resilience in conjunction with enzyme cyclisation. While it is unlikely that a single linker will be universally applicable with enzyme cyclisation due to the variation in distance between termini, the optimised linker could either be designed such that it is modular or scalable, or be used alongside flexible linkers to maximise the scope of the linker-assisted cyclisation platform.

To develop an optimised linker for use in enzyme cyclisation, the L9 structured linker identified in Chapter 4 could be used as the template for directed evolution. L9 linker-appended SnoopLigase cyclisation was effective at improving the thermal resilience of AppA and QB. Since directed evolution has previously been successfully used to screen for thermostable enzyme variants, it could be applied to the directed evolution of linker-appended cyclised enzyme variants with improved thermal stability (Brissos et al., 2014; Zhou et al., 2015). A potential alternative strategy for directed evolution is yeast surface display, in which protein libraries displayed on yeast are subject to heat shocks prior to screening using flow cytometry (Traxlmayr and Shusta, 2017). To ensure the selected linkers variants are optimised to confer generic thermal stability, the enzymes could be varied between cycles of directed evolution.

For an enzyme stabilisation platform to be directly applicable for industrial use, it must be effective, scalable and economically profitable (Chapman et al., 2018; Silva et al., 2018). Catalyst reusability is often advantageous in cost efficiency and is therefore desirable (Chapman et al., 2018). Though SnoopLigase can be re-used for a minimum of eight reaction cycles with no reductions in product formation, SnoopLigase is not currently suited to serving as a reusable enzyme cyclisation platform for industrial use (Buldun et al., 2018). SnoopLigase association with its cyclisation product is ideal to maximise the conferred improvements in thermal resilience. Furthermore, cyclised enzyme purification from SnoopLigase requires either the production of peptide competitor or enzyme exposure to high imidazole concentrations, neither of which are well-suited for scaling up ahead of industrial application.

By selecting for SnoopLigase variants with weaker interactions with their conjugation products, substrate turnover could be engineered into SnoopLigase through directed evolution. Doing so would come at the cost of the option of conjugate purification but would greatly enhance the reusability of SnoopLigase in the production of many batches of cyclised enzyme. A SnoopLigase variant with increased turnover that allows for efficient cyclisation could then be immobilised on to solid supports for use in fixed-bed reactors for large-scale catalyst production.

Alternatively, the strong interaction between SnoopLigase and its conjugate product could be harnessed to increase functionality. Solid-phase immobilisation of SnoopLigase followed by enzyme cyclisation would result in immobilised, cyclised enzyme that could be used for applications such as microfluidic immobilised enzyme reactors, enzyme-based biosensors and paper-based diagnostic devices (Basso and Serban, 2019; Nery and Kubota, 2016; Zhu et al., 2020).

In this thesis, industrial catalysis conditions for phytases in animal feed was modelled using heating challenges in bacterial cleared lysate. However, heating in cleared lysate is a crude approximation of actual conditions for phytase steam treatment, which is conducted in the presence of ingredients such as wheat bran, at 15 ~ 16% moisture, reaching temperatures ranging between 92 ~ 104 °C (Rebello et al., 2017). To more accurately recreate steam treatment conditions, SnoopLigase-cyclised phytases could be applied to wheat bran and heated under low-moisture conditions in an autoclave or microwave.

An aspect of SnoopLigase cyclisation that was notable for its industrial applicability was the ability to confer thermal resilience in the presence of extraneous proteins. In Chapter 3, SnoopLigase cyclisation proved superior to

SpyRing cyclisation during heat incubation in cleared lysate. This could be indicative of a lower tendency for aggregation in the RrgA C-terminal domain compared to the CnaB2 domain. The ability of the SnoopLigase cyclisation system to resist aggregation and confer thermal resilience in the presence of extraneous proteins could be improved through directed evolution to ensure that SnoopLigase-cyclised enzymes are able to withstand the rigours of industrial processes (Ebo et al., 2020). Screening enzymes cyclised by SnoopLigase variants for residual activity following heat incubation in cell lysate could yield a SnoopLigase variant with improved robustness of thermal resilience.

Bibliography

AB Vista Quantum Blue: Enhanced E.coli Phytase | AB Vista.

Acevedo-Rocha, C.G., Hoebenreich, S., and Reetz, M.T. (2014). Iterative saturation mutagenesis: A powerful approach to engineer proteins by systematically simulating darwinian evolution. Methods Mol. Biol. *1179*, 103–128.

Ahuja, K., and Rawat, A. (2019). Animal Feed Enzymes Market Share, Growth Projections 2026. Glob. Mark. Insights.

Ahvazi, B., and Steinert, P.M. (2003). A model for the reaction mechanism of the transglutaminase 3 enzyme. Exp. Mol. Med. *35*, 228–242.

Alegre-Cebollada, J., Badilla, C.L., and Fernández, J.M. (2010). Isopeptide bonds block the mechanical extension of pili in pathogenic Streptococcus pyogenes. J. Biol. Chem. *285*, 11235–11242.

Andersson, A.M.C., Buldun, C.M., Pattinson, D.J., Draper, S.J., and Howarth, M. (2019). SnoopLigase peptide-peptide conjugation enables modular vaccine assembly. Sci. Rep. *9*, 1–13.

Antos, J.M., Popp, M.W., Ernst, R., Chew, G., Spooner, E., and Ploegh, H.L. (2009a). A Straight Path to Circular Proteins. J. Biol. Chem. *284*, 16028–16036.

Antos, J.M., Chew, G.-L., Guimaraes, C.P., Yoder, N.C., Grotenbreg, G.M., Popp, M.W.-L., and Ploegh, H.L. (2009b). Site-Specific N- and C-Terminal Labeling of a Single Polypeptide Using Sortases of Different Specificity. J. Am. Chem. Soc. *131*, 10800–10801.

Aon, J.C., Caimi, R.J., Taylor, A.H., Lu, Q., Oluboyede, F., Dally, J., Kessler, M.D., Kerrigan, J.J., Lewis, T.S., Wysocki, L.A., et al. (2008). Suppressing posttranslational

gluconoylation of heterologous proteins by metabolic engineering of Escherichia coli. Appl. Environ. Microbiol. *74*, 950–958.

Arnold, F.H., and Geurgiou, G. (2014). Directed Evolution Library Creation - Methods and Protocols. Methods Mol. Biol. *1179*, 315–333.

Asquith, R.S., Otterburn, M.S., and Sinclair, W.J. (1974). Isopeptide Crosslinks?Their Occurrence and Importance in Protein Structure. Angew. Chemie Int. Ed. English *13*, 514–520.

Baase, W.A., Liu, L., Tronrud, D.E., and Matthews, B.W. (2010). Lessons from the lysozyme of phage T4. Protein Sci. *19*, 631–641.

Baldwin, A.J., Busse, K., Simm, A.M., and Dafydd Jones, D. (2008). Expanded molecular diversity generation during directed evolution by trinucleotide exchange (TriNEx). Nucleic Acids Res. *36*, 77.

Basso, A., and Serban, S. (2019). Industrial applications of immobilized enzymes—A review. Mol. Catal. *479*, 110607.

Batey, S., and Clarke, J. (2006). Apparent cooperativity in the folding of multidomain proteins depends on the relative rates of folding of the constituent domains. Proc. Natl. Acad. Sci. U. S. A. *103*, 18113–18118.

Batey, S., Nickson, A.A., and Clarke, J. (2008). Studying the folding of multidomain proteins. HFSP.

Bedford, M.R. (2000). Exogenous enzymes in monogastric nutrition - Their current value and future benefits. Anim. Feed Sci. Technol. *86*, 1–13.

Bednar, D., Beerens, K., Sebestova, E., Bendl, J., Khare, S., Chaloupkova, R., Prokop, Z., Brezovsky, J., Baker, D., and Damborsky, J. (2015). FireProt: Energy- and Evolution-Based Computational Design of Thermostable Multiple-Point Mutants. PLOS Comput. Biol. *11*, e1004556.

Bergeron, L.M., Gomez, L., Whitehead, T.A., and Clark, D.S. (2009). Self-renaturing enzymes: Design of an enzyme-chaperone chimera as a new approach to enzyme stabilization. Biotechnol. Bioeng. *102*, 1316–1322.

Bhavsar, K., and Khire, J.M. (2014). Current research and future perspectives of phytase bioprocessing. RSC Adv. *4*, 26677–26691.

Bianconi, A., Ciasca, G., Tenenbaum, A., Battisti, A., and Campi, G. (2012). Temperature and solvent dependence of the dynamical landscape of tau protein conformations. J. Biol. Phys. *38*, 169–179.

Bilen, J., and Bakir, U. (1998). The effect of crosslinking on thermal inactivation of cellulases. In Progress in Biotechnology, (Elsevier), pp. 151–156.

Blatch, G.L., and Lässle, M. (1999). The tetratricopeptide repeat: A structural motif mediating protein-protein interactions. BioEssays *21*, 932–939.

Bommarius, A.S., and Paye, M.F. (2013). Stabilizing biocatalysts. Chem. Soc. Rev. *42*, 6534–6565.

Boney, J.W., Jaczynski, J., Weidhaas, J.L., Bergeron, A.N., and Moritz, J.S. (2018). The effects of steam conditioning and antimicrobial inclusion on feed manufacturing and inactivation of Enterococcus faecium, a Salmonella surrogate. J. Appl. Poult. Res. *27*, 472–482.

Borgo, B., and Havranek, J.J. (2012). Automated selection of stabilizing mutations in designed and natural proteins. Proc. Natl. Acad. Sci. U. S. A. *109*, 1494–1499.

Bornscheuer, U.T., Huisman, G.W., Kazlauskas, R.J., Lutz, S., Moore, J.C., and Robins, K. (2012). Engineering the third wave of biocatalysis. Nature *485*, 185–194.

Borra, R., and Camarero, J.A. (2013). Recombinant expression of backbone-cyclized polypeptides. Biopolymers *100*, 502–509.

Brissos, V., Gonçalves, N., Melo, E.P., and Martins, L.O. (2014). Improving Kinetic or Thermodynamic Stability of an Azoreductase by Directed Evolution. PLoS One *9*, e87209.

Brune, K.D., Leneghan, D.B., Brian, I.J., Ishizuka, A.S., Bachmann, M.F., Draper, S.J., Biswas, S., and Howarth, M. (2016). Plug-and-Display: decoration of Virus-Like Particles via isopeptide bonds for modular immunization. Sci. Rep. *6*, 1–13.

Buldun, C.M., Jean, J.X., Bedford, M.R., and Howarth, M. (2018). SnoopLigase Catalyzes Peptide-Peptide Locking and Enables Solid-Phase Conjugate Isolation. J. Am. Chem. Soc. *140*, 3008–3018.

Buß, O., Rudat, J., and Ochsenreither, K. (2018). FoldX as Protein Engineering Tool: Better Than Random Based Approaches? Comput. Struct. Biotechnol. J. *16*, 25–33.

Cao, L., van Rantwijk, F., and Sheldon, R. a (2000). Cross-linked enzyme aggregates: a simple and effective method for the immobilization of penicillin acylase. Org. Lett. *2*, 1361–1364.

Cao, L., Wang, W., Yang, C., Yang, Y., Diana, J., Yakupitiyage, A., Luo, Z., and Li, D. (2007). Application of microbial phytase in fish feed. Enzyme Microb. Technol. *40*, 497–507.

Chapman, J., Ismail, A., and Dinu, C. (2018). Industrial Applications of Enzymes: Recent Advances, Techniques, and Outlooks. Catalysts *8*, 238.

Charbonneau, D.M., and Beauregard, M. (2013). Role of Key Salt Bridges in Thermostability of G. thermodenitrificans EstGtA2: Distinctive Patterns within the New Bacterial Lipolytic Enzyme Family XV. PLoS One *8*, e76675.

Chen, X., Zaro, J., and Shen, W.-C. (2012). Fusion Protein Linkers: Property, Design and Functionality.

Chen, X., Zaro, J.L., and Shen, W.C. (2013). Fusion protein linkers: Property, design and

functionality. Adv. Drug Deliv. Rev. *65*, 1357–1369.

Choi, J.-M., Han, S.-S., and Kim, H.-S. (2015). Industrial applications of enzyme biocatalysis: Current status and future aspects. Biotechnol. Adv. *33*, 1443–1454.

Ciasca, G., Campi, G., Battisti, A., Rea, G., Rodio, M., Papi, M., Pernot, P., Tenenbaum, A., and Bianconi, A. (2012). Continuous thermal collapse of the intrinsically disordered protein tau is driven by its entropic flexible domain. Langmuir *28*, 13405–13410.

Clark, R.J., and Craik, D.J. (2010). Native chemical ligation applied to the synthesis and bioengineering of circular peptides and proteins. Biopolymers *94*, 414–422.

Copeland, R.A. (2013). Evaluation of Enzyme Inhibitors in Drug Discovery: A Guide for Medicinal Chemists and Pharmacologists (John Wiley & Sons).

Costa, S., Almeida, A., Castro, A., and Domingues, L. (2014). Fusion tags for protein solubility, purification, and immunogenicity in Escherichia coli: The novel Fh8 system. Front. Microbiol. *5*.

Cowieson, A.J., Wilcock, P., and Bedford, M.R. (2011). Super-dosing effects of phytase in poultry and other monogastrics. Worlds. Poult. Sci. J. *67*, 225–235.

Cox, V.E., and Gaucher, E.A. (2014). Engineering proteins by reconstructing evolutionary adaptive paths. Methods Mol. Biol. *1179*, 353–363.

Cozzi, R., Malito, E., Lazzarin, M., Nuccitelli, A., Castagnetti, A., Bottomley, M.J., Margarit, I., Maione, D., and Rinaudo, C.D. (2015). Structure and assembly of group B streptococcus pilus 2b backbone protein. PLoS One *10*.

Dalal, S., Kapoor, M., and Gupta, M.N. (2007). Preparation and characterization of combi-CLEAs catalyzing multiple non-cascade reactions. J. Mol. Catal. B Enzym. *44*, 128–132.

Dennig, A., Shivange, A. V., Marienhagen, J., and Schwaneberg, U. (2011).

OmniChange: The Sequence Independent Method for Simultaneous Site-Saturation of Five Codons. PLoS One *6*, e26222.

Der, B.S., Kluwe, C., Miklos, A.E., Jacak, R., Lyskov, S., Gray, J.J., Georgiou, G., Ellington, A.D., and Kuhlman, B. (2013). Alternative Computational Protocols for Supercharging Protein Surfaces for Reversible Unfolding and Retention of Stability. PLoS One *8*.

Dersjant-Li, Y., Awati, A., Schulze, H., and Partridge, G. (2015). Phytase in non-ruminant animal nutrition: A critical review on phytase activities in the gastrointestinal tract and influencing factors. J. Sci. Food Agric. *95*, 878–896.

DiCosimo, R., McAuliffe, J., Poulose, A.J., and Bohlmann, G. (2013). Industrial use of immobilized enzymes. Chem. Soc. Rev. *42*, 6437.

Dombkowski, A.A., Sultana, K.Z., and Craig, D.B. (2014). Protein disulfide engineering. FEBS Lett. *588*, 206–212.

Dong, T., Zhao, L., Huang, Y., and Tan, X. (2010). Preparation of cross-linked aggregates of aminoacylase from Aspergillus melleus by using bovine serum albumin as an inert additive. Bioresour. Technol. *101*, 6569–6571.

Dou, J., Vorobieva, A.A., Sheffler, W., Doyle, lindsey A., Park, H., Bick, M.J., Mao, B., Foight, G.W., Yen lee, M., Gagnon, lauren A., et al. (2018). De novo design of a fluorescence-activating β-barrel. Nature.

Duan, X., Li, Y., Rajan, N.K., Routenberg, D.A., Modis, Y., and Reed, M.A. (2012). Quantification of the affinities and kinetics of protein interactions using silicon nanowire biosensors. Nat Nanotechnol *7*, 401–407.

Earl, L.A., Bi, S., and Baum, L.G. (2011). Galectin multimerization and lattice formation are regulated by linker region structure. Glycobiology *21*, 6–12.

Ebo, J.S., Guthertz, N., Radford, S.E., and Brockwell, D.J. (2020). Using protein

engineering to understand and modulate aggregation. Curr. Opin. Struct. Biol. *60*, 157–166.

Elcock, A.H. (1998). The stability of salt bridges at high temperatures: Implications for hyperthermophilic proteins. J. Mol. Biol. *284*, 489–502.

Fairhead, M., and Howarth, M. (2015). Site-specific biotinylation of purified proteins using BirA. Methods Mol. Biol. *1266*, 171–184.

Farber, P.J., and Mittermaier, A. (2008). Side chain burial and hydrophobic core packing in protein folding transition states. Protein Sci. *17*, 644–651.

Feng, J., Chen, Y., Pu, J., Yang, X., Zhang, C., Zhu, S., Zhao, Y., Yuan, Y., Yuan, H., and Liao, F. (2011). An improved malachite green assay of phosphate: Mechanism and application. Anal. Biochem. *409*, 144–149.

Fernandes, J.I.M., Horn, D., Ronconi, E.J., Buzim, R., Lima, F.K., and Pazdiora, D.A. (2019). Effects of Phytase Superdosing on Digestibility and Bone Integrity of Broilers. J. Appl. Poult. Res. *28*, 390–398.

Fink, A.L. (2005). Natively unfolded proteins. 35–41.

Finn, T.E., Nunez, A.C., Sunde, M., and Easterbrook-Smith, S.B. (2012). Serum albumin prevents protein aggregation and amyloid formation and retains chaperone-like activity in the presence of physiological ligands. J. Biol. Chem. *287*, 21530–21540.

Flory, P.J. (1956). Theory of Elastic Mechanisms in Fibrous Proteins. J. Am. Chem. Soc. *78*, 5222–5235.

Fox, J.D., Routzahn, K.M., Bucher, M.H., and Waugh, D.S. (2003). Maltodextrin-binding proteins from diverse bacteria and archaea are potent solubility enhancers. FEBS Lett. *537*, 53–57.

Fromant, M., Blanquet, S., and Plateau, P. (1995). Direct Random Mutagenesis of Gene-

Sized DNA Fragments Using Polymerase Chain Reaction. Anal. Biochem. *224*, 347–353.

Fu, H., Grimsley, G.R., Razvi, A., Scholtz, J.M., and Pace, C.N. (2009). Increasing protein stability by improving Beta-turns. Proteins Struct. Funct. Bioinforma. *77*, 491–498.

Galarneau, A., Primeau, M., Trudeau, L.E., and Michnick, S.W. (2002). β-Lactamase protein fragment complementation assays as in vivo and in vitro sensors of protein-protein interactions. Nat. Biotechnol. *20*, 619–622.

Gao, D.-Y., Sun, X.-B., Liu, M.-Q., Liu, Y.-N., Zhang, H.-E., Shi, X.-L., Li, Y.-N., Wang, J.-K., Yin, S.-J., and Wang, Q. (2019). Characterization of Thermostable and Chimeric Enzymes via Isopeptide Bond-Mediated Molecular Cyclization. J. Agric. Food Chem. *67*, 6837–6846.

Garcia-Galan, C., Berenguer-Murcia, Á., Fernandez-Lafuente, R., and Rodrigues, R.C. (2011). Potential of different enzyme immobilization strategies to improve enzyme performance. Adv. Synth. Catal. *353*, 2885–2904.

Garrett, J.B., Kretz, K.A., O'Donoghue, E., Kerovuo, J., Kim, W., Barton, N.R., Hazlewood, G.P., Short, J.M., Robertson, D.E., and Gray, K.A. (2004). Enhancing the thermal tolerance and gastric performance of a microbial phytase for use as a phosphate-mobilizing monogastric-feed supplement. Appl. Environ. Microbiol. *70*, 3041–3046.

Gasteiger, E., Hoogland, C., Gattiker, A., Duvaud, S., Wilkins, M.R., Appel, R.D., and Bairoch, A. (2005). Protein Identification and Analysis Tools on the ExPASy Server. In The Proteomics Protocols Handbook, (Totowa, NJ: Humana Press), pp. 571–607.

Gaucher, E.A., Govindarajan, S., and Ganesh, O.K. (2008). Palaeotemperature trend for Precambrian life inferred from resurrected proteins. Nature *451*, 704–707.

Gekko, K., and Timasheff, S.N. (1981). Mechanism of Protein Stabilization by Glycerol: Preferential Hydration in Glycerol-Water Mixtures. Biochemistry *20*, 4667–4676.

Gen Lei, X., Weaver, J.D., Mullaney, E., Ullah, A.H., and Azain, M.J. (2012). Phytase, a

New Life for an “Old” Enzyme.

Gessler, N.N., Serdyuk, E.G., Isakova, E.P., and Deryabina, Y.I. (2018). Phytases and the Prospects for Their Application (Review). Appl. Biochem. Microbiol. *54*, 352–360.

Gibson, D.G., Young, L., Chuang, R.Y., Venter, J.C., Hutchison, C.A., and Smith, H.O. (2009). Enzymatic assembly of DNA molecules up to several hundred kilobases. Nat. Methods *6*, 343–345.

Gilbert, C., Howarth, M., Harwood, C.R., and Ellis, T. (2017). Extracellular Self-Assembly of Functional and Tunable Protein Conjugates from *Bacillus subtilis*. ACS Synth. Biol. *6*, 957–967.

Goldenberg, D.P., and Creighton, T.E. (1983). Circular and circularly permuted forms of bovine pancreatic trypsin inhibitor. J. Mol. Biol. *165*, 407–413.

Goldenzweig, A., Goldsmith, M., Hill, S.E., Gertman, O., Laurino, P., Ashani, Y., Dym, O., Unger, T., Albeck, S., Prilusky, J., et al. (2016). Automated Structure- and Sequence-Based Design of Proteins for High Bacterial Expression and Stability. Mol. Cell *63*, 337–346.

Gontia, I., and Tiwari, S. (2013). Molecular Characterization and Comparative Phylogenetic Analysis of Phytases from Fungi with Their Prospective Applications. Food Technol. Biotechnol. *51*, 313–326.

Greiner, R., and Konietzny, U. (2006). Phytase for food application. Food Technol. Biotechnol. *44*, 125–140.

Gruninger, R.J., Thibault, J., Capeness, M.J., Till, R., Mosimann, S.C., Sockett, R.E., Selinger, B.L., and Lovering, A.L. (2014). Structural and Biochemical Analysis of a Unique Phosphatase from Bdellovibrio bacteriovorus Reveals Its Structural and Functional Relationship with the Protein Tyrosine Phosphatase Class of Phytase. PLoS One *9*, e94403.

Guddat, L.W., McAlpine, A.S., Hume, D., Hamilton, S., de Jersey, J., and Martin, J.L. (1999). Crystal structure of mammalian purple acid phosphatase. Structure *7*, 757–767.

Guerrero-Olazarán, M., Rodríguez-Blanco, L., Gerardo Carreon-Treviño, J., Gallegos-López, J.A., and Viader-Salvadó, J.M. (2010). Expression of a Bacillus Phytase C Gene in Pichia pastoris and Properties of the Recombinant Enzyme. Appl. Environ. Microbiol. *76*, 5601–5608.

Gupta, R.K., Gangoliya, S.S., and Singh, N.K. (2015). Reduction of phytic acid and enhancement of bioavailable micronutrients in food grains. J. Food Sci. Technol. *52*, 676–684.

Ha, N.C., Oh, B.C., Shin, S., Kim, H.J., Oh, T.K., Kim, Y.O., Choi, K.Y., and Oh, B.H. (2000). Crystal structures of a novel, thermostable phytase in partially and fully calcium-loaded states. Nat. Struct. Biol. *7*, 147–153.

Haefner, S., Knietsch, A., Scholten, E., Braun, J., Lohscheidt, M., and Zelder, O. (2005). Biotechnological production and applications of phytases. Appl. Microbiol. Biotechnol. *68*, 588–597.

Heck, T., Pham, P.H., Yerlikaya, A., Thöny-Meyer, L., and Richter, M. (2014). Sortase A catalyzed reaction pathways: A comparative study with six SrtA variants. Catal. Sci. Technol. *4*, 2946–2956.

Hu, X., Hu, H., Melvin, J.A., Clancy, K.W., McCafferty, D.G., and Yang, W. (2011). Autocatalytic intramolecular isopeptide bond formation in Gram-positive bacterial pili: A QM/MM simulation. J. Am. Chem. Soc. *133*, 478–485.

Huang, R., Chen, H., Zhou, W., Ma, C., and Zhang, Y.H.P. (2018). Engineering a thermostable highly active glucose 6-phosphate dehydrogenase and its application to hydrogen production in vitro. Appl. Microbiol. Biotechnol. *102*, 3203–3215.

Iwai, H., and Plückthun, A. (1999). Circular β-lactamase: Stability enhancement by

cyclizing the backbone. FEBS Lett. *459*, 166–172.

Iwai, H., Lingel, A., and Plückthun, A. (2001). Cyclic Green Fluorescent Protein Produced in Vivo Using an Artificially Split PI-PfuI Intein from Pyrococcus furiosus. J. Biol. Chem. *276*, 16548–16554.

Iyer, P. V., and Ananthanarayan, L. (2008). Enzyme stability and stabilization-Aqueous and non-aqueous environment. Process Biochem. *43*, 1019–1032.

Jelesarov, I., and Karshikoff, A. (2009). Defining the role of salt bridges in protein stability. Methods Mol. Biol. *490*, 227–260.

Jermutus, L., Tessier, M., Pasamontes, L., Van Loon, A.P.G.M., and Lehmann, M. (2001). Structure-based chimeric enzymes as an alternative to directed enzyme evolution: Phytase as a test case. J. Biotechnol. *85*, 15–24.

Jia, X., Kwon, S., Wang, C.-I.A., Huang, Y.-H., Chan, L.Y., Tan, C.C., Rosengren, K.J., Mulvenna, J.P., Schroeder, C.I., and Craik, D.J. (2014). Semienzymatic cyclization of disulfide-rich peptides using Sortase A. J. Biol. Chem. *289*, 6627–6638.

Johannes, T.W., Woodyer, R.D., and Zhao, H. (2005). Directed evolution of a thermostable phosphite dehydrogenase for NAD(P)H regeneration. Appl. Environ. Microbiol. *71*, 5728–5734.

Johnsson, N., and Varshavsky, A. (1994). Split ubiquitin as a sensor of protein interactions in vivo. Proc. Natl. Acad. Sci. U. S. A. *91*, 10340–10344.

Jones, F.T. (2011). A review of practical Salmonella control measures in animal feed. J. Appl. Poult. Res. *20*, 102–113.

Jorquera, M., Martínez, O., Maruyama, F., Marschner, P., and De La Luz Mora, M. (2008). Current and future biotechnological applications of bacterial phytases and phytase-producing bacteria. Microbes Environ. *23*, 182–191.

Kang, H.J., and Baker, E.N. (2009). Intramolecular Isopeptide Bonds Give Thermodynamic and Proteolytic Stability to the Major Pilin Protein of Streptococcus pyogenes *.

Kang, H.J., and Baker, E.N. (2011). Intramolecular isopeptide bonds: Protein crosslinks built for stress? Trends Biochem. Sci. *36*, 229–237.

Kang, H.J., Coulibaly, F., Clow, F., Proft, T., and Baker, E.N. (2007). Stabilizing isopeptide bonds revealed in gram-positive bacterial pilus structure. Science (80-.). *318*, 1625–1628.

Katchalski-Katzir, E. (1993). Immobilized enzymes--learning from past successes and failures. Trends Biotechnol. *11*, 471–478.

Kellogg, E.H., Leaver-Fay, A., and Baker, D. (2011). Role of conformational sampling in computing mutation-induced changes in protein structure and stability. Proteins Struct. Funct. Bioinforma. *79*, 830–838.

Kerovuo, J., Lauraeus, M., Nurminen, P., Kalkkinen, N., and Apajalahti, J. (1998). Isolation, characterization, molecular gene cloning, and sequencing of a novel phytase from Bacillus subtilis. Appl. Environ. Microbiol. *64*, 2079–2085.

Kerovuo, J., Rouvinen, J., and Hatzack, F. (2000). Analysis of myo-inositol hexakisphosphate hydrolysis by Bacillus phytase : indication of a novel reaction mechanism.

Kim, C.-S., Pierre, B., Ostermeier, M., Looger, L.L., and Kim, J.R. (2009a). Enzyme stabilization by domain insertion into a thermophilic protein. Protein Eng. Des. Sel. *22*, 615–623.

Kim, C., Pierre, B., Ostermeier, M., Looger, L.L., and Kim, J.R. (2009b). Enzyme stabilization by domain insertion into a thermophilic protein. Protein Eng. Des. Sel. *22*, 615–623.

Klein, J.S., Jiang, S., Galimidi, R.P., Keeffe, J.R., Bjorkman, P.J., and Regan, L. (2014). Design and characterization of structured protein linkers with differing flexibilities. Protein Eng. Des. Sel. *27*, 325–330.

Klibanov, A.M. (1983). Stabilization of Enzymes against Thermal Inactivation. Adv. Appl. Microbiol. *29*, 1–28.

Kohda, K., Tsuji, Y., Takagi, M., and Imanaka, T. (1996). Cloning and functional analysis of molecular chaperone genes from Bacillus stearothermophilus SIC1. Biotechnol. Lett. *18*, 1061–1066.

Konietzny, U., and Greiner, R. (2004). Bacterial phytase: Potential application, in vivo function and regulation of its synthesis. Brazilian J. Microbiol. *35*, 11–18.

Korendovych, I. V. (2018). Rational and semirational protein design. In Methods in Molecular Biology, (Humana Press Inc.), pp. 15–23.

Kostrewa, D., Wyss, M., D'Arcy, A., and Van Loon, A.P.G.M. (1999). Crystal structure of Aspergillus niger pH 2.5 acid phosphatase at 2.4 Å resolution. J. Mol. Biol. *288*, 965–974.

Kuhlman, B., Yang, H.Y., Boice, J.A., Fairman, R., and Raleigh, D.P. (1997). An exceptionally stable helix from the ribosomal protein L9: Implications for protein folding and stability. J. Mol. Biol. *270*, 640–647.

Kumar, S., Tsai, C.J., Ma, B., and Nussinov, R. (2000). Contribution of salt bridges toward protein thermostability. J. Biomol. Struct. Dyn. *17*, 79–85.

van Langen, L.M., Selassa, R.P., van Rantwijk, F., and Sheldon, R. a (2005). Cross-linked aggregates of (R)-oxynitrilase: a stable, recyclable biocatalyst for enantioselective hydrocyanation. Org. Lett. *7*, 327–329.

Laothanachareon, T., Champreda, V., Sritongkham, P., Somasundrum, M., and Surareungchai, W. (2008). Cross-linked enzyme crystals of organophosphate hydrolase for electrochemical detection of organophosphorus compounds. World J. Microbiol.

Biotechnol. *24*, 3049–3055.

Lawrence, M.S., Phillips, K.J., and Liu, D.R. (2007). Supercharging Proteins Can Impart Unusual Resilience. J. Am. Chem. Soc. *129*, 10110–10112.

Lee, S.A., and Bedford, M.R. (2016). Inositol - An effective growth promotor? Worlds. Poult. Sci. J. *72*, 743–760.

Lee, S.A., Nagalakshmi, D., Raju, M.V.L.N., Rama Rao, S. V., and Bedford, M.R. (2017). Effect of phytase superdosing, myo-inositol and available phosphorus concentrations on performance and bone mineralisation in broilers. Anim. Nutr. *3*, 247–251.

Lehmann, M., and Wyss, M. (2001). Engineering proteins for thermostability: The use of sequence alignments versus rational design and directed evolution. Curr. Opin. Biotechnol. *12*, 371–375.

Lehmann, M., Kostrewa, D., Wyss, M., Brugger, R., D'Arcy, A., Pasamontes, L., and van Loon, A. (2000). From DNA Sequence to Improved Functionality: Using Protein Sequence Comparisons to Rapidly Design a Thermostable Consensus Phytase. Protein Eng. *13*.

Levinthal, C. (1969). How to fold graciously. In Mossbaun Spectroscopy in Biological Systems Proceedings, pp. 22–24.

Li, S., Yang, X., Yang, S., Zhu, M., and Wang, X. (2012). Technology prospecting on enzymes: application, marketing and engineering. Comput. Struct. Biotechnol. J. *2*, e201209017.

Liao, S.M., Du, Q.S., Meng, J.Z., Pang, Z.W., and Huang, R.B. (2013). The multiple roles of histidine in protein interactions. Chem. Cent. J. *7*, 44.

Lin-Goerke, J.L., Robbins, D.J., and Burczak, J.D. (1997). PCRr-based random mutagenesis using manganese and reduced DNTP concentration. Biotechniques *23*, 409–412.

Liu, T., Wang, Y., Luo, X., Li, J., Reed, S.A., Xiao, H., Young, T.S., and Schultz, P.G. (2016). Enhancing protein stability with extended disulfide bonds. Proc. Natl. Acad. Sci. U. S. A. *113*, 5910–5915.

Liu, Z., Cao, S., Liu, M., Kang, W., and Xia, J. (2019). Self-Assembled Multienzyme Nanostructures on Synthetic Protein Scaffolds. ACS Nano *13*, 11343–11352.

Lopez-Gallego, F., Batencor, L., Hidalgo, A., Mateo, C., Fernandez-Lafuente, R., and Guisan, J.M. (2005). One-Pot Conversion of Cephalosporin C to 7-Aminocephalosporanic Acid in the Absence of Hydrogen Peroxide. Adv. Synth. Catal. *347*, 1804–1810.

López-Gallego, F., Fernandez-Lorente, G., Rocha-Martin, J., Bolivar, J.M., Mateo, C., and Guisan, J.M. (2013). Stabilization of enzymes by multipoint covalent immobilization on supports activated with glyoxyl groups. Methods Mol. Biol. *1051*, 59–71.

Luckarift, H.R., Naik, R.R., and Stone, M.O. (2004). Enzyme immobilization in a biomimetic silica support. Nat. Biotechnol. *22*, 211–213.

Luke, J.M., Carnes, A.E., Sun, P., Hodgson, C.P., Waugh, D.S., and Williams, J.A. (2011). Thermostable tag (TST) protein expression system: Engineering thermotolerant recombinant proteins and vaccines. J. Biotechnol. *151*, 242–250.

Madan, B., and Mishra, P. (2014). Directed evolution of bacillus licheniformis lipase for improvement of thermostability. Biochem. Eng. J. *91*, 276–282.

Magnusson, A.O., Szekrenyi, A., Joosten, H., Finnigan, J., Charnock, S., and Fessner, W. (2019). nanoDSF as screening tool for enzyme libraries and biotechnology development. FEBS J. *286*, 184–204.

Main, E.R.G., Xiong, Y., Cocco, M.J., D'Andrea, L., and Regan, L. (2003). Design of stable α-helical arrays from an idealized TPR motif. Structure *11*, 497–508.

Marcos, E., Chidyausiku, T.M., Mcshan, A.C., Evangelidis, T., Nerli, S., Carter, L., Nivón,

L.G., Davis, A., Oberdorfer, G., Tripsianes, K., et al. (2018). De novo design of a non-local β-sheet protein with high stability and accuracy. Nat. Struct. Mol. Biol. *25*, 1028–1034.

Marrs, B., Delagrave, S., and Murphy, D. (1999). Novel approaches for discovering industrial enzymes. Curr. Opin. Microbiol. *2*, 241–245.

Masson, G.R., Burke, J.E., Ahn, N.G., Anand, G.S., Borchers, C., Brier, S., Bou-Assaf, G.M., Engen, J.R., Englander, S.W., Faber, J., et al. (2019). Recommendations for performing, interpreting and reporting hydrogen deuterium exchange mass spectrometry (HDX-MS) experiments. Nat. Methods *16*, 595–602.

Mateo, C., Palomo, J.M., Fernandez-Lorente, G., Guisan, J.M., and Fernandez-Lafuente, R. (2007). Improvement of enzyme activity, stability and selectivity via immobilization techniques. Enzyme Microb. Technol. *40*, 1451–1463.

McLachlan, M.J., Johannes, T.W., and Zhao, H. (2008). Further improvement of phosphite dehydrogenase thermostability by saturation mutagenesis. Biotechnol. Bioeng. *99*, 268–274.

Mcnaughton, B.R., Cronican, J.J., Thompson, D.B., and Liu, D.R. (2009). Mammalian cell penetration , siRNA transfection , and DNA transfection by supercharged proteins. *106*.

Meng, F.G., Hong, Y.K., He, H.W., Lyubarev, A.E., Kurganov, B.I., Yan, Y. Bin, and Zhou, H.M. (2004). Osmophobic effect of glycerol on irreversible thermal denaturation of rabbit creatine kinase. Biophys. J. *87*, 2247–2254.

Millard, C.B., Shnyrov, V.L., Newstead, S., Shin, I., Roth, E., Silman, I., and Weiner, L.E. V (2003). Stabilization of a metastable state of Torpedo californica acetylcholinesterase by chemical chaperones. Protein Sci. *12*, 2337–2347.

Miranda, V., Wilson, L., Cárdenas, C., and Illanes, A. (2011). Reactivation of immobilized penicillin G acylase: Influence of cosolvents and catalytic modulators. J. Mol. Catal. B

Enzym. *68*, 77–82.

Mishra, R., Seckler, R., and Bhat, R. (2005). Efficient refolding of aggregation-prone citrate synthase by polyol osmolytes: How well are protein folding and stability aspects coupled? J. Biol. Chem. *280*, 15553–15560.

Mishra, R., Bhat, R., and Seckler, R. (2007). Chemical chaperone-mediated protein folding: Stabilization of P22 tailspike folding intermediates by glycerol. Biol. Chem. *388*, 797–804.

Miyawaki, O., Ma, G., Horie, T., Hibi, A., Ishikawa, T., and Kimura, S. (2008). Thermodynamic, kinetic, and operational stabilities of yeast alcohol dehydrogenase in sugar and compatible osmolyte solutions. Enzyme Microb. Technol. *43*, 495–499.

Miyazaki, K., and Arnold, F.H. (1999). Exploring nonnatural evolutionary pathways by saturation mutagenesis: Rapid improvement of protein function. J. Mol. Evol. *49*, 716–720.

Morris, A.L., MacArthur, M.W., Hutchinson, E.G., and Thornton, J.M. (1992). Stereochemical quality of protein structure coordinates. Proteins Struct. Funct. Genet. *12*, 345–364.

Murray, M.-Y. (2011). Comprehensive Biotechnology (Elsevier).

Nannemann, D.P., Birmingham, W.R., Scism, R.A., and Bachmann, B.O. (2011). Assessing directed evolution methods for the generation of biosynthetic enzymes with potential in drug biosynthesis. Future Med. Chem. *3*, 803–819.

Nery, E.W., and Kubota, L.T. (2016). Evaluation of enzyme immobilization methods for paper-based devices-A glucose oxidase study. J. Pharm. Biomed. Anal. *117*, 551–559.

Nguyen, G.K.T., Wang, S., Qiu, Y., Hemu, X., Lian, Y., and Tam, J.P. (2014). Butelase 1 is an Asx-specific ligase enabling peptide macrocyclization and synthesis. Nat. Chem. Biol. *10*, 732–738.

Nguyen, G.K.T., Kam, A., Loo, S., Jansson, A.E., Pan, L.X., and Tam, J.P. (2015). Butelase 1: A Versatile Ligase for Peptide and Protein Macrocyclization. J. Am. Chem. Soc. *137*, 15398–15401.

Nguyen, G.K.T., Qiu, Y., Cao, Y., Hemu, X., Liu, C.-F., and Tam, J.P. (2016a). Butelase-mediated cyclization and ligation of peptides and proteins. Nat. Protoc. *11*, 1977–1988.

Nguyen, G.K.T., Qiu, Y., Cao, Y., Hemu, X., Liu, C.F., and Tam, J.P. (2016b). Butelase-mediated cyclization and ligation of peptides and proteins. Nat. Protoc. *11*, 1977–1988.

Nielsen, P.H., and Wenzel, H. (2007). Enzyme Technology LCA Case Studies 514 Environmental Assessment of Ronozyme ® P5000 CT Phytase as an Alternative to Inorganic Phosphate Supplementation to Pig Feed Used in Intensive Pig Production. Int J LCA *12*, 514–520.

Niesen, F.H., Berglund, H., and Vedadi, M. (2007). The use of differential scanning fluorimetry to detect ligand interactions that promote protein stability. Nat. Protoc. *2*, 2212–2221.

Nixon, A., and Firestine, S. (2000). Rational and Irrational Design of Proteins and Their Use in Biotechnology. IUBMB Life *49*, 181–187.

Nunes, C.S., and Kumar, V. (2018). Enzymes in Human and Animal Nutrition (Elsevier).

Odii, B.O., and Coussons, P. (2014). Biological functionalities of transglutaminase 2 and the possibility of its compensation by other members of the transglutaminase family. ScientificWorldJournal. *2014*, 714561.

Oh, B.C., Choi, W.C., Park, S., Kim, Y.O., and Oh, T.K. (2004). Biochemical properties and substrate specificities of alkaline and histidine acid phytases. Appl. Microbiol. Biotechnol. *63*, 362–372.

Okafor, C.D., Pathak, M.C., Fagan, C.E., Bauer, N.C., Cole, M.F., Gaucher, E.A., and Ortlund, E.A. (2018). Structural and Dynamics Comparison of Thermostability in Ancient,

Modern, and Consensus Elongation Factor Tus. Structure *26*, 118-129.e3.

Óskarsson, K.R., Sævarsson, A.F., and Kristjánsson, M.M. (2020). Thermostabilization of VPR, a kinetically stable cold adapted subtilase, via multiple proline substitutions into surface loops. Sci. Rep. *10*.

Pace, C.N., Grimsley, G.R., Thomson, J.A., and Barnett, B.J. (1988). Conformational Stability and Activity of Ribonuclease T1 With Zero, One, and Two Intact Disulfide Bonds - PubMed. J. Biol. Chem. *263*.

Packer, M.S., and Liu, D.R. (2015). Methods for the directed evolution of proteins. Nat. Rev. Genet. *16*, 379–394.

Pantoliano, M.W., Whitlow, M., Wood, J.F., Dodd, W., Hardman, K.D., Rollence, M.L., and Bryan, P.N. (1989). Large Increases in General Stability for Subtilisin BPN' through Incremental Changes in the Free Energy of Unfolding^ (Tanford).

Paraskevopoulou, V., and Falcone, F. (2018). Polyionic Tags as Enhancers of Protein Solubility in Recombinant Protein Expression. Microorganisms *6*, 47.

Park, K., Shen, B.W., Parmeggiani, F., Huang, P.S., Stoddard, B.L., and Baker, D. (2015). Control of repeat-protein curvature by computational protein design. Nat. Struct. Mol. Biol. *22*, 167–174.

Parmeggiani, F., Huang, P.-S., Vorobiev, S., Xiao, R., Park, K., Caprari, S., Su, M., Jayaraman, S., Mao, L., Janjua, H., et al. (2015). A General Computational Approach for Repeat Protein Design.

Parthiban, V., Gromiha, M.M., and Schomburg, D. (2006). CUPSAT: prediction of protein stability upon point mutations. Nucleic Acids Res. *34*, 239–242.

Paterson, N.G., and Baker, E.N. (2011). Structure of the Full-Length Major Pilin from Streptococcus pneumoniae: Implications for Isopeptide Bond Formation in Gram-Positive Bacterial Pili. PLoS One *6*, e22095.

Pecher, P., and Arnold, U. (2009). The effect of additional disulfide bonds on the stability and folding of ribonuclease A. Biophys. Chem. *141*, 21–28.

Pelletier, J.N., Arndt, K.M., Plückthun, A., and Michnick, S.W. (1999). An in vivo library-versus-library selection of optimized protein- protein interactions. Nat. Biotechnol. *17*, 683–690.

van Pelt, S., Quignard, S., Kubáč, D., Sorokin, D.Y., van Rantwijk, F., and Sheldon, R.A. (2008). Nitrile hydratase CLEAs: The immobilization and stabilization of an industrially important enzyme. Green Chem. *10*, 395–400.

Perler, F.B., Olsen, G.J., and Adam, E. (1997). Compilation and analysis of intein sequences. Nucleic Acids Res. *25*, 1087–1093.

Persichetti, R., St. Clair, N., Griffith, J., Navia, M., and Margolin, A. (1995). Cross-linked enzyme crystals. J. Am. Chem. Soc. *117*, 2732–2737.

Peschke, T., Rabe, K.S., and Niemeyer, C.M. (2017). Orthogonal Surface Tags for Whole-Cell Biocatalysis. Angew. Chemie Int. Ed. *56*, 2183–2186.

Phelan, P., Gorfe, A.A., Jelesarov, I., Marti, D.N., Warwicker, J., and Bosshard, H.R. (2002). Salt bridges destabilize a leucine zipper designed for maximized ion pairing between helices. Biochemistry *41*, 2998–3008.

Pickart, C.M. (2001). Mechanisms Underlying Ubiquitination. Annu. Rev. Biochem. *70*, 503–533.

Pierre, B., Xiong, T., Hayles, L., Guntaka, V.R., and Kim, J.R. (2011). Stability of a Guest Protein Depends on Stability of a Host Protein in Insertional Fusion. Biotechnol. Bioeng. *108*, 1011–1020.

Pollard, T.D. (2010). MBOC technical perspective: A guide to simple and informative binding assays. Mol. Biol. Cell *21*, 4061–4067.

Popp, M.W., Dougan, S.K., Chuang, T., Spooner, E., and Ploegh, H.L. (2011). Sortase-catalyzed transformations that improve the properties of cytokines. *108*.

Pretty, J.N., Mason, C.F., Nedwell, D.B., Hine, R.E., Leaf, S., and Dils, R. (2003). Environmental costs of freshwater eutrophication in England and Wales. Environ. Sci. Technol. *37*, 201–208.

Pucci, F., Bourgeas, R., and Rooman, M. (2016). Predicting protein thermal stability changes upon point mutations using statistical potentials: Introducing HoTMuSiC. Sci. Rep. *6*, 1–9.

Purkayastha, A., and Kang, T.J. (2019). Stabilization of Proteins by Covalent Cyclization. Biotechnol. Bioprocess Eng. *24*, 702–712.

Qi, X., and Xiong, S. (2017). Intein-mediated backbone cyclization of VP1 protein enhanced protection of CVB3-induced viral myocarditis. Sci. Rep. *7*, 41485.

Qu, J., Cao, S., Wei, Q., Zhang, H., Wang, R., Kang, W., Ma, T., Zhang, L., Liu, T., Wing-Ngor Au, S., et al. (2019). Synthetic Multienzyme Complexes, Catalytic Nanomachineries for Cascade Biosynthesis in Vivo. ACS Nano *13*, 9895–9906.

Rämisch, S., Weininger, U., Martinsson, J., Akke, M., and André, I. (2014). Computational design of a leucine-rich repeat protein with a predefined geometry. Proc. Natl. Acad. Sci. U. S. A. *111*, 17875–17880.

Rao, D.E.C.S., Rao, K.V., and Reddy, V.D. (2008). Cloning and expression of *Bacillus* phytase gene (*phy*) in *Escherichia coli* and recovery of active enzyme from the inclusion bodies. J. Appl. Microbiol. *105*, 1128–1137.

Raran-Kurussi, S., and Waugh, D.S. (2012). The Ability to Enhance the Solubility of Its Fusion Partners Is an Intrinsic Property of Maltose-Binding Protein but Their Folding Is Either Spontaneous or Chaperone-Mediated. PLoS One *7*, e49589.

Rebello, S., Jose, L., Sindhu, R., and Aneesh, E.M. (2017). Molecular advancements in

the development of thermostable phytases. Appl. Microbiol. Biotechnol. *101*, 2677–2689.

Reddy, N.R., Sathe, S.K., and Salunkhe, D.K. (1982). Phytates in legumes and cereals. Adv. Food Res. *28*, 1–92.

Reetz, M.T., Bocola, M., Carballeira, J.D., Zha, D., and Vogel, A. (2005). Expanding the Range of Substrate Acceptance of Enzymes: Combinatorial Active-Site Saturation Test. Angew. Chemie *117*, 4264–4268.

Reetz, M.T., Carballeira, J.D., and Vogel, A. (2006). Iterative Saturation Mutagenesis on the Basis of B Factors as a Strategy for Increasing Protein Thermostability. Angew. Chemie Int. Ed. *45*, 7745–7751.

Ribeiro, V., Salguero, S.C., Gomes, G., Barros, V.R.S.M., Silva, D.L., Barreto, S.L.T., Rostagno, H.S., Hannas, M.I., and Albino, L.F.T. (2016). Efficacy and phosphorus equivalency values of two bacterial phytases (Escherichia coli and Citrobacter braakii) allow the partial reduction of dicalcium phosphate added to the diets of broiler chickens from 1 to 21 days of age. Anim. Feed Sci. Technol. *221*, 226–233.

Rigden, D.J. (2008). The histidine phosphatase superfamily: Structure and function. Biochem. J. *409*, 333–348.

Rigoldi, F., Donini, S., Redaelli, A., Parisini, E., and Gautieri, A. (2018). Review: Engineering of thermostable enzymes for industrial applications. APL Bioeng. *2*, 011501.

Risso, V.A., Gavira, J.A., Mejia-Carmona, D.F., Gaucher, E.A., and Sanchez-Ruiz, J.M. (2013). Hyperstability and substrate promiscuity in laboratory resurrections of precambrian β-lactamases. J. Am. Chem. Soc. *135*, 2899–2902.

Rodríguez-Fernández, D.E., Parada, J.L., Medeiros, A.B.P., De Carvalho, J.C., Lacerda, L.G., Rodríguez-León, J.A., and Soccol, C.R. (2013). Concentration by ultrafiltration and stabilization of phytase produced by solid-state fermentation. Process Biochem. *48*, 374–379.

Rosenfeld, L., Heyne, M., Shifman, J.M., and Papo, N. (2016). Protein Engineering by Combined Computational and In Vitro Evolution Approaches. Trends Biochem. Sci. *41*, 421–433.

Rossi, F., Charlton, C.A., and Blau, H.M. (1997). Monitoring protein-protein interactions in intact eukaryotic cells by β-galactosidase complementation. Proc. Natl. Acad. Sci. U. S. A. *94*, 8405–8410.

Ruller, R., Alponti, J., Deliberto, L.A., Zanphorlin, L.M., Machado, C.B., and Ward, R.J. (2014). Concommitant adaptation of a GH11 xylanase by directed evolution to create an alkali-tolerant/ thermophilic enzyme. Protein Eng. Des. Sel. *27*, 255–262.

Sadeghi, M., Naderi-Manesh, H., Zarrabi, M., and Ranjbar, B. (2006). Effective factors in thermostability of thermophilic proteins. Biophys. Chem. *119*, 256–270.

Sakaguchi, M., Osaku, K., Maejima, S., Ohno, N., Sugahara, Y., Oyama, F., and Kawakita, M. (2014). Highly conserved salt bridge stabilizes a proteinase K subfamily enzyme, Aqualysin I, from Thermus aquaticus YT-1. AMB Express *4*, 1–12.

Sanchez-Romero, I., Ariza, A., Wilson, K.S., Skjøt, M., Vind, J., De Maria, L., Skov, L.K., and Sanchez-Ruiz, J.M. (2013). Mechanism of Protein Kinetic Stabilization by Engineered Disulfide Crosslinks. PLoS One *8*, e70013.

Sauer, R.T., Hehir, K., Stearman, R.S., Weiss, M.A., Jeitler-Nilsson, A., Suchanek, E.G., and Pabo, C.O. (1986). An Engineered Intersubunit Disulfide Enhances the Stability and DNA Binding of the N-Terminal Domain of λ Repressor. Biochemistry *25*, 5992–5998.

Schenk, G., Ge, Y., Carrington, L.E., Wynne, C.J., Searle, I.R., Carroll, B.J., Hamilton, S., and De Jersey, J. (1999). Binuclear metal centers in plant purple acid phosphatases: Fe-Zn in sweet potato and Fe-Zn in soybean. Arch. Biochem. Biophys. *370*, 183–189.

Schmid, R.D. (1979). Stabilized soluble enzymes. (Springer, Berlin, Heidelberg), pp. 41–118.

Schoene, C., Fierer, J.O., Paul Bennett, S., and Howarth, M. (2014). SpyTag/SpyCatcher Cyclization Confers Resilience to Boiling on a Mesophilic Enzyme. Angew Chem Int Ed Engl *53*, 6101–6104.

Schoene, C., Bennett, S.P., and Howarth, M. (2016a). SpyRing interrogation: analyzing how enzyme resilience can be achieved with phytase and distinct cyclization chemistries. Sci. Rep. *6*, 21151.

Schoene, C., Bennett, S.P., and Howarth, M. (2016b). SpyRings Declassified. In Methods in Enzymology, pp. 149–167.

Schoene, C., Bennett, S.P., and Howarth, M. (2016c). SpyRing interrogation: analyzing how enzyme resilience can be achieved with phytase and distinct cyclization chemistries. Sci. Rep. *6*, 21151.

Schoonen, L., Nolte, R.J.M., and Hest, J.C.M. Van (2016). Highly efficient enzyme encapsulation in a protein nanocage : towards enzyme catalysis in a cellular nanocompartment mimic. Nanoscale *8*, 14467–14472.

Schumann, F.H., Varadan, R., Tayakuniyil, P.P., Grossman, J.H., Camarero, J.A., and Fushman, D. (2015). Changing the topology of protein backbone: The effect of backbone cyclization on the structure and dynamics of a SH3 domain. Front. Chem. *3*, 26.

Schweida, D., Barraud, P., Regl, C., Loughlin, F.E., Huber, C.G., Cabrele, C., and Schubert, M. (2019). The NMR signature of gluconoylation: a frequent N-terminal modification of isotope-labeled proteins. J. Biomol. NMR *73*, 71–79.

Scott, C.P., Abel-Santos, E., Wall, M., Wahnon, D.C., and Benkovic, S.J. (1999). Production of cyclic peptides and proteins in vivo. Proc. Natl. Acad. Sci. U. S. A. *96*, 13638–13643.

Seng Wong, T., Lan Tee, K., Hauer, B., and Schwaneberg, U. (2004). Sequence saturation mutagenesis (SeSaM): a novel method for directed evolution. Nucleic Acids

Res. *32*.

Senior, A.W., Evans, R., Jumper, J., Kirkpatrick, J., Sifre, L., Green, T., Qin, C., Žídek, A., Nelson, A.W.R., Bridgland, A., et al. (2019). Protein structure prediction using multiple deep neural networks in the 13th Critical Assessment of Protein Structure Prediction (CASP13). Proteins Struct. Funct. Bioinforma. *87*, 1141–1148.

Senior, A.W., Evans, R., Jumper, J., Kirkpatrick, J., Sifre, L., Green, T., Qin, C., Žídek, A., Nelson, A.W.R., Bridgland, A., et al. (2020). Improved protein structure prediction using potentials from deep learning. Nature *577*, 706–710.

Shah, S., Sharma, A., and Gupta, M.N. (2006). Preparation of cross-linked enzyme aggregates by using bovine serum albumin as a proteic feeder. Anal. Biochem. *351*, 207–213.

Sheinerman, F.B., Norel, R., and Honig, B. (2000). Electrostatic aspects of protein-protein interactions. Curr. Opin. Struct. Biol. *10*, 153–159.

Sheldon, R.A. (2011). Characteristic features and biotechnological applications of cross-linked enzyme aggregates (CLEAs). Appl. Microbiol. Biotechnol. *92*, 467–477.

Sheldon, R., Schoevaart, R., and Van Langen, L. (2005). Cross-linked enzyme aggregates (CLEAs): A novel and versatile method for enzyme immobilization (a review). Biocatal. Biotransformation *23*, 141–147.

Shin, S., Ha, N.C., Oh, B.C., Oh, T.K., and Oh, B.H. (2001). Enzyme mechanism and catalytic property of beta propeller phytase. Structure *9*, 851–858.

Shivange, A. V., Marienhagen, J., Mundhada, H., Schenk, A., and Schwaneberg, U. (2009). Advances in generating functional diversity for directed protein evolution. Curr. Opin. Chem. Biol. *13*, 19–25.

Si, M., Xu, Q., Jiang, L., and Huang, H. (2016a). SpyTag/SpyCatcher Cyclization Enhances the Thermostability of Firefly Luciferase. PLoS One *11*, e0162318.

Si, M., Xu, Q., Jiang, L., and Huang, H. (2016b). SpyTag/SpyCatcher Cyclization Enhances the Thermostability of Firefly Luciferase. PLoS One *11*, e0162318.

Siadat, O.R., Lougarre, A., Lamouroux, L., Ladurantie, C., and Fournier, D. (2006). The effect of engineered disulfide bonds on the stability of Drosophila melanogaster acetylcholinesterase. BMC Biochem. *7*, 12.

Siddiqui, K.S., Poljak, A., Guilhaus, M., Feller, G., D'Amico, S., Gerday, C., and Cavicchioli, R. (2005). Role of disulfide bridges in the activity and stability of a cold-active α-amylase. J. Bacteriol. *187*, 6206–6212.

Siebold, C., and Erni, B. (2002). Intein-mediated cyclization of a soluble and a membrane protein in vivo: Function and stability. Biophys. Chem. *96*, 163–171.

Sikorski, R.S., Boguski, M.S., Goebl, M., and Hieter, P. (1990). A repeating amino acid motif in CDC23 defines a family of proteins and a new relationship among genes required for mitosis and RNA synthesis. Cell *60*, 307–317.

Silva, C., Martins, M., Jing, S., Fu, J., and Cavaco-Paulo, A. (2018). Practical insights on enzyme stabilization. Crit. Rev. Biotechnol. *38*, 335–350.

Silver, D., Huang, A., Maddison, C.J., Guez, A., Sifre, L., Van Den Driessche, G., Schrittwieser, J., Antonoglou, I., Panneershelvam, V., Lanctot, M., et al. (2016). Mastering the game of Go with deep neural networks and tree search. Nature *529*, 484–489.

Simeonov, P., Berger-hoffmann, R., Hoffmann, R., and Stra, N. (2011). Surface supercharged human enteropeptidase light chain shows improved solubility and refolding yield. Protein Eng. Des. Sel. *24*, 261–268.

Singh, P.K. (2008). Significance of phytic acid and supplemental phytase in chicken nutrition: a review. Worlds. Poult. Sci. J. *64*.

Singh, R., Kumar, M., Mittal, A., Praveen, •, and Mehta, K. Microbial enzymes: industrial

progress in 21st century.

Singh, R., Kumar, M., Mittal, A., and Mehta, P.K. (2016). Microbial enzymes: industrial progress in 21st century. 3 Biotech *6*.

Sommerfeld, V., Schollenberger, M., Kühn, I., and Rodehutscord, M. (2018). Interactive effects of phosphorus, calcium, and phytase supplements on products of phytate degradation in the digestive tract of broiler chickens. Poult. Sci. *97*, 1177–1188.

Song, L., Siguier, B., Dumon, C., Bozonnet, S., and O'donohue, M.J. (2012). Engineering better biomass-degrading ability into a GH11 xylanase using a directed evolution strategy.

Speight, R. (2016). Biotechnology in the development of improved phytases.

Stayton, P.S., Freitag, S., Klumb, L.A., Chilkoti, A., Chu, V., Penzotti, J.E., To, R., Hyre, D., Le Trong, I., Lybrand, T.P., et al. (1999). Streptavidin-biotin binding energetics. Biomol. Eng. *16*, 39–44.

Steiner, K., and Schwab, H. (2012). Recent advances in rational approaches for enzyme engineering. Comput. Struct. Biotechnol. J. *2*, e201209010.

Stemmer, W.P.C. (1994). DNA shuffling by random fragmentation and reassembly: In vitro recombination for molecular evolution. Proc. Natl. Acad. Sci. U. S. A. *91*, 10747–10751.

Stranges, P.B., Palla, M., Kalachikov, S., Nivala, J., Dorwart, M., Trans, A., Kumar, S., Porel, M., Chien, M., Tao, C., et al. (2016). Design and characterization of a nanopore-coupled polymerase for single-molecule DNA sequencing by synthesis on an electrode array. Proc. Natl. Acad. Sci. U. S. A. *113*, E6749–E6756.

Sun, F., Zhang, W. Bin, Mahdavi, A., Arnold, F.H., and Tirrell, D.A. (2014). Synthesis of bioactive protein hydrogels by genetically encoded SpyTag-SpyCatcher chemistry. Proc. Natl. Acad. Sci. U. S. A. *111*, 11269–11274.

Sun, X.B., Cao, J.W., Wang, J.K., Lin, H.Z., Gao, D.Y., Qian, G.Y., Park, Y.D., Chen, Z.F., and Wang, Q. (2019). SpyTag/SpyCatcher molecular cyclization confers protein stability and resilience to aggregation. N. Biotechnol. *49*, 28–36.

Takahashi, H., Arai, M., Takenawa, T., Sota, H., Qui, H.X., and Iwakura, M. (2007). Stabilization of hyperactive dihydrofolate reductase by cyanocysteine-mediated backbone cyclization. J. Biol. Chem. *282*, 9420–9429.

Talekar, S., Joshi, A., Joshi, G., Kamat, P., Haripurkar, R., and Kambale, S. (2013). Parameters in preparation and characterization of cross linked enzyme aggregates (CLEAs). RSC Adv. *3*, 12485–12511.

Tarasava, K., and Freisinger, E. (2014). An optimized intein-mediated protein ligation approach for the efficient cyclization of cysteine-rich proteins. Protein Eng. Des. Sel. *27*, 481–488.

Teilum, K., Olsen, J.G., and Kragelund, B.B. (2011). Protein stability, flexibility and function. Biochim. Biophys. Acta - Proteins Proteomics *1814*, 969–976.

Thornton, J.M., and Sibanda, B.L. (1983). Amino and carboxy-terminal regions in globular proteins. J. Mol. Biol. *167*, 443–460.

Trabi, M., and Craik, D.J. (2002). Circular proteins - No end in sight. Trends Biochem. Sci. *27*, 132–138.

Traxlmayr, M.W., and Shusta, E. V. (2017). Directed evolution of protein thermal stability using yeast surface display. In Methods in Molecular Biology, (Humana Press Inc.), pp. 45–65.

Trevino, S.R., Schaefer, S., Scholtz, J.M., and Pace, C.N. (2007). Increasing Protein Conformational Stability by Optimizing β-Turn Sequence. J. Mol. Biol. *373*, 211–218.

Trevizano, L.M., Ventorim, R.Z., De Rezende, S.T., Silva, F.P., and Guimarães, V.M. (2012). Thermostability improvement of Orpinomyces sp. xylanase by directed evolution.

J. Mol. Catal. B Enzym. *81*, 12–18.

Vagenende, V., Yap, M.G.S., and Trout, B.L. (2009). Mechanisms of protein stabilization and prevention of protein aggregation by glycerol. Biochemistry *48*, 11084–11096.

Vanhercke, T., Ampe, C., Tirry, L., and Denolf, P. (2005). Reducing mutational bias in random protein libraries. Anal. Biochem. *339*, 9–14.

Veggiani, G., Nakamura, T., Brenner, M.D., Gayet, R. V., Yan, J., Robinson, C. V., and Howarth, M. (2016). Programmable polyproteams built using twin peptide superglues. Proc. Natl. Acad. Sci. U. S. A. *113*, 1202–1207.

Voloshchuk, N., Chen, L., Li, Q., and Liang, J.F. (2017). Peptide oligomers from ultra-short peptides using sortase. Biochem. Biophys. Reports *10*, 1–6.

Voutilainen, S.P., Murray, P.G., Tuohy, M.G., and Koivula, A. (2010). Expression of Talaromyces emersonii cellobiohydrolase Cel7A in Saccharomyces cerevisiae and rational mutagenesis to improve its thermostability and activity. Protein Eng. Des. Sel. *23*, 69–79.

Walk, C.L., and Olukosi, O.A. (2019). Influence of graded concentrations of phytase in high-phytate diets on growth performance, apparent ileal amino acid digestibility, and phytate concentration in broilers from hatch to 28 D post-hatch | Elsevier Enhanced Reader. Pooultry Sci. *98*, 3884–3893.

Walk, C.L., Santos, T.T., and Bedford, M.R. (2014). Influence of superdoses of a novel microbial phytase on growth performance, tibia ash, and gizzard phytate and inositol in young broilers. Poult. Sci. *93*, 1172–1177.

Walters, B.T., Mayne, L., Hinshaw, J.R., Sosnick, T.R., and Englander, S.W. (2013). Folding of a large protein at high structural resolution. Proc. Natl. Acad. Sci. U. S. A. *110*, 18898–18903.

Wang, J., Wang, Y., Wang, X., Zhang, D., Wu, S., and Zhang, G. (2016a). Enhanced

thermal stability of lichenase from Bacillus subtilis 168 by SpyTag/SpyCatcher-mediated spontaneous cyclization. Biotechnol. Biofuels *9*, 79.

Wang, J., Wang, Y., Wang, X., Zhang, D., Wu, S., and Zhang, G. (2016b). Enhanced thermal stability of lichenase from Bacillus subtilis 168 by SpyTag/SpyCatcher-mediated spontaneous cyclization. Biotechnol. Biofuels *9*.

Wang, M., Si, T., and Zhao, H. (2012). Biocatalyst development by directed evolution. Bioresour. Technol. *115*, 117–125.

Wang, Y., Tian, J., Xiao, Y., Wang, Y., Sun, H., Chang, Y., and Luo, H. (2019a). SpyTag/SpyCatcher cyclization enhances the thermostability and organic solvent tolerance of l-phenylalanine aldolase. Biotechnol. Lett. *41*, 987–994.

Wang, Y., Tian, J., Xiao, Y., Wang, Y., Sun, H., Chang, Y., and Luo, H. (2019b). SpyTag/SpyCatcher cyclization enhances the thermostability and organic solvent tolerance of l-phenylalanine aldolase. Biotechnol. Lett. *41*, 987–994.

Wang, Y., Chang, Y., Jia, R., Sun, H., Tian, J.W., Luo, H., Yu, H., and Shen, Z. (2020). SpyTag/SpyCatcher cyclization and covalent immobilization in enhancing cephalosporin C acylase stability. Process Biochem. *95*, 260–268.

Watanabe, K., Ohkuri, T., Yokobori, S.I., and Yamagishi, A. (2006). Designing thermostable proteins: Ancestral mutants of 3-isopropylmalate dehydrogenase designed by using a phylogenetic tree. J. Mol. Biol. *355*, 664–674.

van de Waterbeemd, M., Llauró, A., Snijder, J., Valbuena, A., Rodríguez-Huete, A., Fuertes, M.A., de Pablo, P.J., Mateu, M.G., and Heck, A.J.R. (2017). Structural Analysis of a Temperature-Induced Transition in a Viral Capsid Probed by HDX-MS. Biophys. J. *112*, 1157–1165.

Wijma, H.J., Fürst, M.J.L.J., and Janssen, D.B. (2018). A Computational Library Design Protocol for Rapid Improvement of Protein Stability: FRESCO. In Methods in Molecular

Biology, (Humana Press Inc.), pp. 69–85.

Williams, C.L. (2014). Evaluation of Phytate and Phytase Interactions and Phytase Phase-Feeding on Bird Performance, Bone Characteristics and Meat Quality in Young Growing Broilers.

Williams, N.K., Liepinsh, E., Watt, S.J., Prosselkov, P., Matthews, J.M., Attard, P., Beck, J.L., Dixon, N.E., and Otting, G. Stabilization of Native Protein Fold by Intein-Mediated Covalent Cyclization.

Wood, D.W., and Camarero, J.A. (2014). Intein applications: From protein purification and labeling to metabolic control methods. J. Biol. Chem. *289*, 14512–14519.

Woyengo, T.A., and Nyachoti, C.M. (2011). Review: Supplementation of phytase and carbohydrases to diets for poultry. Can. J. Anim. Sci. *91*, 177–192.

Wu, L. zhi, Ma, B. liang, Sheng, Y. biao, and Wang, W. (2008a). Equilibrium and kinetic analysis on the folding of hen egg lysozyme in the aqueous-glycerol solution. J. Mol. Struct. *891*, 167–172.

Wu, S., Wu, J., Liu, Y., and Ju, H. (2008b). Conductive and Highly Catalytic Nanocage for Assembly and Improving Function of Enzyme. Chem. Mater. *20*, 1397–1403.

Xiao, H., Bao, Z., and Zhao, H. (2015). High throughput screening and selection methods for directed enzyme evolution. Ind. Eng. Chem. Res. *54*, 4011–4020.

Xu, C., Xu, Q., Huang, H., and Jiang, L. (2018). Enhancing the stability of trehalose synthase via SpyTag/SpyCatcher cyclization to improve its performance in industrial biocatalysts. Biosci. Biotechnol. Biochem. *82*, 1473–1479.

Yamashiro, K., Yokobori, S.-I., Koikeda, S., and Yamagishi, A. (2010). Improvement of Bacillus circulans β-amylase activity attained using the ancestral mutation method. Protein Eng. Des. Sel. *23*, 519–528.

Yin, S., Ding, F., and Dokholyan, N. V. (2007). Eris: An automated estimator of protein stability [2]. Nat. Methods *4*, 466–467.

Yu, K., Liu, C., Kim, B.G., and Lee, D.Y. (2015). Synthetic fusion protein design and applications. Biotechnol. Adv. *33*, 155–164.

Yumura, K., Akiba, H., Nagatoishi, S., Kusano-Arai, O., Iwanari, H., Hamakubo, T., and Tsumoto, K. (2017). Use of SpyTag/SpyCatcher to construct bispecific antibodies that target two epitopes of a single antigen. J. Biochem. *162*, 203–210.

Zakeri, B., and Howarth, M. (2010). Spontaneous intermolecular amide bond formation between side chains for irreversible peptide targeting. J. Am. Chem. Soc. *132*, 4526–4527.

Zakeri, B., Fierer, J.O., Celik, E., Chittock, E.C., Schwarz-Linek, U., Moy, V.T., and Howarth, M. (2012). Peptide tag forming a rapid covalent bond to a protein, through engineering a bacterial adhesin. Proc. Natl. Acad. Sci. U. S. A. *109*, E690-7.

Zavodszky, M., Chen, C.-W., Huang, J.-K., Zolkiewski, M., Wen, L., and Krishnamoorthi, R. (2001). Disulfide bond effects on protein stability: Designed variants of Cucurbita maxima trypsin inhibitor-V . Protein Sci. *10*, 149–160.

Zhang, S., Ma, C., and Chalfie, M. (2004). Combinatorial marking of cells and organelles with reconstituted fluorescent proteins. Cell *119*, 137–144.

Zhang, W., Mullaney, E.J., and Xin, G.L. (2007). Adopting selected hydrogen bonding and ionic interactions from Aspergillus fumigatus phytase structure improves the thermostability of Aspergillus niger PhyA phytase. Appl. Environ. Microbiol. *73*, 3069–3076.

Zhao, Z., Fu, J., Dhakal, S., Johnson-buck, A., Liu, M., Zhang, T., Woodbury, N.W., Liu, Y., Walter, N.G., and Yan, H. (2016). Nanocaged enzymes with enhanced catalytic activity and increased stability against protease digestion. Nat. Commun. *7*, 1–9.

Zhou, C., Xue, Y., and Ma, Y. (2015). Evaluation and directed evolution for thermostability improvement of a GH 13 thermostable α-glucosidase from Thermus thermophilus TC11. BMC Biotechnol. *15*, 97.

Zhou, Y.B., Cao, J.W., Sun, X.B., Wang, H., Gao, D.Y., Li, Y.N., Wu, K.Y., Wang, J.K., Qian, G.Y., and Wang, Q. (2020). Enhanced stability of a rumen-derived xylanase using SpyTag/SpyCatcher cyclization. World J. Microbiol. Biotechnol. *36*, 33.

Zhu, Y., Chen, Q., Shao, L., Jia, Y., and Zhang, X. (2020). Microfluidic immobilized enzyme reactors for continuous biocatalysis. React. Chem. Eng. *5*, 9–32.

平淑珍, 赵仲麟, 林敏, 陆伟, 陈明, 张维, and 燕永亮 (2010). CN101638642A - Cyclized phytase with improved heat stability and proteinase resistance - Google Patents.

(2011). European Food Safety Authority. EFSA J. *9*.

(2013). European Food Safety Authority. EFSA J. *11*, 3433.